NTNU

Norwegian University of
Science and Technology

Early History Matching of the Ivar Aasen Field

Øystein Hølland

Petroleum Geoscience and Engineering
Submission date: June 2017
Supervisor: Jon Kleppe, IGP
Co-supervisor: Kjell Christoffersen, Aker BP ASA
Geir Frode Kvilaas, Aker BP ASA

Norwegian University of Science and Technology
Department of Geoscience and Petroleum

Abstract

Dynamic reservoir simulation models are used to better understand the reservoir and predict future reservoir performance. Once a field starts to produce, a continuous flow of dynamic data becomes available in terms of production data and measurements. Integrating this information through history matching is crucial in improving the reservoir understanding and the predictive power of the reservoir model. The purpose of this study is to investigate what new knowledge about the Ivar Aasen field could be gained from the reservoir's reactions to the first months of production.

Through a manual history matching the Ivar Aasen reservoir model was successfully adjusted to better represent the production data and measurements. A higher rate of depletion in the model compared in the field at two of the producers was fixed by increasing the reservoir volume and permeability in the area around them. Reducing the permeability in the aquifer counteracted the larger depletion seen at the injectors in the model.

The results from the manual history matching were partly supported by a computer assisted history matching study. The study also brought an opportunity to highlight the main differences between manual and assisted history matching. Due to the difficulties in implementing either methods in a way that is quick and easy, and gives high quality results, a sound use of both is recommended.

Samandrag

Dynamiske reservoarsimuleringsmodellar vert brukte til å skjøne reservoaret betre og føreseia framtidig reservoaryting. I det eit felt vert sett i produksjon, vert ein kontinuerlig straum av dynamiske data tilgjengelege i form av produksjonsdata og målingar. Å integrere denne informasjonen gjennom ei historietilpasning er avgjerande for å betre reservoarforståinga og reservoarmodellen si prediktive kraft. Hensikta med denne studien er å undersøkje kva for ny kunnskap om Ivar Aasen-feltet som kan hentast frå reservoaret sine reaksjonar på dei første månadane med produksjon.

Gjennom ei manuell historietilpasning vart reservoarmodellen på Ivar Aasen vellukka justert for å betre representere produksjonsdata og målingar. Eit raskare trykkfall i modellen enn på feltet ved to av produsentane vart ordna ved å auke reservoarvolumet og permeabiliteten i området rundt dei. Ved å redusere permeabiliteten i vatnsona motverka dette det høgare trykkfallet ved injektorane i modellen.

Resultata frå den manuelle hm vart til dels støtta av ei dataassistert historietilpasning. Den assisterte studien var også eit høve til å rette merksemd mot dei viktigaste skilnadane mellom manuell og assistert historietilpasning. Som følgje av vanskane med å implementere nokon av metodane raskt og enkelt, og samstundes oppnå resultat med høg kvalitet, er ein nøktern bruk av begge tilrådd.

Preface

This master's thesis was carried out during the spring of 2017 at Department of Geoscience and Petroleum, Norwegian University of Science and Technology (NTNU).

Acknowledgements

First and furthermost I would like to thank Aker BP ASA for the opportunity to work with a real field case, for the use of workspace, equipment, and experienced professionals available to answer any questions. Special thanks to my co-supervisors at Aker BP, Kjell Christoffersen and Geir Frode Kvilaas, for guidance in struggles with reservoir technology, software and thesis writing.

A great thank to my supervisor Professor Jon Kleppe (NTNU), for always having the door open and welcoming any questions.

Finally, I would like to thank Resoptima AS, for answering my questions regarding assisted history matching and their ResX software.

Table of Contents

List of Figures

List of Tables

1 Introduction

Almost all decisions regarding optimization of hydrocarbon production are based on reservoir simulations. The reservoir simulation model is thus instrumental in the work towards maximizing the field value. Before any hydrocarbon is produced, the simulation model is built on the basis of geophysical, petrophysical and geological interpretations, in addition to well tests. The well tests are the only sources to dynamic data used to construct the dynamic reservoir model. The rest of the data are considered static, they do not change with time. The uncertainties associated with all the data sources, in addition to the scarce dynamic data at hand, make the prediction of fluid flow difficult.

The production data, for instance production rates and pressures, typically are the first full field dynamic data gathered. A natural action is thus to integrate these data into the reservoir model in order to improve its predictive power. To adjust the reservoir model, for it to fit the new information better, is called history matching. Over the lifetime of a field all kinds of available information needs to be integrated continuously, to reduce uncertainty, improve the model and maximize field value. History matching methods are commonly divided into manual history matching and computer assisted history matching. Manual history matching is carried out by manual adjustments of reservoir parameters, while a computer performs the optimization in computer assisted history matching.

The Aker BP operated Ivar Aasen field came into production last winter. Over the course of the spring increasing amounts of dynamic data have become available. The new data needs to be integrated into the current reservoir model in order to efficiently make use of it in reservoir management decisions.

The purpose of this study is to investigate what new knowledge about the Ivar Aasen field could be gained from the reservoir's reactions to the first few months of production. The study is performed through a manual history matching. The Ivar Aasen reservoir model, which was solely based on information gathered prior to production start, is conditioned to new production data. The results from the manual history matching are compared with the results from a computer assisted history matching study, using the ensemble based ResX software. The results from repeat formation tester (RFT) surveys performed during drilling of two new injection wells after production start are also examined.

Having results from one manual and one assisted history matching, based on the same data, also provide the foundation for a comparison of the two classes of history matching.

2 History Matching

Numerical reservoir simulation models are constructed based on the best available information at that time, with the objective of predicting future reservoir production and performance (Mattax and Dalton, 1990). When production data is at hand, comparing the behaviour of the model to the actual field's behaviour can be used to evaluate the model. If the model is unable to reproduce the performance of the reservoir, one can expect the ability to predict future performance to be at least equally bad. In order to make a match the model is adjusted. The procedure of modifying the model, until it approximately reproduce the behaviour of the actual field, is called history matching (Dadashpour, 2009).

The objective of history matching is to exploit the new information to get a better reservoir model, and (more importantly) a better understanding of the reservoir. The better understanding should then put one in a position to make better decisions regarding for instance drainage strategy, production allocation and infill wells. And in turn increase field value.

The general form of the history matching problem is to find a vector of reservoir model variables $\boldsymbol{m}$ that solves

$$g(\boldsymbol{m}) = \boldsymbol{d}_{obs} \tag{2.1}$$

where $\boldsymbol{d}_{\text{obs}}$ is a vector of observed reservoir behaviour, and $g(\ )$ is the model that predicts reservoir behaviour (Oliver and Chen, 2011).

History matching is an inverse type of problem (Oliver and Chen, 2011). Instead of using the cause of an action to estimate the action, the action (measured rates, pressures etc.) is used to estimate the cause (reservoir properties). This makes the problem over-determined, possibly having multiple sets of reservoir variables able to solve the problem adequately.

The data matched during a traditional history matching procedure typically are pressure, water/oil ratio (WOR), gas/oil ratio (GOR), water/gas ratio, water and gas arrival times and fluid saturation from cores, well logs, and chemical tracer tests (Mattax and Dalton, 1990).

Although one seeks to minimize the uncertainty in the different types of data used for history matching, there will always be some measurement errors. This is particularly true if the properties are not measured directly. Examples of this are production rates based on choke openings and formation pressure monitoring with gauges placed some distance up the well. However, model error is often more dominating, e.g. a tool can often have a high precision on

pressure measurement, but this precision can rarely be captured by a coarsely gridded reservoir model. No matter the source of error, one should not spend vast amounts of time to achieve a better match than the uncertainties would suggest.

The most important goal of history matching is to improve the predictive power of the reservoir model. However, a high match quality do not necessarily imply high prediction quality (Cancelliere et al., 2011). Gjesdal (2015) advocates for running predictions as part of the quality control. By running the last part of history in prediction mode, with real production constraints (inlet pressures, capacities etc.), the predictive power can be estimated. An example of model validation is found in Perrone et al. (2017). By leaving production data from the latest period out of the history matching, it can be used for validation of the model.

Modern history matching needs to integrate all available data, not just production data, in order to utilize all the available information and reduce uncertainties. Gjesdal (2015) lists the following data types as suitable to integrate (Figure 2.1):

- Simulation results
- Structural framework
- Reservoir characterization and initial volumes
- CH logging and down-hole measurements
- Well positions and perforated intervals
- Production and injection rates
- 4D seismic
- Tracer responses

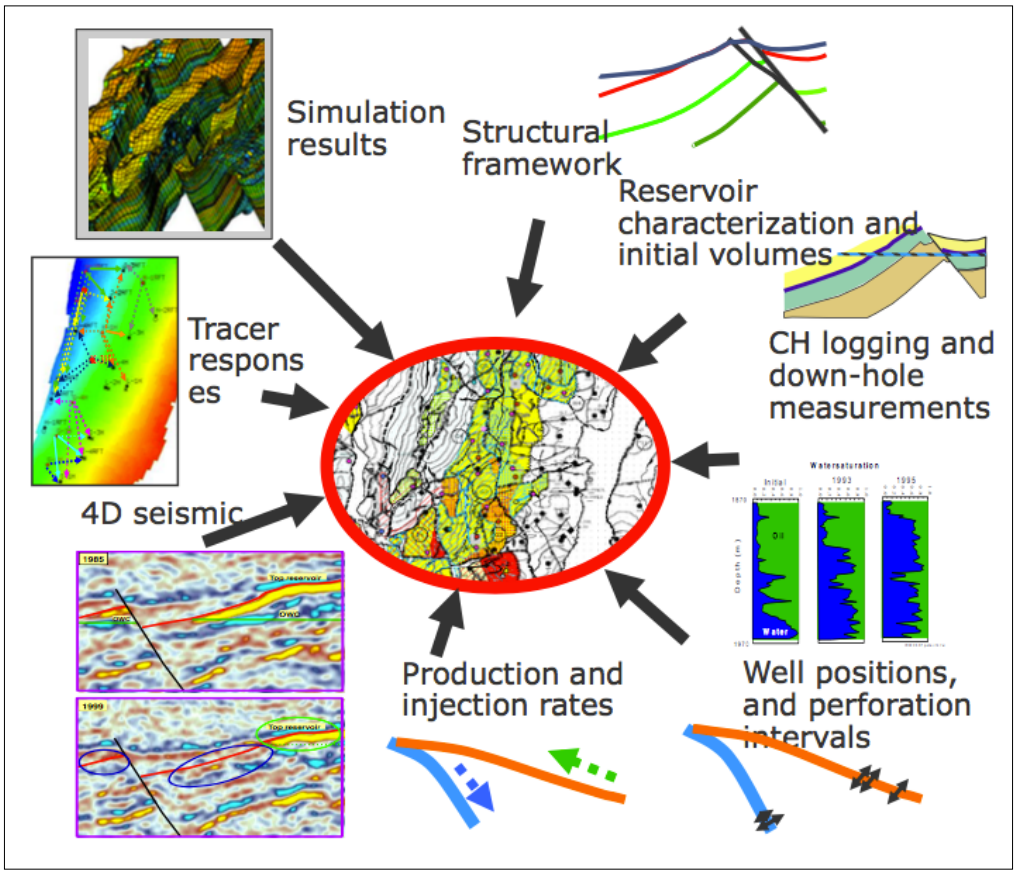

Figure 2.1 Integration of all available information

From Gjesdal (2015)

The diversity in the data sources has turned history matching into a highly cross-disciplinary procedure, compared to traditional history matching of production data. Hopefully this change will improve the legitimacy of the history-matched models across the disciplines.

In the literature history matching methods are commonly divided into manual history matching (single model) and computer assisted history matching (multiple models). The two classes will be given a closer look in the following subchapters.

2.1 Manual History Matching

Traditionally, history matching is a trial and error exercise, adjusting one or a few reservoir model parameters at a time, analysing the effect of the adjustments, and then repeating. The goal of a manual history match procedure is to find one single new model that better reproduces the measured data from the field. The complex nature of the reservoir model can make history matching both time-consuming and frustrating (Mattax and Dalton, 1990). In addition, this single matched model is inconsistent with the fact that multiple models, with widely different adjustments, can yield a sufficient match. Ending up with only one matched

model also makes uncertainty studies difficult (Gjesdal, 2015). Never the less, manual history matching is still common (Cancelliere et al., 2011).

In order to simplify the history matching process, and make it more efficient, Gjesdal (2015) suggests a stepwise approach. The steps are shown in Figure 2.2. The main motivations behind this methodology are to start with a global perspective and a limited number of matching parameters. Step by step the matching parameters becomes more detailed.

	History matching steps	Modifiers
1	Match average reservoir pressure (during analysis phase focus on delta pressure/depletion)	Pore volume, rock compressibility, fault transmissibility, permeability, asuifer paramters/pressure support, vertical/lateral communication....
2	Match RFT pressures	Pore volume, rock compressibility, fault transmissibility, permeability, aquifer paramters/pressure support, vertical/lateral communication.....
3	Match average GOR and WCT	Fault transmissibilty, vertical/lateral communication, relative permeability, facies proportions
4	Match well GOR and WCT	Relative permeability, fault transmissibility, vertical/lateral communication, well PI, near wellbore permeability
5	Match/quality check well PLT, open hole logs and tracer data	Relative permeability, fault transmissibility, vertical lateral communication, well PI, near well bore permeability
6	Match well shut in pressures	Reservoir communication, near well bore connectivity
7	Calibrate wells for predictions	Well PI, skin factor

Figure 2.2 A systematic approach to history matching

From Gjesdal (2015)

This approach is also applicable for computer assisted history matching, especially if the number of parameters that can be calibrated simultaneously is the limiting factor of the method.

2.2 Assisted History Matching

The timely manner of manual history matching has over the last decades driven forward research in automatic (computer) methods for reservoir model calibration. However, the complexity of the reservoir models, and the variations from field to field, have made it hard to find an optimal fully automatic method (Cancelliere et al., 2011). Thus, semi-automatic or assisted history matching (AHM) seems more viable.

The AHM methods use a misfit function to quantify the difference between the simulated and observed responses

$$g(\boldsymbol{m}) = \boldsymbol{d}_{obs} + \varepsilon \tag{2.2}$$

An algorithm then seeks to minimize the misfit function and thereby find the best approximate model. What parameters to adjust can for instance be determined by sensitivities, a quantification of which actions directs one towards the goal.

2.2.1 Methods

Over the last decades there have been numerous attempts to come up with an efficient and reliable algorithm for AHM. However, no method has yet gained reputation as the industry standard for real field cases.

Some of the proposed methods are:

- Ensemble Kalman filter (EnKF) (Evensen, 1994)
- Ensemble Kalman smoother (EnKS) (Evensen and Van Leeuwen, 2000)
- Iterative ensemble Kalman smoother (Chen and Oliver, 2013)
- Randomized maximum likelihood (RML) (Khaninezhad and Jafarpour, 2013)
- Evolutionary algorithms (Oliver and Chen, 2011)
- Gauss-Newton (Tan, 1995)

Most of the latest AHM methods are based on a stochastic generation of an ensemble of reservoir models (realizations). A number of static models are populated with stochastically (Monte Carlo) picked values for the different properties in each grid block. The randomness is constrained by confidence intervals given by the user. The intervals, or distributions, are established based on measurement errors, uncertainty in the geologically interpretations, seismic uncertainty and so on. The goal is thus that the ensemble of static models captures the uncertainty in the input data.

Each of these static models are converted into reservoir simulation models and simulated with the real production history. They are then compared with field and production data that needs to be integrated into the reservoir model. How the data are integrated, i.e. how the different AHM methods history match the ensemble of models, vary from method to method as the misfit function and sensitivities are stated differently. Some methods actively use learning between the models, while other use discarding of models. Assimilation of new data can be carried out simultaneously or sequentially. At the end of the matching procedure, one ends up

with an ensemble of history-matched models. This ensemble is more suited for uncertainty quantification of production forecast compared to a single matched model (Cancelliere et al., 2011).

To illuminate what differences might exist between AHM algorithms, a short discussion of two methods frequently mentioned in the literature, EnKF and RML, follows. The methods are similar, both using an ensemble of realizations. However, EnKF conditions the models to new data sequentially, while RML is non-sequential (Fossum et al., 2012). In addition, for a non-linear model (like most reservoir models) more differences appear:

- RML can be iterative, EnKF is not
- RML uses gradients/sensitivities that are specific to the realization when a realization is changed, EnKF uses the covariance of the entire ensemble to change each realization

When the number of variables are relatively small, evolutionary algorithms are often the standard approach for assisted history matching (Oliver and Chen, 2011). The inspiration behind this class of algorithms is the process occurring in biological evolution. The algorithms are population-based, using mutation and recombination of the reservoir models to create new models. Which models survive and which are discarded from the ensemble is determined by a fitness function based predominantly on data mismatch.

The EnKF has historically been given most attention in the literature. However, its limitations have become more and more apparent in recent years, and research has been put into the EnKS, which is a modified EnKF. The ResX software uses an iterative version of the EnKS. In the next chapter, the focus will thus be on the ensemble Kalman filter and the ensemble Kalman smoother.

2.2.2 Workflow

An example of a workflow used in ensemble based integration of dynamic data is shown in Figure 2.3. As the closed circle indicates, the knowledge gained from the matched models should also be used as input to the next reservoir modelling. This continuous, circular approach shifts the focus from model optimization to increased reservoir understanding and the involved uncertainty, which are more important as new data continuously becomes available.

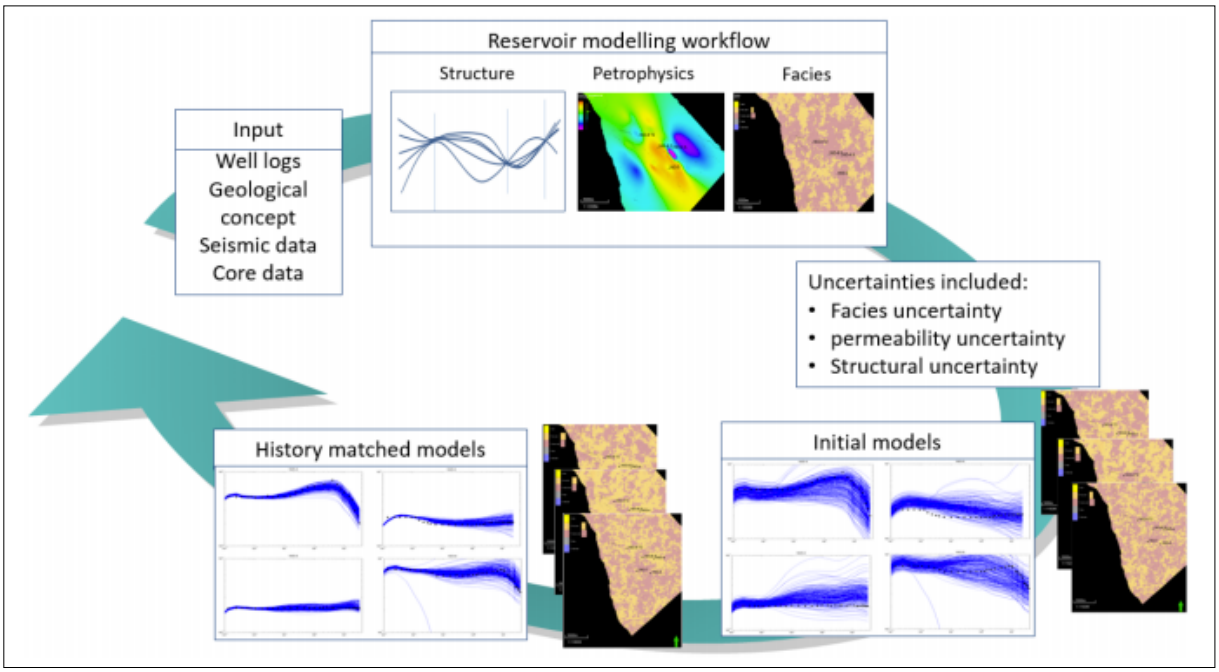

Figure 2.3 Overview of integrated reservoir modelling workflow

From Sætrom et al. (2016)

2.2.3 Parameterization

The traditional manual history matching is often limited by problems associated with adjustment of numerous parameters simultaneously (Cancelliere et al., 2011). The challenges are mostly related to the complex nature of the reservoir model and its parameter interdependencies. The AHM methods are more suited to handle a large number of parameters at the same time, where statistics and stochastic algorithms are used to tackle the complex problems. Although the AHM methods are more capable of managing numerous parameters, the selection of parameters to adjust is still essential.

In order to describe the reservoir fluid dynamics parameters like porosity, permeability etc., are assigned to each grid block. With a large grid the total number of parameters soon exceeds what can be calibrated based on the available data or constraints (Cancelliere et al., 2011).

2.2.4 Quality Check

An assisted history matching study utilizes large quantities of data. The initial models typically include petrophysical, geophysical and geological interpretations in addition to modelled representations of the wells and completions. How realistic the initial models turn out to be is of course strongly dependent on the quality of the input data, and how it is implemented.

During the history matching, the results produced by the models are compared to the measured results by the AHM algorithms. The quality of the analysis (and in turn the quality of the match) relies on comparability in the result pairs. Extra rounds of ensemble generation and history matching can be used to correct any inadequate implementations and inconsistencies.

3 Ensemble Kalman Filters

The EnKF was presented by Evensen (1994) as a stochastic (Monte Carlo) alternative to the deterministic extended Kalman filter. The motivation behind EnKF was to reduce the computational power needed when dealing with nonlinear dynamics in large state spaces. It has later been used in reservoir characterization to solve the general state and parameter estimation problem (Aanonsen et al., 2009). Some of the benefits of the EnKF are no need for derivation of tangent linear operator or adjoint equations, as well as no backward integration in time (Evensen, 2009).

3.1 Kalman Filters

The Kalman filter uses a series of noisy measurements to approximate the state of a linear dynamical system (Aanonsen et al., 2009). Since it was first presented in 1960 much research has been done on the Kalman filter, and multiple extensions and alternatives are introduced (Evensen, 2009).

3.2 Derivation of EnKF

The statistical notation used in the following derivations is explained in Appendix A Statistical Definitions.

3.2.1 Representation of Error Statistics

The EnKF differs from the Kalman filter and the extended Kalman filter in the way error statistics is treated (Aanonsen et al., 2009). Traditionally, the error covariance matrices for the predicted and analysed estimate, $\boldsymbol{C}^{\boldsymbol{f}}_{\psi\psi}$ and $\boldsymbol{C}^{\boldsymbol{a}}_{\psi\psi}$, are defined as

$$\boldsymbol{C}^{\boldsymbol{f}}_{\psi\psi} = \overline{(\psi^f - \psi^t)(\psi^f - \psi^t)^T} \tag{3.1}$$

$$\boldsymbol{C}^{\boldsymbol{a}}_{\psi\psi} = \overline{(\psi^a - \psi^t)(\psi^a - \psi^t)^T} \tag{3.2}$$

where ψ^f is the predicted state vector, ψ^t is the true state vector and ψ^a is the analysed state vector. State vectors are vectors containing all reservoir parameters. With an infinite ensemble size the ensemble average converges to the expectation value (Evensen, 2009). But since the true state, ψ^t, is unknown, the ensemble covariance matrices can be defined around the ensemble mean,

$$(\boldsymbol{C}^{e}_{\psi\psi})^{f} = \overline{\left(\psi^{f} - \overline{\psi^{f}}\right)\left(\psi^{f} - \overline{\psi^{f}}\right)^{T}} \tag{3.3}$$

$$(\boldsymbol{C}^{e}_{\psi\psi})^{a} = \overline{(\psi^{a} - \overline{\psi^{a}})(\psi^{a} - \overline{\psi^{a}})^{T}} \tag{3.4}$$

With this notation the ensemble mean is interpreted as the best estimate, and the spreading of the ensemble is interpreted as the error around the ensemble mean.

There will exist an infinite number of ensembles yielding an error covariance equal to $\boldsymbol{C}^{e}_{\psi\psi}$, since the error covariances in equations (3.3) and (3.4) are defined as averages. The error statistics can thus instead be represented with a suitable ensemble of model states. As stated in Appendix A, the error of the Monte Carlo sampled ensemble will decrease with sample size, proportional to $1/N^{1/2}$.

Given an ensemble of N model states with n dimensions, each of the model states is represented by a single point in an n-dimensional state space. When N goes to infinity, the set of points can be described by a probability density function

$$f(\psi) = \frac{dN}{N} \tag{3.5}$$

where dN is the amount of points located within a small unit volume, and N is the total amount of points. The probability density function (pdf), or the ensemble representing the pdf, can be used to compute statistical moments (mean, covariance etc.). The infinite ensemble of model states can thus be used to represent the information of the full pdf (Evensen, 2009).

3.2.2 Prediction of Error Statistics

The use of a Monte Carlo method for solving of the time evolution equation of the probability density of the model state was shown in Evensen (1994). This was in contrast to the extended Kalman filter, which uses the approximate error covariance equation.

The imperfectness and model errors of a nonlinear model make it possible to write the time evolution as a stochastic differential equation

$$d\psi = \boldsymbol{G}(\psi)dt + \boldsymbol{h}(\psi)d\boldsymbol{q} \tag{3.6}$$

Making a time step will lead to change in ψ, accompanied by a random influence from the stochastic forcing term $\boldsymbol{h}(\psi)d\boldsymbol{q}$. The forcing term represents the model error, where the $d\boldsymbol{q}$

term describes a vector Brownian motion process with covariance $\boldsymbol{C}_{qq}dt$. $\boldsymbol{G}$ is the non-linear model operator.

The Fokker-Planck equation can be derived when additive Gaussian model errors forming a Markov process are used (Evensen, 2009). It defines the time evolution of the probability density $f(\psi)$ of the model state,

$$\frac{\partial f}{\partial t} + \sum_i \frac{\partial (g_i f)}{\partial \psi_i} = \frac{1}{2} \sum_{i,j} \frac{\partial^2 f \left(\boldsymbol{h} \boldsymbol{C}_{qq} \boldsymbol{h}^T \right)_{ij}}{\partial \psi_i \partial \psi_j} \tag{3.7}$$

where g_i is the component i in the model operator $\boldsymbol{G}$ and $\boldsymbol{h}\boldsymbol{C}_{qq}\boldsymbol{h}^T$ is the covariance matrix for the model errors. Fokker-Planck is a fundamental equation describing the time evolution of error statistics.

The probability density function of a linear model for a Gauss-Markov process with initial conditions from a normal distribution will be described completely by its mean and covariance (this is used in the Kalman filter). For a non-linear model, this will not generally be the case. Approximate equations for the statistical moments can however be solved, since they determine the mean path and the dispersion about the path. This is used by the extended Kalman filter.

Instead the EnKF uses a Monte Carlo method method to approximately sample from the posterior pdf. As discussed the probability density is represented by an ensemble of model states. The stochastic differential equation (3.6) is used to integrate all the state models forward in time according to the model dynamics. This process is equivalent to solving the Fokker-Planck equation.

The derivation of the Fokker-Planck equation can become very complex due to the stochastic terms in the nonlinear model operator of some dynamical models. However, the equation is not needed. It is sufficient to know that it exists and that it can be solved.

3.2.3 Analysis Scheme

The definitions of $\boldsymbol{C}^{f}_{\psi\psi}$ and $\boldsymbol{C}^{a}_{\psi\psi,}$ (given by (3.1) and (3.2)) is used in the analysis scheme of the Kalman filter. In the following an analysis scheme using the ensemble covariances (given by (3.3) and (3.4)) is derived. The observations must be treated as random variables with mean equal to the first guess, and covariance equal to $\boldsymbol{C}_{\varepsilon\varepsilon}$. The ensemble of observations is defined as

$$\boldsymbol{d}_j = \boldsymbol{d} + \boldsymbol{\epsilon}_j \tag{3.8}$$

where j counts the ensemble members up to N, the ensemble size.

The ensemble covariance matrix of the measurement errors, $\boldsymbol{\varepsilon}$, is defined as

$$\boldsymbol{C}^{e}_{\epsilon\epsilon} = \overline{\boldsymbol{\epsilon}\boldsymbol{\epsilon}^{\mathrm{T}}} \tag{3.9}$$

With an infinite number of state models in the ensemble, the matrix will converge to $\boldsymbol{C}_{\varepsilon\varepsilon}$, the actual covariance matrix.

In the analysis step of EnKF, each model state is updated using

$$\psi^{a}_{j} = \psi^{f}_{j} + \left(\boldsymbol{C}^{e}_{\psi\psi}\right)^{f}\boldsymbol{M}^{T}\left(\boldsymbol{M}\left(\boldsymbol{C}^{e}_{\psi\psi}\right)^{f}\boldsymbol{M}^{T} + \boldsymbol{C}^{e}_{\varepsilon\varepsilon}\right)^{-1}\left(\boldsymbol{d}_j - \boldsymbol{M}\psi^{f}_{j}\right) \tag{3.10}$$

where $\boldsymbol{M}$ is the measurement matrix. Given a finite number of ensemble members, (3.10) will be an approximation.

This analysis is performed every time measurements are available, as seen in Figure 3.1. The blue arrows represent the forward ensemble integration, the red arrows are the introduction of measurements, and the green arrows are the EnKF update algorithm.

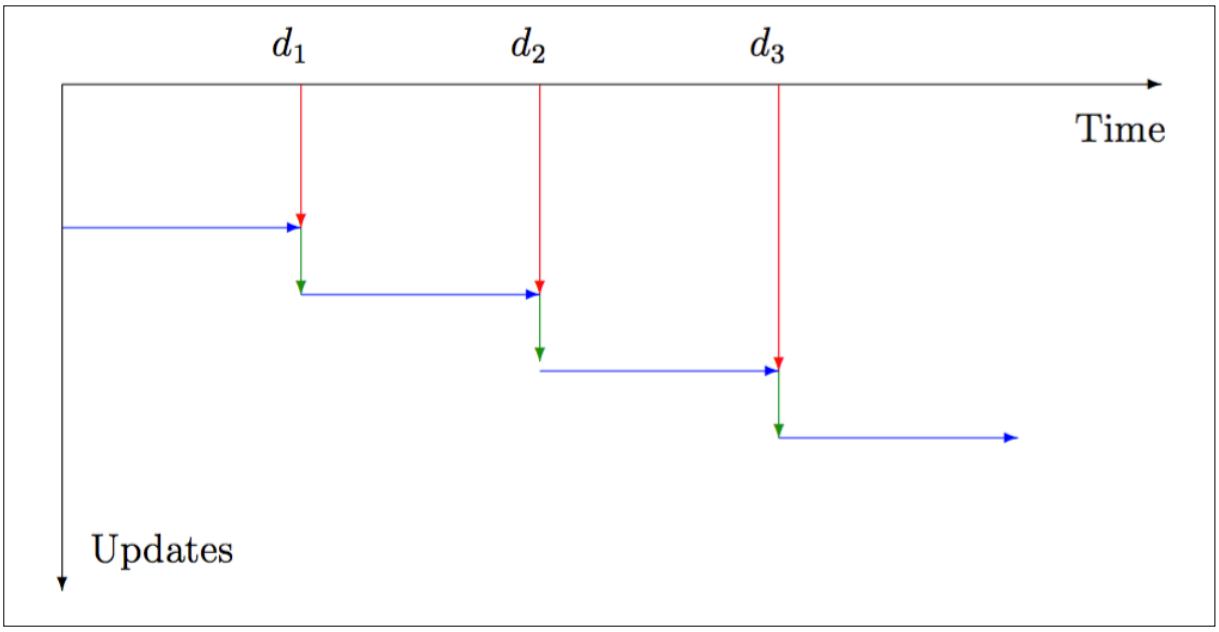

Figure 3.1 Illustration of the updating procedure used in EnKF

From Evensen (2009)

From (3.10) it can be implied that (with an ensemble size close to infinite)

$$\overline{\psi^a} = \overline{\psi^f} + \left(\boldsymbol{C}^e_{\psi\psi}\right)^f \boldsymbol{M}^T \left(\boldsymbol{M}\left(\boldsymbol{C}^e_{\psi\psi}\right)^f \boldsymbol{M}^T + \boldsymbol{C}^e_{\varepsilon\varepsilon}\right)^{-1} \left(\overline{\boldsymbol{d}} - \boldsymbol{M}\overline{\psi^f}\right) \tag{3.11}$$

where $\overline{\boldsymbol{d}} = \boldsymbol{d}$ is the first guess vector of measurements.

The analysed error covariance estimate, $\left(\boldsymbol{C}^e_{\psi\psi}\right)^a$, can then derive from the analysis scheme. Equations (3.10) and (3.11) is used to find

$$\psi^a_j - \overline{\psi^a} = (\boldsymbol{I} - \boldsymbol{K_e M})\left(\psi^f_j - \overline{\psi^f}\right) + \boldsymbol{K_e}\left(\boldsymbol{d_j} - \overline{\boldsymbol{d}}\right) \tag{3.12}$$

where the Kalman gain, $\boldsymbol{K}_e$, is defined as

$$\boldsymbol{K}_e = \left(\boldsymbol{C}^e_{\psi\psi}\right)^f \boldsymbol{M}^T \left(\boldsymbol{M}\left(\boldsymbol{C}^e_{\psi\psi}\right)^f \boldsymbol{M}^T + \boldsymbol{C}^e_{\varepsilon\varepsilon}\right)^{-1} \tag{3.13}$$

The following derivation is then used to obtain the error covariance matrix

$$
\begin{aligned}
\left(\boldsymbol{C}_{\psi\psi}^{e}\right)^{a} &= \overline{(\psi^{a}-\overline{\psi^{a}})(\psi^{a}-\overline{\psi^{a}})^{T}} \\
&= \overline{((\boldsymbol{I}-\boldsymbol{K}_{e}\boldsymbol{M})\left(\psi^{f}-\overline{\psi^{f}}\right)+\boldsymbol{K}_{e}\left(\boldsymbol{d}-\overline{\boldsymbol{d}}\right)(\dots)^{T}} \\
&= (\boldsymbol{I}-\boldsymbol{K}_{e}\boldsymbol{M})\overline{\left(\psi^{f}-\overline{\psi^{f}}\right)\left(\psi^{f}-\overline{\psi^{f}}\right)^{T}}(\boldsymbol{I}-\boldsymbol{K}_{e}\boldsymbol{M})^{T} \\
&+ \boldsymbol{K}_{e}\overline{\left(\boldsymbol{d}-\overline{\boldsymbol{d}}\right)\left(\boldsymbol{d}-\overline{\boldsymbol{d}}\right)^{T}}\boldsymbol{K}_{e}^{T} \\
&= (\boldsymbol{I}-\boldsymbol{K}_{e}\boldsymbol{M})\left(C_{\psi\psi}^{e}\right)^{f}(\boldsymbol{I}-\boldsymbol{M}^{\boldsymbol{T}}\boldsymbol{K}_{\boldsymbol{e}}^{\boldsymbol{T}})+\boldsymbol{K}_{e}\boldsymbol{C}_{\epsilon\epsilon}^{e}\boldsymbol{K}_{e}^{T} \\
&= \left(\boldsymbol{C}_{\psi\psi}^{e}\right)^{f}-\boldsymbol{K}_{e}\boldsymbol{M}\left(\boldsymbol{C}_{\psi\psi}^{e}\right)^{f}-\left(\boldsymbol{C}_{\psi\psi}^{e}\right)^{f}\boldsymbol{M}^{T}\boldsymbol{K}_{e}^{T} \\
&+ \boldsymbol{K}_{e}\left(\boldsymbol{M}\left(\boldsymbol{C}_{\psi\psi}^{e}\right)^{f}\boldsymbol{M}^{T}+\boldsymbol{C}_{\epsilon\epsilon}^{e}\right)\boldsymbol{K}_{e}^{T} \\
&= (\boldsymbol{I}-\boldsymbol{K}_{e}\boldsymbol{M})\left(\boldsymbol{C}_{\psi\psi}^{e}\right)^{f}
\end{aligned}
\tag{3.14}
$$

3.2.4 Discussion

There has been shown that the results of the EnKF are strongly dependent on the prior parameter uncertainty given by the user (Jafarpour and Tarrahi, 2011). If the ranges of the parameters are given too narrow, the EnKF updates will not be able to correct it. Another weakness of the EnKF is the Gaussian approximation used in the update scheme (Skjervheim and Evensen, 2011). When the approximation becomes too severe it can lead to unphysical solutions and numerical instabilities. The EnKF is particularly hard to apply for strongly non-Gaussian problems, like facies estimation and changes to the numerical grid.

3.3 The Ensemble Kalman Smoother

EnKS is an alternative method for data assimilation. It can be regarded as an extension of the EnKF, as it uses the ensemble covariance not only in space, but also backward in time (Evensen, 2009). That means that all previous steps are analysed every time new measurements becomes available. EnKS is otherwise identical to EnKF, an ensemble is used to represent the possible model states, and based on their covariance the ensemble is conditioned every time new measurements is available. The first guess of EnKS is the EnKF solution, and the smoother estimate provides an improvement of this (Evensen and Van Leeuwen, 2000). It is also better suited for handling of non-linear dynamics, which is crucial in reservoir simulation.

The updating procedure of EnKS is illustrated in Figure 3.2. As for EnKF the blue arrows represent the forward ensemble integration, the red arrows are the introduction of measurements, and the green arrows are the EnKF algorithm updates. The magenta arrows represent the backwards in time EnKS updates, which is done after the EnKF update every time measurements are available.

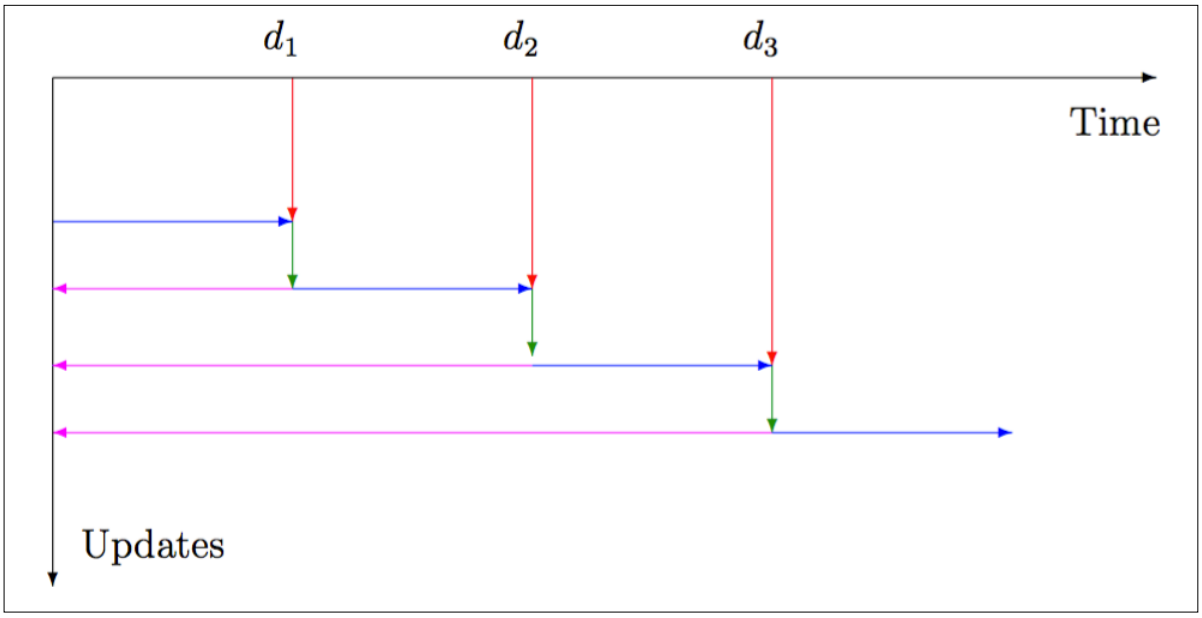

Figure 3.2 Illustration of the updating procedure used in EnKS

From Evensen (2009)

4 ResX

ResX is a commercially available computer assisted history matching and forecasting software built on ensemble based methods (Resoptima, 2017). The software is developed by Resoptima, a company specialized in development of software and consulting regarding reservoir modelling and reservoir management. ResX is a plug-in for Petrel, and is integrated with the reservoir simulators ECLIPSE and INTERSECT, all software by Schlumberger.

4.1 Optimization Algorithm

The data assimilation process used by ResX is the iterative ensemble Kalman smoother (Resoptima, 2017). The method is similar to EnKS, except that each smoother update is split into several iterations. The iterations make it better suited for handling of non-linear dynamics (Ma et al., 2017). In addition, splitting the updating into smaller steps prevents overshooting and limits the adjustments.

4.2 Workflow

A typical ResX workflow is illustrated in Figure 4.1. What software is used during the steps is shown to the right. Petrel is used for initial preparation: defining reservoir uncertainties and making the initial ensemble. The history matching part is conducted by ResX: the ensemble analysis, the ensemble based simulation study and the result analysis.

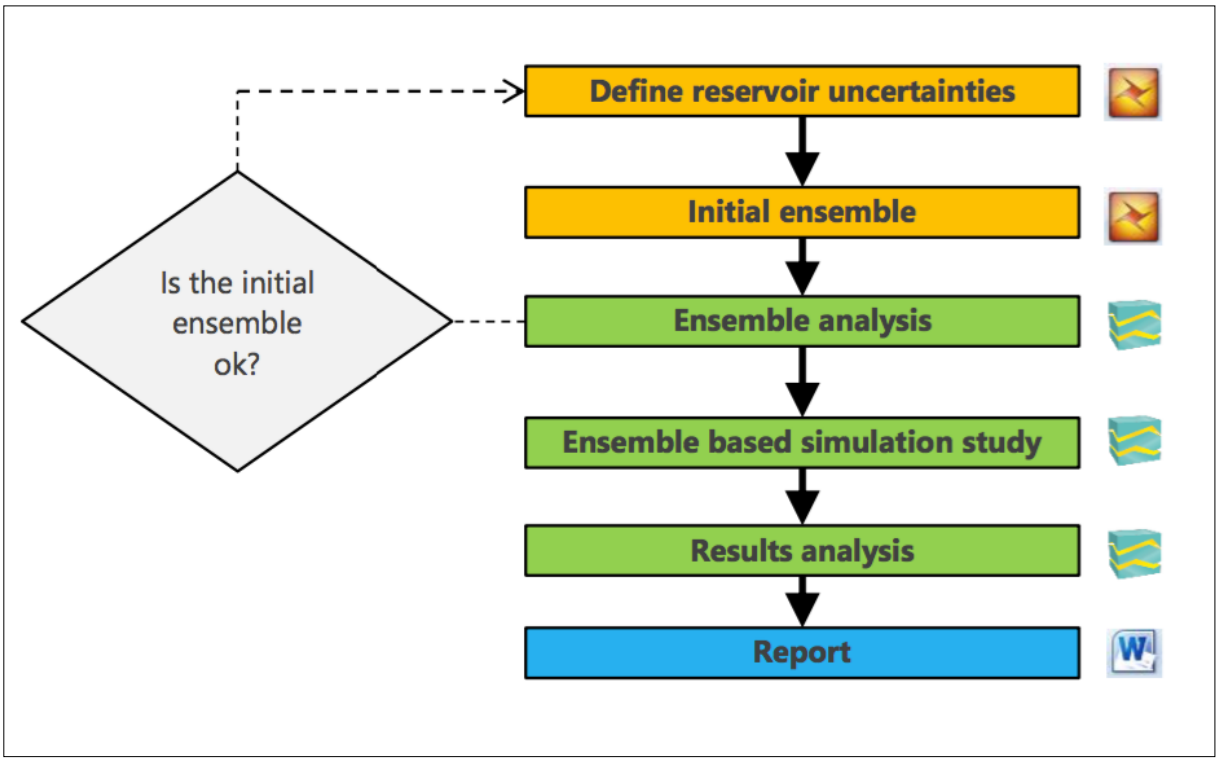

Figure 4.1 ResX workflow

From Resoptima (2016)

4.2.1 Reservoir Uncertainty

The workflow starts out with quantification of the uncertainty of reservoir parameters like porosity, permeability, saturation and fault transmissibility. A distribution and a range is given by the user. The distribution can be based on well logs or input from geology and geophysics, or be set uniform, log-uniform or truncated normal. The ranges dictate the span in properties in the initial ensemble, and must be set sufficiently wide. Then the history matching algorithm is allowed to explore all possibilities from the start of.

4.2.2 Initial Ensemble

Based on well logs, seismic data, core data and reservoir uncertainties, the petrophysical properties are generated on the geological grid. If necessary, the properties are then rescaled to fit the simulation grid, and the initial ensemble of simulation models are created. The possible differences between the simulation models are illustrated in Figure 4.2, where the WCTs of an initial ensemble are plotted. A majority of the ensemble members give values far from the measured water cut, which is seen as dots in the figure. With only a few models with

WCT close to the measured ones, one would probably revise the process behind the initial ensemble. This would potentially ease the work of the AHM algorithm.

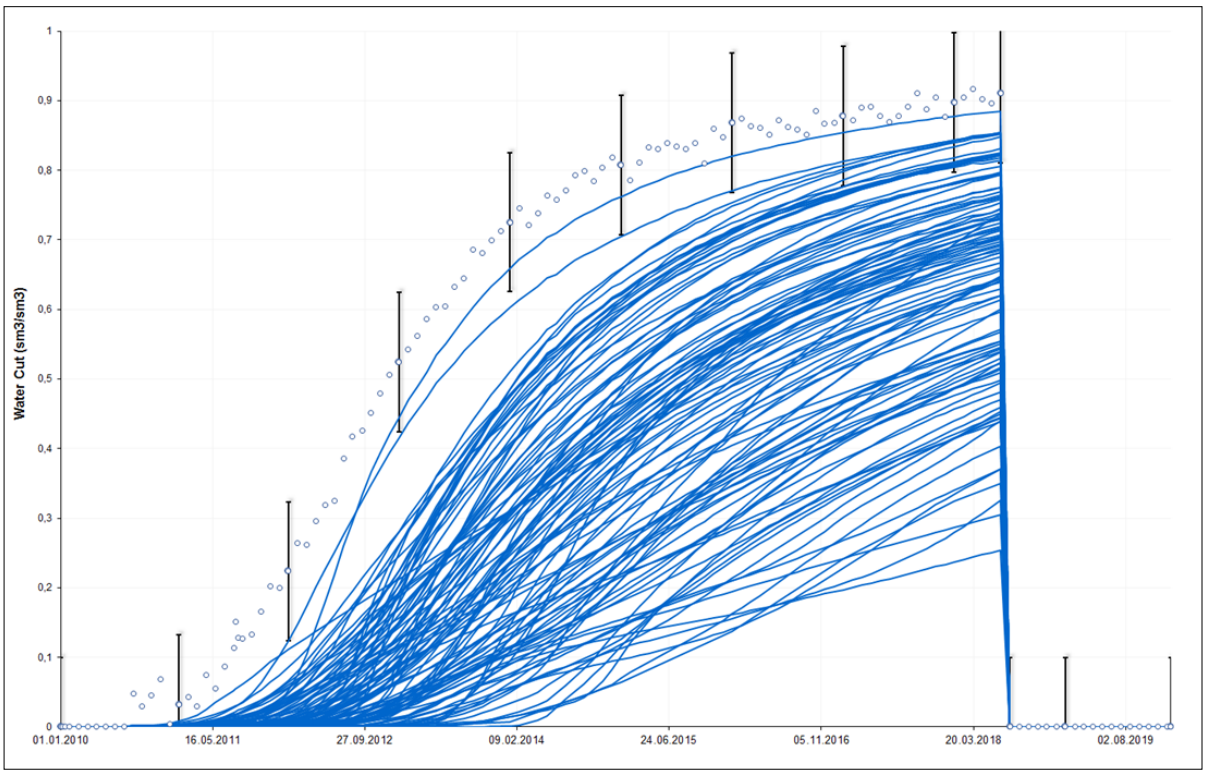

Figure 4.2 Water cuts of an initial ensemble

From Resoptima (2017)

4.2.3 Objective Function

When the initial ensemble is ready, what parameters to include in the objective function need to be defined (Resoptima, 2016). The parameters included in the objection function are later tried matched in the history matching procedure. The tolerance accepted for each source of data is then specified. The tolerances are given either absolute or relative (with a minimum value).

4.2.4 Model Uncertainties

Next step is to define model uncertainties, i.e. to specify the history matching variables. If desired, the static variables, like porosity and permeability, can be held unchanged through the procedure by checking the passthrough box (Resoptima, 2016). The rest of the static, and all the dynamic variables, are each given a minimum and a maximum value, which they must end up between after the history matching. As for the reservoir uncertainties, the model uncertainties need to be set wide, to allow the algorithm to go to extremes if needed.

4.2.5 Localization

To reduce the probability of dubious correlations, one can define what area around a well data from the well will influence. This can also be further refined with respect to what measurements are influencing what variables in what radius. This is the same mechanism used in geostatistics when defining variograms for the different properties modelled.

4.2.6 History Matching Run

When all initial models are constructed and other preparations are made, it is time to condition the model to field and production data. As mentioned, ResX utilizes the iterative ensemble Kalman smoother for assimilation. Since the smoother part of the update is conducted in several steps, the number of iterations needs to be specified. The impact of each step has to be controlled by a data inflation scheme (Resoptima, 2016). The data inflation can be defined in several ways:

- Constant – one coefficient for all iterations
- Linear – linearly decreasing coefficients per iteration
- Logarithmic – logarithmically decreasing coefficients per iteration
- Slope – decreasing coefficients per iteration, controlled by user defined slope

To prevent failed cases from running for hours and hours, a maximum allowed simulation time can also be specified.

Figure 4.3 show water cuts of an ensemble after being conditioned to historical data. Compared to the initial ensemble in Figure 4.2, the water cuts of different ensemble members closer resemble the production data and the variations between them are also greatly reduced.

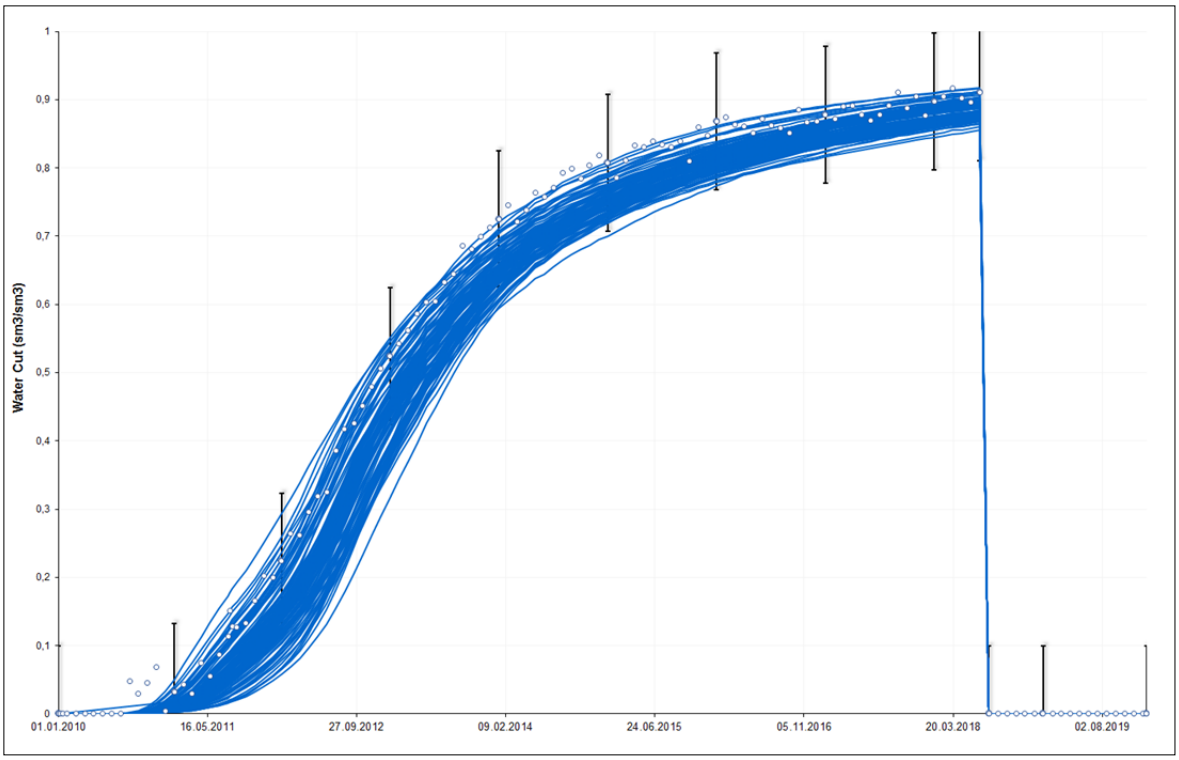

Figure 4.3 Water cuts of a history-matched ensemble

From Resoptima (2017)

4.2.7 Forecasting

The history-matched ensemble is then typically used to perform a prediction study, forecasting future performance of the field. The range in results produced by the models regarding pressure development, oil production, water cut, GOR etc. are used for uncertainty quantification. At this point AHM methods are superior to manual history matching.

Extra runs of creation of initial ensemble and of the history matching are made if the forecasting, or any earlier steps, turns out sub-optimal. The knowledge gained from the process is now used to improve the settings of the next run.

5 Well Testing

Well testing is a type of formation evaluation. As for other forms of formation evaluation, the goal is to obtain knowledge about the reservoir that in turn can be used to improve the geologic model (Jelmert, 2013). Traditional well testing analysis is based on simplified analytical models and graphical technics. The procedure goes as follows: Give the well one or more perturbations in flow, then measure the pressure response at the same well and match the response to a mathematical model (equation or graph). Depending on the rock and fluid, properties the response will vary form well to well. Combining the mathematical model found with known properties (from geology, core analysis, well logging, seismic, etc.), unknown parameters can be determined.

5.1 Productivity of Wells

The productivity index, PI, of a well is defined as the production rate per unit drawdown,

$$PI = \frac{q}{\Delta p} \tag{5.1}$$

PI is thus a measure of how much the well is able to produce with a given pressure difference between the well and the formation. The PI is not necessarily constant.

Assuming a cylinder shaped reservoir with the well in the centre, the flow is controlled by the diffusivity equation (Jelmert, 2013)

$$\frac{1}{r}\frac{\partial}{\partial r}\left(r\frac{\partial p}{\partial r}\right) = \frac{\varphi \mu c_t}{k}\frac{\partial p}{\partial t} \tag{5.2}$$

where r is the radius from the well to a given point, φ is the porosity of the formation, μ is the viscosity of the reservoir fluid, c_t is the total compressibility and k is the permeability.

Steady state flow, where the flow in and out of the drainage area is the same, makes the pressure independent of time. Then the right side of (5.2) becomes zero.

Interference between production wells and geological features can construct no-flow boundaries. They are characterized by no pressure difference perpendicular to the boundary. With a cylindrical geometry, the boundary condition becomes:

$$\frac{\partial p}{\partial r} = 0 \tag{5.3}$$

Under this condition the derivative of pressure, i.e. the depletion rate, becomes constant for all values of r. This pseudo-steady state flow shares important characteristics with steady state.

5.2 Flow Equations

For steady- and pseudo-steady state flow, Darcy's law gives the production rate:

$$q = \frac{2\pi khr}{\mu B}\frac{dp}{dr} \tag{5.4}$$

where h is the height of the formation and B is the formation volume factor. Under the assumptions that the μB-product is independent of pressure, that the flow rate is independent of time and constant pressure boundaries, integration of (5.4) by separation of variables leads to:

$$\Delta p = p_e - p_w = \frac{q\mu B}{2\pi kh} ln\frac{r_e}{r_w} \tag{5.5}$$

where p_e is the pressure at reservoir boundary, p_w is the well pressure, r_e is the external radius of the reservoir and r_w is the radius of the well.

A skin factor S may account for non-ideal conditions:

$$\Delta p = p_e - p_w = \frac{q\mu B}{2\pi kh}\left(ln\frac{r_e}{r_w} + S\right) \tag{5.6}$$

It may be shown that for pseudo-steady state, the equation becomes:

$$\Delta p = \bar{p} - p_w = \frac{q\mu B}{2\pi kh}\left(ln\frac{r_e}{r_w} - \frac{3}{4} + S\right) \tag{5.7}$$

where $\bar{p}$ is the average pressure.

5.3 Productivity Index

The productivity index is a way of quantifying the quality of a well. Equation (5.1) can be rewritten as

$$q = PI \cdot \Delta p \tag{5.8}$$

where the PI is assumed constant. The equation then shows up as a straight line in q vs. Δp plot with slope PI.

The productivity index for steady state flow can be computed from (5.6):

$$PI = \frac{q}{\Delta p} = \frac{2\pi kh}{\mu B\left(ln\frac{r_e}{r_w} + S\right)} \tag{5.9}$$

Similarly for pseudo-steady state flow:

$$PI = \frac{2\pi kh}{\mu B\left(ln\frac{r_e}{r_w} - \frac{3}{4} + S\right)} \tag{5.10}$$

5.4 Discussion

A high production rate is beneficial, as it leads to both higher income and more flexibility in production optimization between wells. The production rate might be increased by increased drawdown by changing the choke opening. However, high drawdown is associated with problems like sand- or water production and gas coning. Thus, the drawdown must be limited. As a result, the production rate of the well is highly dependent on the productivity index.

Equations (5.9) and (5.10) show that the well will produce at a higher rate if the numerator is increased or the denominator is decreased for the relevant PI. Increasing the *kh*-product, the flow capacity, will of course improve the productivity. The flow capacity is hard to change as soon as a well is drilled and completed, lack of productivity might however be traced back to it.

Jelmert (2013) lists these ways to decrease the denominator:

- Reducing the skin factor, *S*. By stimulation project, hydraulic fracturing or acid injection.
- Reducing the external radius, r_e. By infill drilling, the drainage area of each individual well is reduced.
- Increasing the wellbore radius, r_w. This is expensive, or even impossible for deep wells.
- Increasing the effective wellbore radius, r_{we}. By fracturing.
- Decreasing the viscosity, μ. By thermal project.

These variables are normally not part of a history matching, as they are more or less known. The skin factors may however be adjusted when calibrating each well prior to a prediction run (Gjesdal, 2015).

6 Comparing Expected and Observed Communication

In the author's previous work (Hølland, 2016), the early reservoir communication on nine Norwegian continental shelf oil fields was examined. The literature study showed that the reservoir communication experienced during production turned out to be relatively similar to what was expected on most fields. However, some reservoir features stood out as more challenging to model. Faults, calcite-cemented beds and shale layers were often expected to have less sealing capacity than later observed.

6.1 Faults

The uncertainty in the sealing capacity of faults proved to be linked to the lack of dynamic data prior to production. Prediction without dynamic data is hard, as the sealing capacity is governed by a complex function with numerous unknown parameters. The proposed measure to be taken was to drill (and perforate) the production wells through multiple fault blocks in order to be less dependent on open faults. This is not revolutionary, horizontal wells are widely used to cut through several fault blocks.

6.2 Low-Permeable Beds

The sealing capacity of layers with low permeability, like calcareous sandstone and shale, showed to be greatly reliant on the lateral extension and continuity. If the layers are interpreted more as lenses, and not continuous layers, the resulting reservoir simulation will predict fluid flow around them. Thus, the model will not be able to reproduce the sealing nature. Reservoir simulations with reduced communication over the potential barriers was suggested for the planning phase, in order to increase the awareness of what role the barriers might play.

Horizontal wells drilled entirely parallel to the layers will suffer from reduced production if the layers are sealing. A well cutting through the layers will have access to greater volumes in case of barriers.

6.2.1 Depositional Environments

In Hølland (2016) the depositional environments of the reservoir rocks were credited a major role in reservoir communication. Both fluvial and shallow marine deposition can serve as excellent reservoir rock, this is however dependent on a number of factors. To illustrate this, key factors in fluvial deposition are presented in the following.

6.2.1.1 Fluvial Depositions

Fluvial depositions include material deposited either inside the river channel or on the surrounding floodplain. To put it broad, due to velocity differences sand is deposited inside the channel during normal flow, while finer material (collectively called mud) is deposited on the floodplain during flooding. When buried, the sand becomes permeable sandstone and the mud becomes less permeable mudstone.

In flat areas, rivers tend to move sideways by eroding on one side and deposit on the other. The lateral movement last until the channel is abandoned, so called avulsion. The building of deposits from a meandering river is illustrated in Figure 6.1.

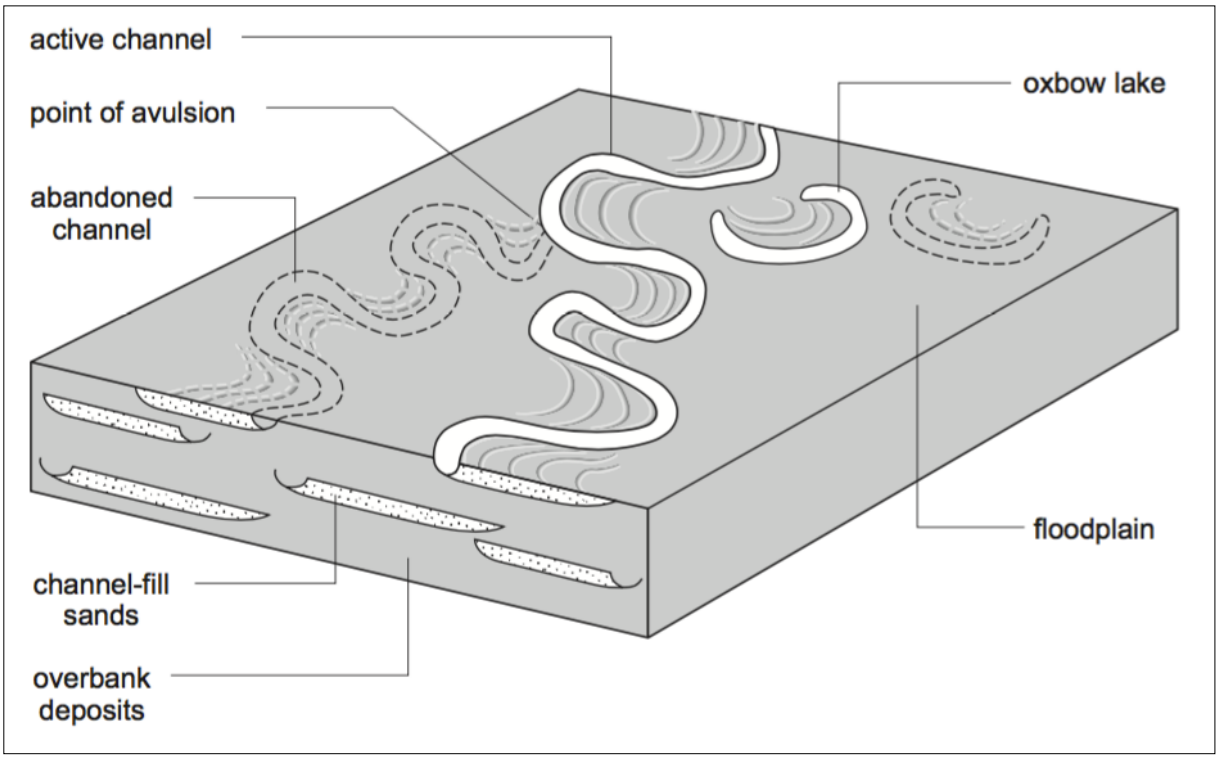

Figure 6.1 Depositional architecture of a meandering river

From Nichols (2009)

The overbank deposits in Figure 6.1 comprise thin sheets of fine sediments resulting from repeated flooding. The rate of subsidence mentioned in Figure 6.2 is a measure of how fast the overbank deposits are building.

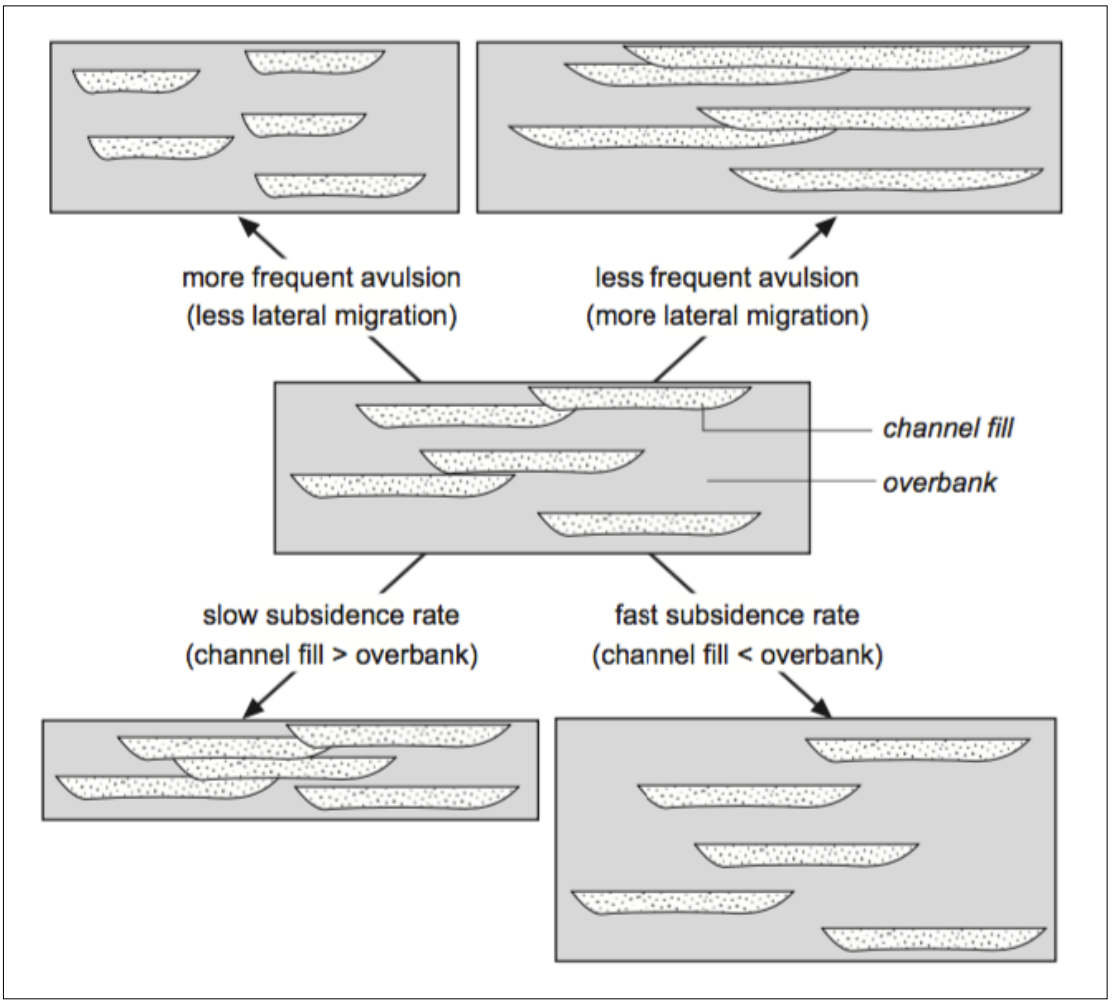

Figure 6.2 Architecture of fluvial deposits

From Nichols (2009)

From Figure 6.2 it is clear that avulsion and subsidence during deposition will strongly influence the fluid flow in a reservoir. If the lateral extent of the sandstone channels is limited by frequent avulsion, neighbouring channels will not be in contact. The mudstone separating them will slow fluid flow and decrease the effective horizontal permeability. The mudstone layer between two vertically adjacent sandstones will impede vertical flow similarly. Hence, fast subsidence rate will be detrimental to effective vertical permeability, as the low-permeability mudstone layers are growing thicker.

In either case, the closer the sand bodies are, the higher the effective permeability. The net to gross ratio (NTG), what share of a limited area that is of high reservoir quality, can thus be indicative of the effective permeability in a fluvial reservoir formation.

7 The Ivar Aasen Field

Ivar Aasen is an oil field in the North Sea operated by Aker BP ASA. It was discovered in 2008 by the 16/1-9 well. The partners of the field, with company shares in brackets, are Statoil ASA (41.4730%), Aker BP ASA (34.7862%), Bayerngas Norge AS (12.3173%), Wintershall Norge AS (6.4615%), VNG Norge AS (3.0230%), Lundin Norway AS (1.3850 %) and OKEA AS (0.5540%). Production of the field started 24.12.2016 (NPD, 2017).

Ivar Aasen is located on the Gudrun Terrace, in the Viking Graben, just west of the Utsira High, as shown in Figure 7.1. This map also shows the positions of the West Cable and Hanz discoveries, which are included in the Ivar Aasen development project (Det norske oljeselskap, 2014). However, due to the fact that they have not been producing during the time frame of the history matching, they are not further considered in this thesis.

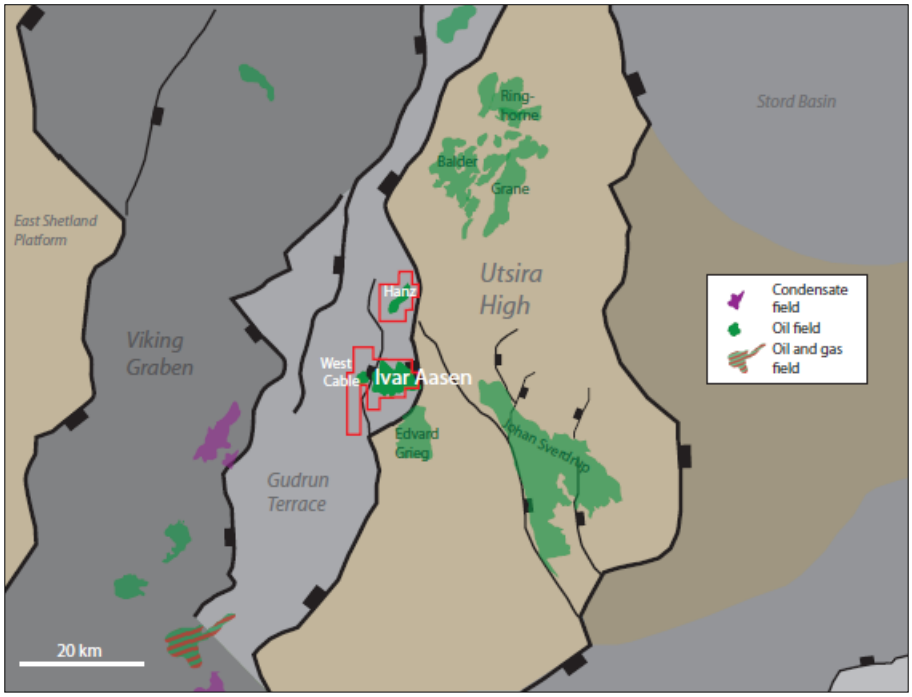

Figure 7.1 Ivar Aasen location

From Det norske oljeselskap (2014)

The Lundin operated Edvard Grieg field is also seen in Figure 7.1. The oil and gas produced from Ivar Aasen are separated from the produced water and sent trough pipelines to Edvard Grieg. There it is mixed with Edvard Grieg oil and gas, processed and further transported.

The main reservoir of Ivar Aasen comprises the Middle Jurassic Vestland Group and the uppermost Triassic Statfjord and Skagerrak formations (Det norske oljeselskap, 2014). The

Vestland Group consists of the Sleipner and Hugin formations. An unconformity makes up the boundary between the Jurrasic and the underlying Triassic Statfjord Group. Further down Skagerrak 2, Wheatering Profile and Skagerrak 1 make up the Hegre Group.

Clean sandstones dominate the Vestland Group. The sands of the Triassic reservoir zones have higher levels of shaliness, which reduces the reservoir quality (Det norske oljeselskap, 2014). The Heather formation serves as the cap rock of the reservoir.

7.1 Sedimentology and Depositional Models

Next follows a description of the sedimentology of Ivar Aasen. The subchapter is written based on Det norske oljeselskap (2014)

7.1.1 Triassic Reservoir Zones

Throughout the late Triassic the larger Viking Graben area is thought to have been dominated by extensive continental basins with fluvial and alluvial deposition. Tectonic events of varying magnitude influenced the deposition. Well logs and seismic indicates relatively uniform thicknesses on the Ivar Aasen structure.

Skagerrak 1 is the deepest reservoir zone of Ivar Aasen. It consists of mixed sand- and mudstone, dominated by mudstone. The sand is either dispersed in the mud or situated in cm-thin laminated or slightly rippled layers. Clasts of calcium carbonate and cracks filled with mudstone are observed in cores from the zone. The listed features indicate a poorly drained floodplain that has later been overgrown. The consistently high mud content throughout the Skagerrak 1 zone makes it almost free of net sand.

The Weathering Profile zone is dominated by reddish-brown sandstone with chaotic and disturbed appearance. Thin calcrete layers, carbonate-cemented spots, caliche clasts and sand-filled fractures are found throughout the zone. A 25 cm thick calcrete layer marks the top of the zone.

Skagerrak 2 is dominated by several meters thick intervals of clean to slightly shaly sandstone. The sandstones are typically fine-grained, with up to pebble-sized mud clasts. Inside the sand intervals there also exist caliche conglomerate beds. Between the sands there is mud-dominated beds. The depositional system in Skagerrak 2 is believed to be continental fluvial and lake or flood basin. The sandstone intervals are therefore assigned to fluvial channels, sand deposited inside the river channels.

The lower part of Statfjord, the Statfjord 1 zone, is similar to the mud-dominated beds the underlying Skagerrak 2. However, the good reservoir sands found there are not present in Statfjord 1. An erosive surface marks the move into the overlying Statfjord 2 zone. It consists of clean, cross-bedded, medium to coarse-grained sandstone. The caliches (and other features) found in the sands of Skagerrak 2 are not present. The bottom of several meters thick, dark shale beds and mudstone/sandstone beds indicates the base of Statfjord 3. The Statfjord 1, 2 and 3 are now merged into one Statfjord reservoir zone.

7.1.2 Latest Triassic to Early Jurassic Development

A doming event (regional uplifting) in the North Sea area facilitated removal of the uppermost Triassic through Lower Jurassic strata by erosion. However, the degree of erosion varies vastly throughout the Ivar Aasen field, leading to different formations, and formation thicknesses, being present in the different wells. The magnitude of the hiatus, about 30 million years of missing sediments, is illustrated in Figure 7.2.

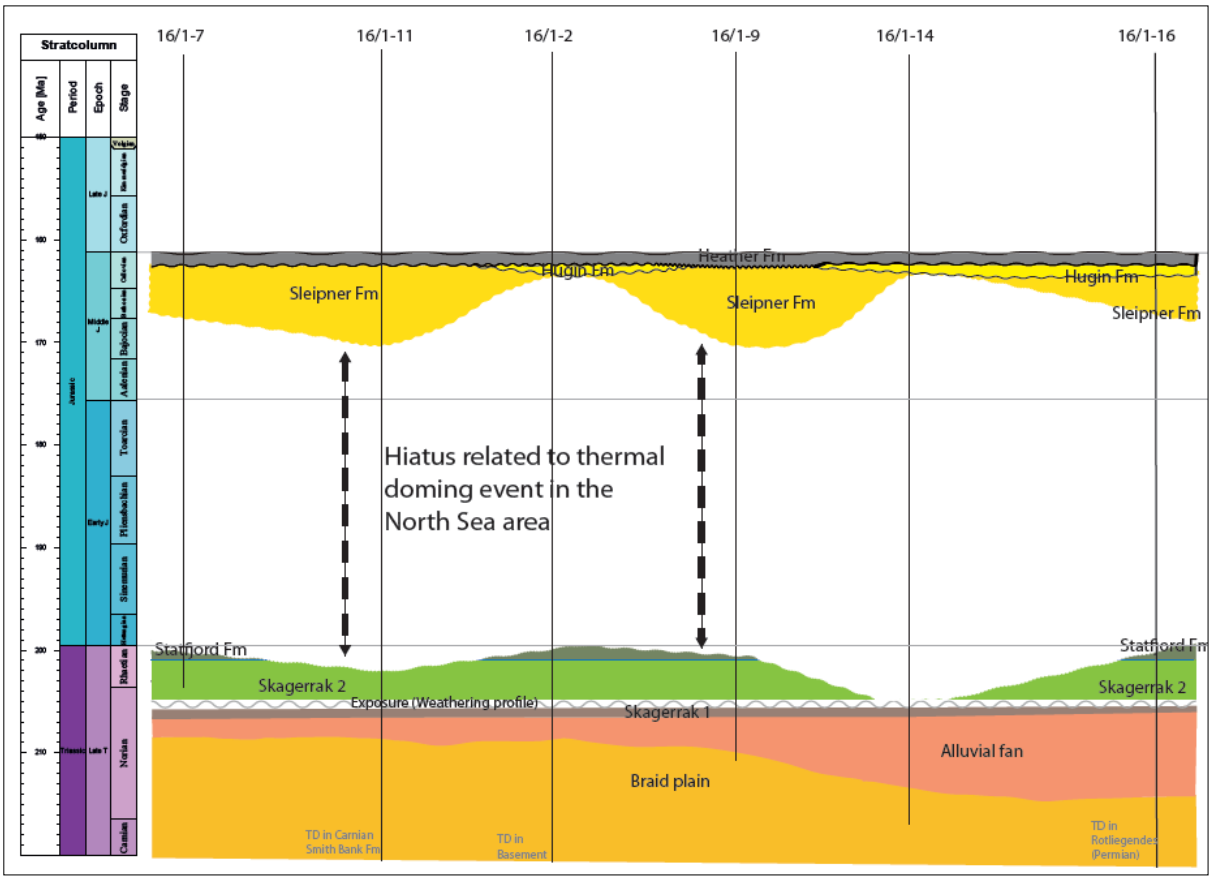

Figure 7.2 Stratigraphic chart

From Det norske oljeselskap (2014)

7.1.3 Middle Jurassic Reservoir Zones

The subdivision of the Vestland Group into the Sleipner and Hugin formations is uncertain unless cores can establish the sedimentological characteristics, as the log patterns are ambiguous. The similarity between terrestrial Sleipner and shallow marine Hugin is explained by marine re-working of terrestrial deposits. The variation in Sleipner and Hugin thicknesses throughout the field is attached to the concept of reworking of Sleipner sediments during deposition of Hugin.

The characteristics of the Sleipner formation deviate between the eastern and western part. In the west, the formation consists of conglomeratic sandstones. The grain size ranges from fine-grained to pebbles, but is dominated by coarse- to very coarse-grained. Cross bedding is the dominant structure, with an average bed set height of 0.4 m. Sands with no particular structure is also present. The most striking heterogeneity in the formation is set up by contrasts in grain size and sorting between bed sets. Eroded boundaries are also common. However, the lack of mud laminae should minimize the permeability anisotropy set up by cross bedding. The

depositional environment is interpreted as continental fluvial succession. The coarser sands stems from braid bars formed during high discharge, while the finer sands were deposited intra-channel during low discharge.

The eastern Sleipner deposits are slightly different from western ones. Here the sandstones are dominated by medium- to coarse-grained. However, the entire range from very fine- to coarse-grained are found, grading into gravelly conglomerates in places. The sands typically become finer moving upwards on a dm- to m-scale. The formation contains large quantities of organic debris, coal and organic-rich clay clasts. Cross stratification and current ripples are the most common sedimentary structures. In places these structures are coated with disturbed mud laminae. The mud laminae are normally below 1 cm thick, compared to the bed set average height of 25 cm. The mud lamination, in addition to grain size differences set up by sorting, represent the main sources of heterogeneity. With relative high permeability sandstone layers adjacent to the mud laminae, the permeability anisotropy will be considerable. The high-energy fluvial system interpreted in the west is substituted by low-lying coastal plain. The eastern area core studied is assumed to represent distributary channels from the coastal plain.

The examined core from the Hugin formation consists of sandstones. The sandstones have grain sizes of medium to coarse, are poorly to moderately sorted and contain observable fractions of dispersed mud. Chaotic appearance and little visible stratification are interpreted to be associated with high degree of reworking by animals. Abundant shell fragments has facilitated considerable carbonate cementation in places. Dispersed organic debris and mud rip-up flakes are also present. The shell debris, and the type of reworking seen, point towards shallow marine origin of the Hugin formation. The lack of wave-generated sedimentary structures is assumed to be caused by water depth below wave base and/or sheltered conditions.

7.2 Faults

The Ivar Aasen Reservoir Management Plan 2014 (Det norske oljeselskap, 2014) states that more faults had been identified since the Plan for Development and Operation (PDO) was submitted in 2012. The adding of faults has continued ever since, as new wells are drilled and the seismic surveys are reprocessed and reinterpreted. This was anticipated in the Reservoir Management Plan, where presence of sub seismic faults (faults too small to be detected by seismic) across the field was assumed.

Back in 2014, the sealing capacity of the faults was uncertain. At production start this was still not determined. By then the base case reservoir simulation model used a common transmissibility multiplier (Tx) of 0.01 to restrict the flow across all faults present in the model. For the ECLIPSE reservoir simulator this corresponds to reducing the effective permeability between two neighbouring grid blocks on each side of a fault by a factor 100 (Schlumberger, 2015). The remaining characteristics used to compute the effective permeability are the assigned permeabilities of the grid blocks, in addition to geometric properties. The reductions in permeability across the faults are made to account for the uncertainty, and make a more robust model.

7.3 Reservoir Fluids

The fluid properties of the Ivar Aasen reservoir are shown in Table 7.1 (Det norske oljeselskap, 2014).

Table 7.1 Ivar Aasen main fluid properties

Parameter	Value	Unit
Reference pressure	245	bar @ GOC
Reservoir temperature	98	°C
Live oil density	0.69	g/cc
Live gas density	0.21	g/cc
Live water density	1.03	g/cc
Live oil viscosity	0.319	cp
Live gas viscosity	0.025	cp
Live water density	0.365	cp
Oil formation volume factor, Bo	1.54	
Gas formation volume factor, Bg	0.0048	

7.4 Drainage Strategy

Depletion for three months and then full pressure maintenance with water injection is selected as drainage strategy for Ivar Aasen (Det norske oljeselskap, 2014). It is thought to give the most robust drainage. Gas injection on the other hand is not expected to increase the reserves enough to compensate for the investment required and the deferred gas sales. The limited upside is related to the flat structure and the heterogeneous sands of the field. There is expected limited pressure support from the relatively small gas cap and the small aquifer. A mobility ratio of water to oil of 0.66, which gives a stable flooding front, is favourable when water flooding is used.

In order to produce from a higher number of fault blocks the production wells are drilled horizontally. Perforation of several fault blocks reduces the risk of the wells draining limited volumes.

7.4.1 Production and Injection Wells

The six horizontal producers of Ivar Aasen are spun out like a fan, with six vertical water injectors placed between them, but farther out to the edges of the field (Figure 7.3). With this configuration the injectors are planned to push the oil towards the producers, and towards the middle of the field. The production wells are completed with inflow control devices (ICD) and swell packs.

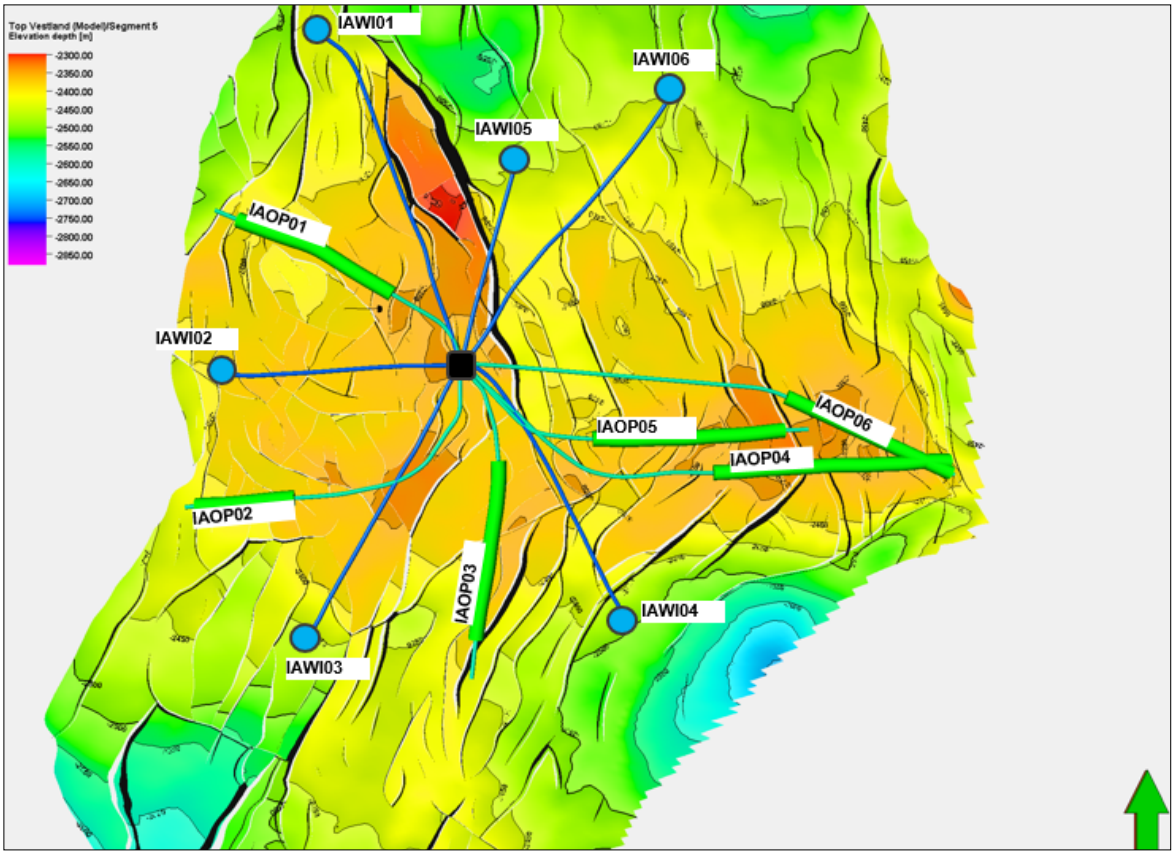

Figure 7.3 Ivar Aasen wells

7.4.1.1 Producers

All production well except IAOP06 (which is not yet drilled) started production during December and January winter 2016/17.

7.4.1.1.1 IAOP01

The horizontal production well IAOP01 started production 24.12.2016. The following Figure 7.4 and Figure 7.5 show cross sections of the well with fluids and formations, respectively.

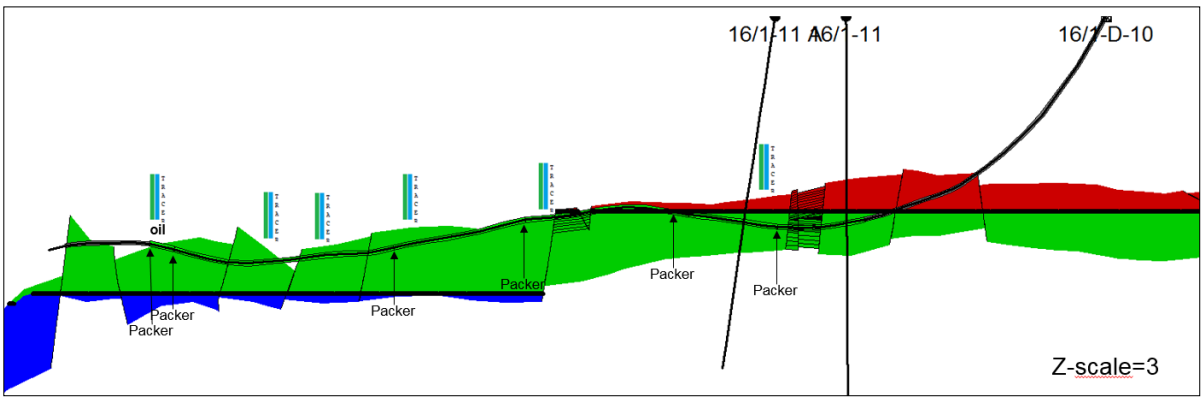

Figure 7.4 IAOP01 cross section with fluids

Gas: Red. Oil: Green. Water: Blue.

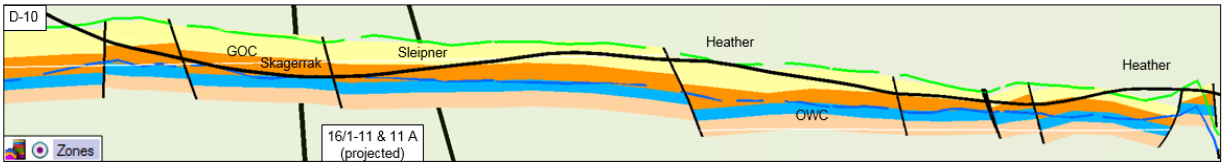

Figure 7.5 IAOP01 cross section with formations

Hugin: Yellow. Sleipner: Light yellow. Statfjord: Grey. Skagerrak 2: Orange. Weathering profile: Blue. Skagerrak 1: Pink. Alluvial fan: Brown.

7.4.1.1.2 IAOP02

The horizontal production well IAOP02 started production 19.01.2017. The following Figure 7.6 and Figure 7.7 show cross sections of the well with fluids and formations, respectively.

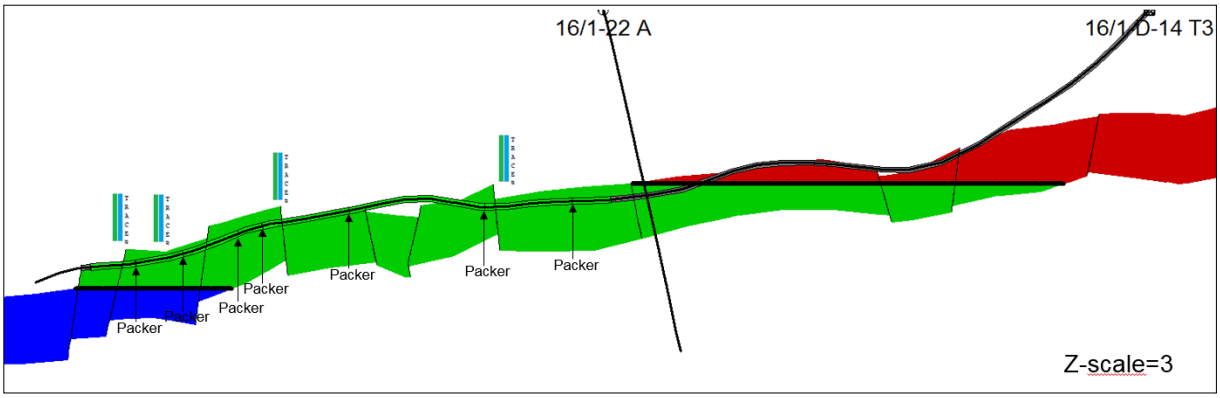

Figure 7.6 IAOP02 cross section with fluids

Gas: Red. Oil: Green. Water: Blue.

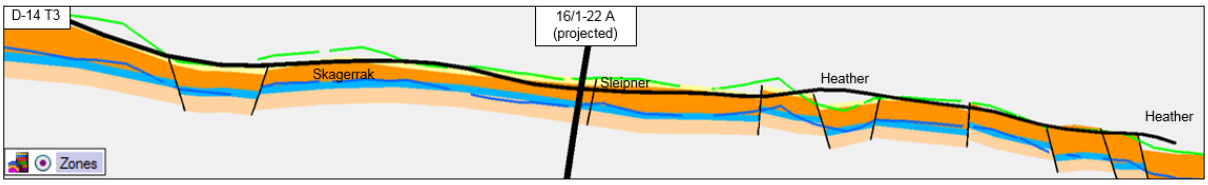

Figure 7.7 IAOP02 cross section with formations

Hugin: Yellow. Sleipner: Light yellow. Statfjord: Grey. Skagerrak 2: Orange. Weathering profile: Blue. Skagerrak 1: Pink. Alluvial fan: Brown.

7.4.1.1.3 IAOP03

The horizontal production well IAOP03 started production 04.01.2017. The following Figure 7.8 and Figure 7.9 show cross sections of the well with fluids and formations, respectively.

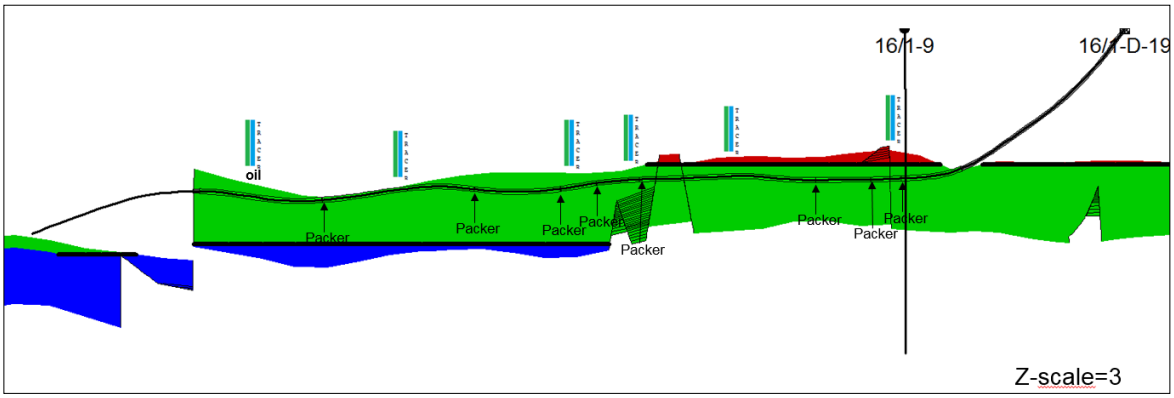

Figure 7.8 IAOP03 cross section with fluids

Gas: Red. Oil: Green. Water: Blue.

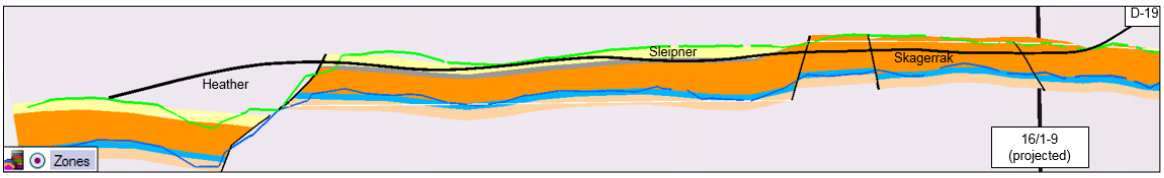

Figure 7.9 IAOP03 cross section with formations

Hugin: Yellow. Sleipner: Light yellow. Statfjord: Grey. Skagerrak 2: Orange. Weathering profile: Blue. Skagerrak 1: Pink. Alluvial fan: Brown.

7.4.1.1.4 IAOP04

The horizontal production well IAOP04 started production 30.12.2017. The following Figure 7.10 and Figure 7.11 show cross sections of the well with fluids and formations, respectively. Unfortunately, the 500 m toe section of the well has not been able to produce at all. The interval starts at the third last packer, just right of the vertical line marked 16/1-16 in Figure 7.10. As seen in the figure the well is here placed well below the gas oil contact (GOC).

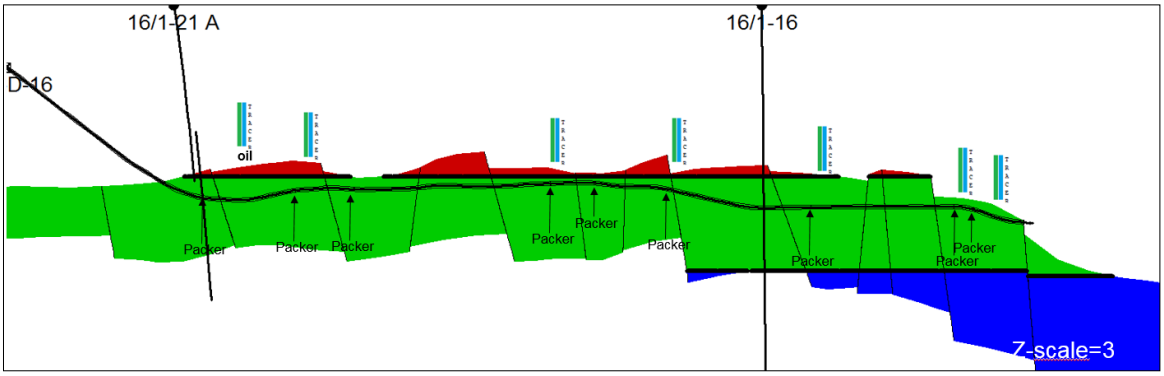

Figure 7.10 IAOP04 cross section with fluids

Gas: Red. Oil: Green. Water: Blue.

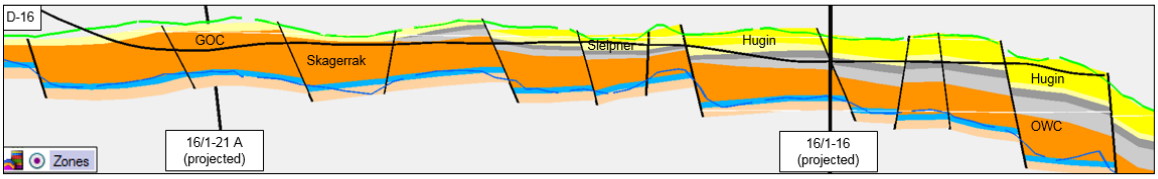

Figure 7.11 IAOP04 cross section with formations

Hugin: Yellow. Sleipner: Light yellow. Statfjord: Grey. Skagerrak 2: Orange. Weathering profile: Blue. Skagerrak 1: Pink. Alluvial fan: Brown.

7.4.1.1.5 IAOP05

The horizontal production well IAOP05 started production 28.01.2017. The following Figure 7.12 and Figure 7.13 show cross sections of the well with fluids and formations, respectively.

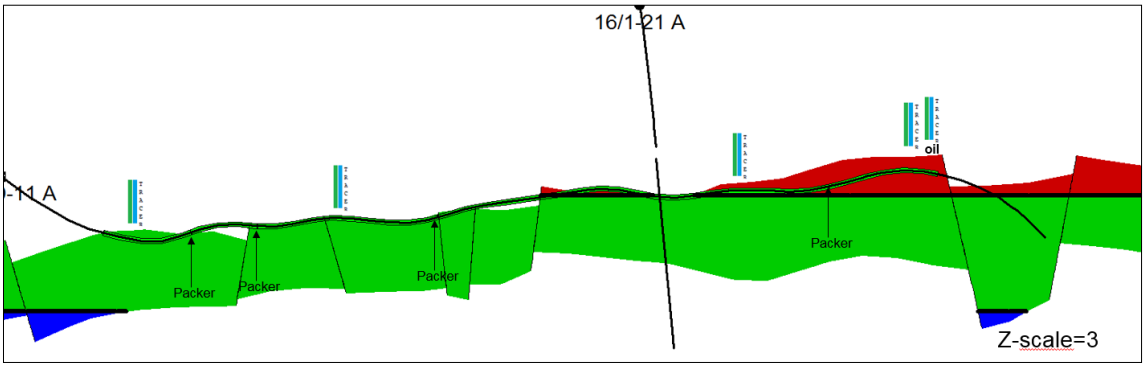

Figure 7.12 IAOP05 cross section with fluids

Gas: Red. Oil: Green. Water: Blue.

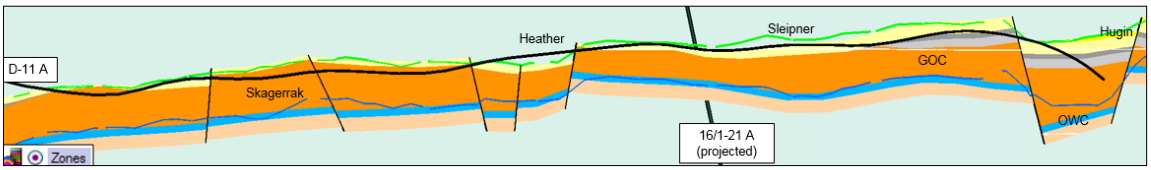

Figure 7.13 IAOP05 cross section with formations

Hugin: Yellow. Sleipner: Light yellow. Statfjord: Grey. Skagerrak 2: Orange. Weathering profile: Blue. Skagerrak 1: Pink. Alluvial fan: Brown.

7.4.1.1.6 IAOP06

The horizontal production well IAOP06 is planned drilled later in 2017. Figure 7.14 shows the expected cross sections of the well with formations.

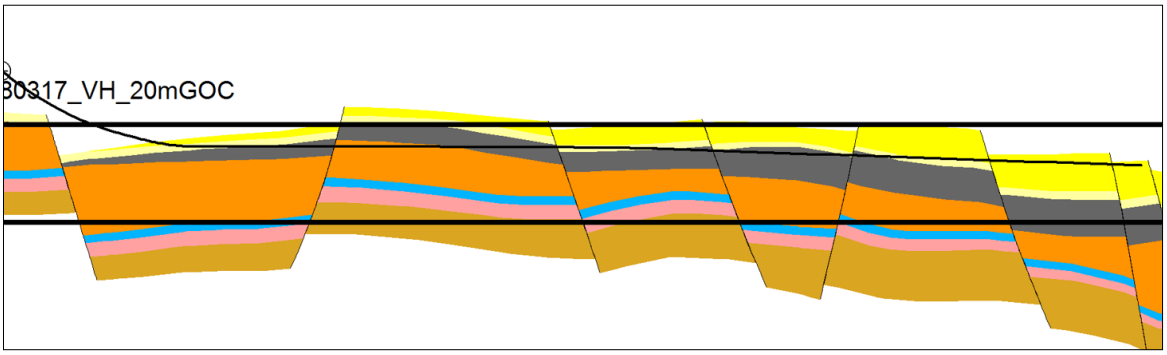

Figure 7.14 IAOP06 cross section with formations

Hugin: Yellow. Sleipner: Light yellow. Statfjord: Grey. Skagerrak 2: Orange. Weathering profile: Blue. Skagerrak 1: Pink. Alluvial fan: Brown.

7.4.1.2 Injectors

Water injection on the Ivar Aasen field started May 2017. All the injectors are (or are planned) perforated in Skagerrak 2. As mentioned in chapter 7.1.1, the Skagerrak 2 zone is believed to originate from fluvial deposition. The efficiency of injection will thus depend on the configuration of the sandstone channels surrounding the wells. As discussed in chapter 6.2.1.1, the NTG can indicate if the sand bodies are connected or not in a fluvial deposition like Skagerrak 2.

7.4.1.2.1 IAWI01

The modelled permeability and NTG prior to drilling of IAWI01 are shown in Figure 7.15. High NTG is expected at the top of Skagerrak 2, where the well is perforated. However, the NTG is decreasing deeper in the zone.

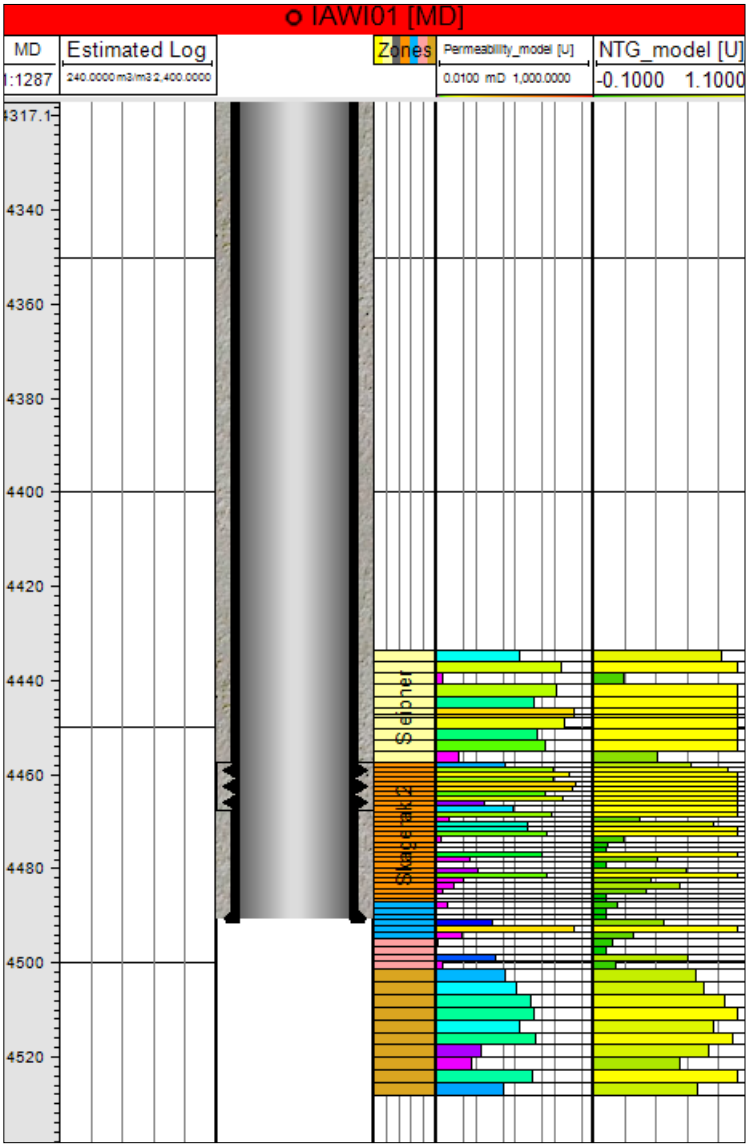

Figure 7.15 IAWI01 permeability and NTG

Hugin: Yellow. Sleipner: Light yellow. Statfjord: Grey. Skagerrak 2: Orange. Weathering profile: Blue. Skagerrak 1: Pink. Alluvial fan: Brown.

7.4.1.2.2 IAWI02

A number of logs from IAWI02 are shown in Figure 7.16. In the log to the far right, the yellow colour indicates NTG. Large parts of Skagerrak 2 show high NTG, but less at the top and at the bottom.

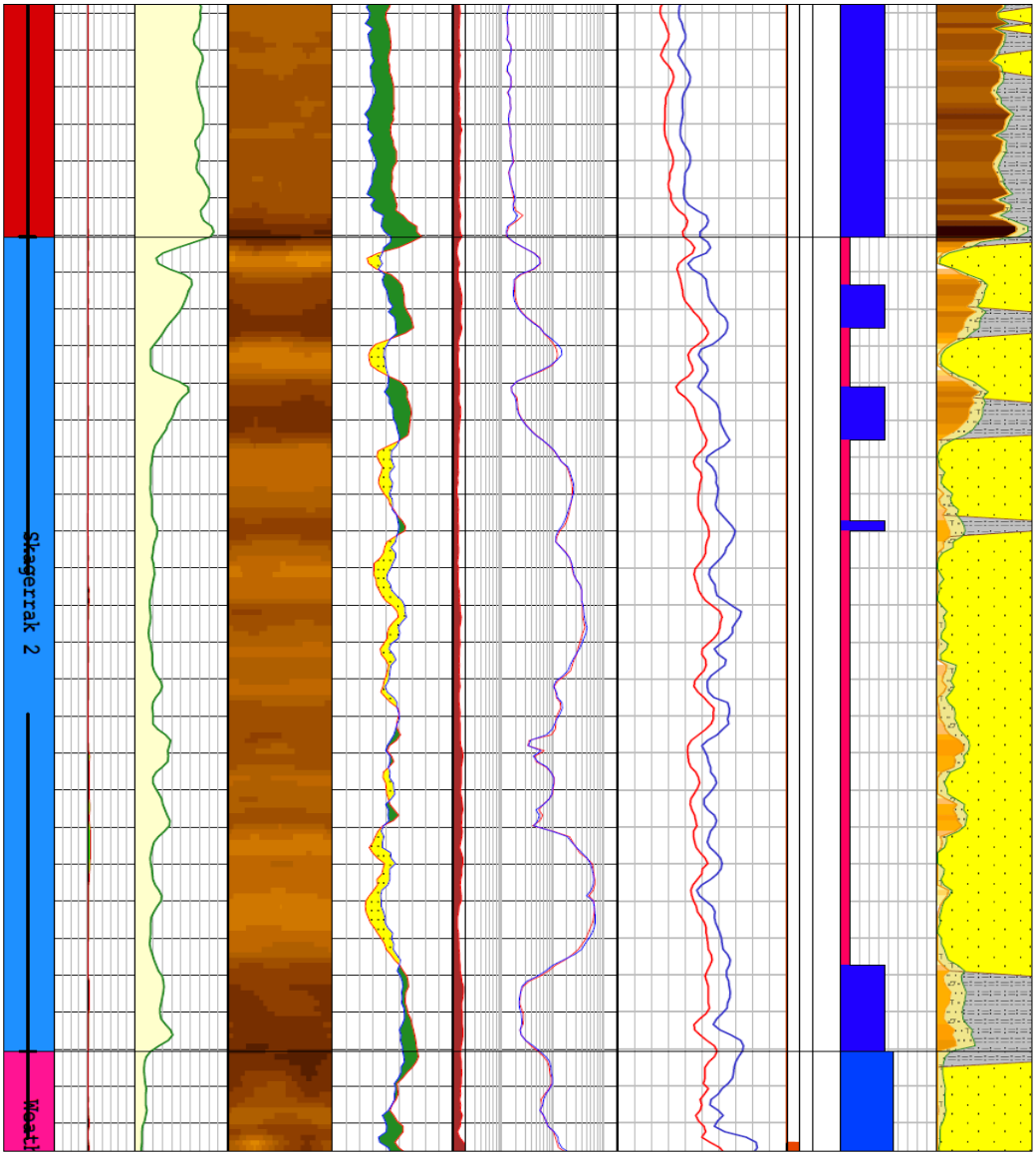

Figure 7.16 IAWI02 well logs

Heather: Red. Hugin: Yellow. Sleipner: Purple. Statfjord: Light blue. Skagerrak 2: Dark blue. Weathering profile: Pink. Skagerrak 1: Green.

7.4.1.2.3 IAWI03

A number of logs from IAWI03 are shown in Figure 7.17. In the log to the far right, the yellow colour indicates NTG. In Skagerrak 2, the NTG are high only in places.

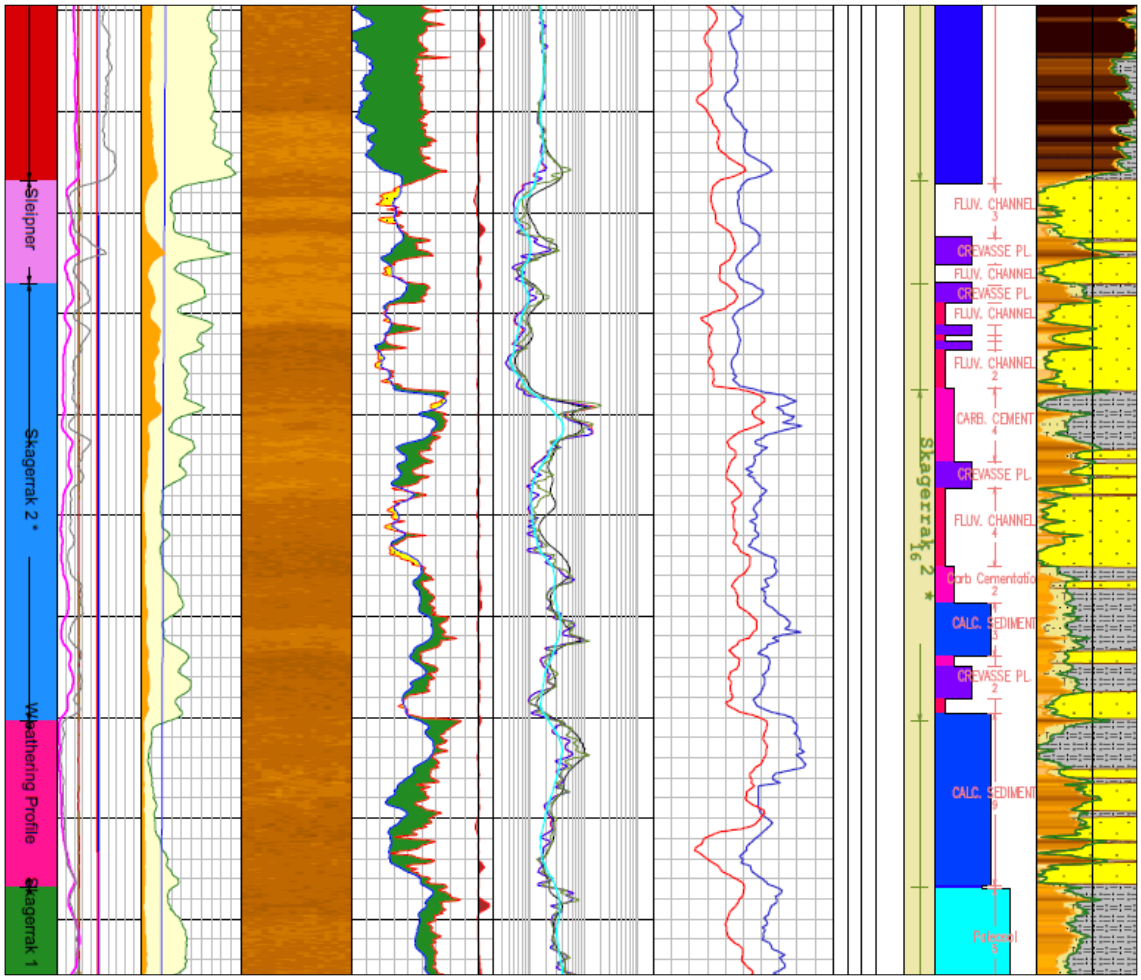

Figure 7.17 IAWI03 well logs

Heather: Red. Hugin: Yellow. Sleipner: Purple. Statfjord: Light blue. Skagerrak 2: Dark blue. Weathering profile: Pink. Skagerrak 1: Green.

7.4.1.2.4 IAWI04

A number of logs from IAWI04 are shown in Figure 7.18. In the log to the far right, the yellow colour indicates NTG. Skagerrak 2 has generally low NTG, it is however higher in the deepest part, where the well is perforated.

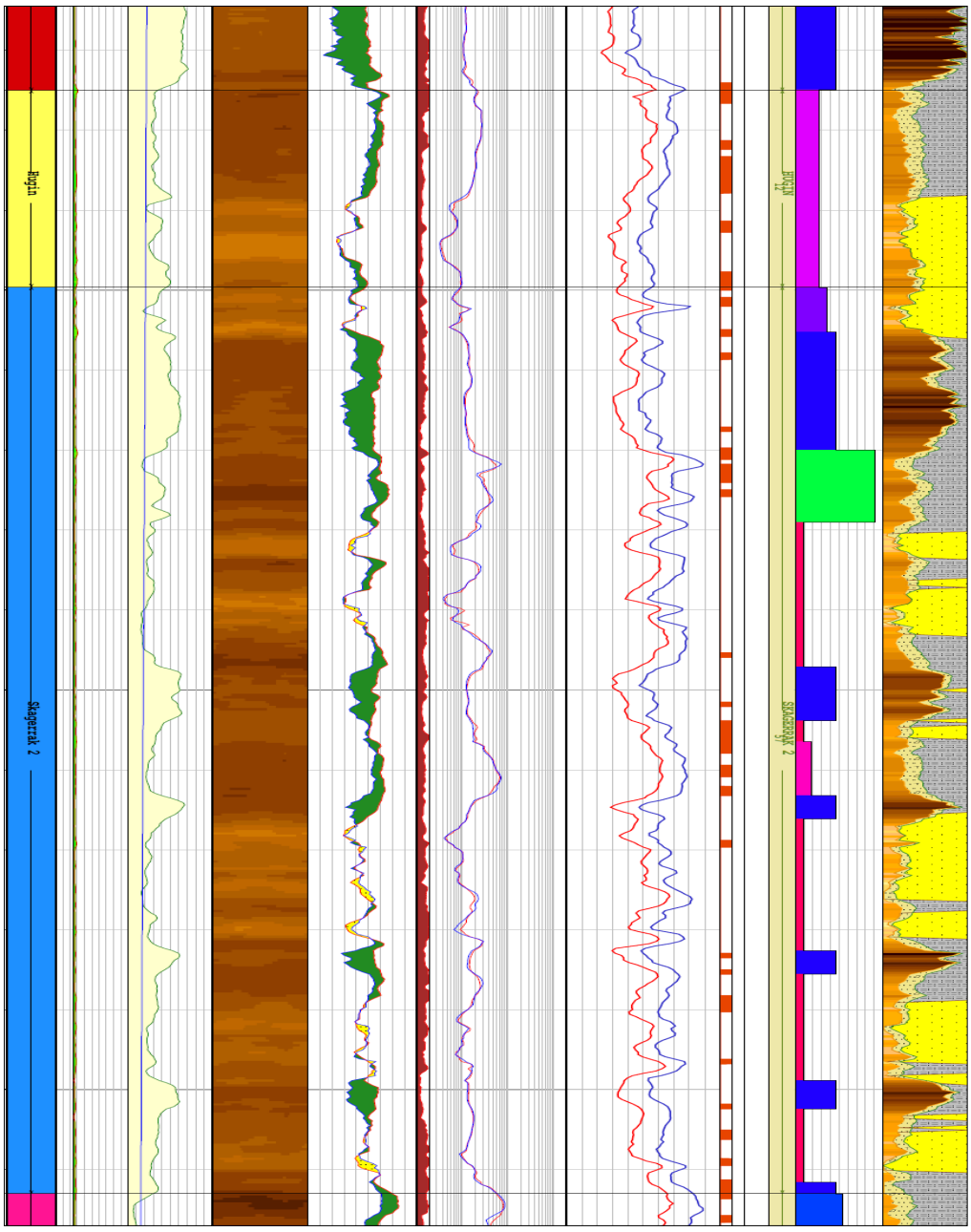

Figure 7.18 IAWI04 well logs

Heather: Red. Hugin: Yellow. Sleipner: Purple. Statfjord: Light blue. Skagerrak 2: Dark blue. Weathering profile: Pink. Skagerrak 1: Green.

7.4.1.2.5 IAWI05

The modelled permeability and NTG prior to drilling of IAWI05 are shown in Figure 7.19. The NTG is expected to be low Skagerrak 2, where the well is planed to be perforated.

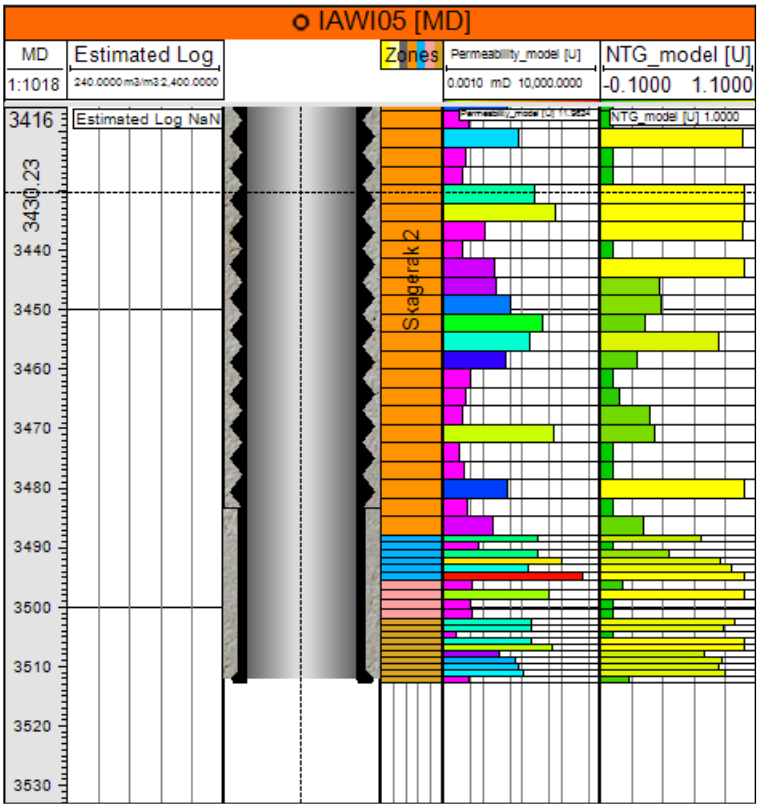

Figure 7.19 IAWI05 permeability and NTG models

Hugin: Yellow. Sleipner: Light yellow. Statfjord: Grey. Skagerrak 2: Orange. Weathering profile: Blue. Skagerrak 1: Pink. Alluvial fan: Brown.

7.4.1.2.6 IAWI06

A number of logs from IAWI06 are shown in Figure 7.20. In the log to the far right, the yellow colour indicates NTG. The NTG is generally low in Skagerrak 2.

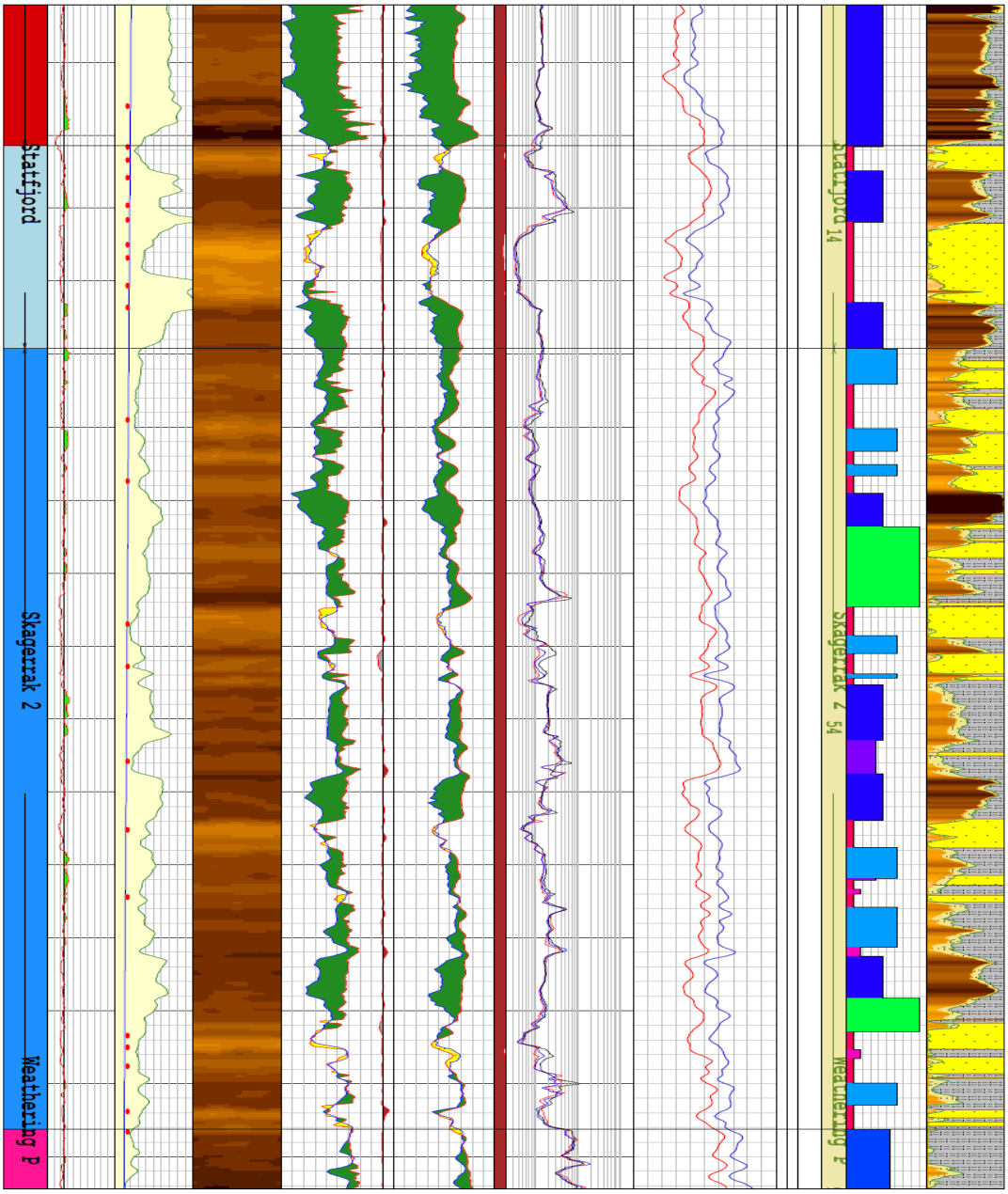

Figure 7.20 IAWI06 well logs

Heather: Red. Hugin: Yellow. Sleipner: Purple. Statfjord: Light blue. Skagerrak 2: Dark blue. Weathering profile: Pink. Skagerrak 1: Green.

8 Manual History Matching

The oil production of the Ivar Aasen field started 24.12.16. The time period tried matched in the manual history match is from production start to 14.03.17. To get familiar with the model and the real reservoir responses, some testing was done prior, with down to a month of production history available.

The ECLIPSE 100 simulator performed the reservoir simulations. In order to launch the simulations, and to compare the observed and simulated responses, the Petrel software was used. Both ECLIPSE and Petrel are Schlumberger products.

Later RFT surveys from the drilling of two new injectors, and an AHM study, performed by the Ivar Aasen subsurface team of Aker BP, with support from Resoptima, became available.

8.1 Observed Data

Oil- and gas production rates and shut-in pressures at the producers, and shut-in pressures at the injectors are used to calibrate the reservoir simulation model in this manual history matching.

8.1.1 Production Rates

The oil- and gas production rates of the field are continuously monitored, and stored for later use. However, the production rates are allocated based on choke openings, and are inherently uncertain. Such sources of error must be kept in mind during history matching. For this work daily average rates are downloaded and imported into Petrel.

In order to launch an ECLIPSE simulation from Petrel, a simulation case, containing all the needed information, has to be defined. This includes the simulation model, adjustments of the model, and a development strategy. The development strategy can be made as history or prediction type, including historical production data or planned future production rates respectively. The simulations of this history matching are run with history type development strategies, based on the imported daily averaged production rates. The maximum step size of the simulations is therefore set to one day to capture the variations from day to day.

In addition, the oil production rates alongside the gas production rates have been used to calculate the gas/oil ratios (GOR) of the producers. These have been compared with the simulated GORs, to confirm the realism in the adjustments done to the reservoir model.

8.1.2 Shut-In Pressures

The shut-in pressures better represent the formation pressure compared to the flowing bottomhole pressure measured during production. The reason for this is the pressure drop related to the flow through the ICD nozzles between the formation and the well.

During the first few months of production of the Ivar Aasen field there have frequently been shut-ins of one or more production wells. These shut-ins have persistently been used to measure the pressure at downhole gauges in the wells. The gauges are placed some distance above the top of the perforated interval of the wells. Thus, the pressures are corrected according to the fluid column in order to be able to compare them with the simulated pressures. This conversion adds uncertainty. However, the uncertainty should be limited, as the distance and density of the fluid column are known.

Three injection wells were drilled in advance of the production start. This was partly done to be able to measure the pressure at locations some distance away from the producer, and make interpretations about greater areas of the reservoir based on it. The fact that the injectors were not injecting the first few months was important. Then accurate measurements of the formation depletion could be done. If they were injecting, shut-ins would be required to get pressure measurements, since over-pressure is needed to push water into the formation. In addition, if the injectors were able to maintain the pressure at the producers (as they are supposed to do) there would be no depletion to match. Thus, only reservoir communication dramatically worse than expected, i.e. very limited communication between injector and producer, would be detected.

8.2 Matching Procedure

The stage that a field is currently at dictates the structure of a history matching. Recalling the stepwise approach to history matching presented in chapter 2, the first step is matching of average reservoir pressure. The reservoir average is hard to determine in the early phase, with few pressure observation points, and little knowledge about what areas are subject to depletion. Next is matching of RFT pressures. The RFT surveys of the two injection wells became available after the matching of production data was completed. However, the RFT surveys are used to add reservoir knowledge, and to comment on the results from the matching of production data.

Further, the reservoir average GOR and water cut (WCT) are matched. No water produced during the matching period made WCT a hard parameter to match. However, gas is coning

down towards the producers from production start of, since the wells are placed high on the structure (the gas cap is not big enough to justify lowering the placement of the producers, which would reduce total recovery in the long run). The gas coning makes the GOR highly dependent on how the grid around the wells is modelled. Thus, the reservoir average GOR is hard to match by only using field wide changes, without focusing on the grid near the wells.

Next step is matching of each well's GOR and WCT. The GORs were used to quality check the changes made to improve the pressure matches. As mentioned, there was no water production. The WCT was therefore not used as a matching parameter. Further, well PLT, open hole logs and tracer data are matched or quality checked. None of these were available during the matching period. Well shut in pressures, which is next, were the main parameter in the manual history matching of the Ivar Aasen field.

8.3 NOV_2016_Facies_Stochastic

The first rounds of history matching were carried out on the reservoir model available at production start. It was based on the geomodel NOV_2016_Facies_Stochastic, which at that time included the latest seismic and petrophysical interpretations. The work on improving the interpretations continued on past production start.

8.3.1 Matching of Pressure at Injectors

The first data tried to match were the pressure monitoring from the water injectors (not injecting) that were drilled prior to production start, IAWI02, IAWI04 and IAWI06. IAWI02 (west) showed a pressure drop during the first month of production of about 0.8 bar, while the measured pressure drop at IAWI04 (south-east) and IAWI06 (north-east) were about 0.2 bar. The big differences in depletion between the injectors are possibly related to the NTG of Skagerrak 2 where the wells are perforated. The low NTG in IAWI04 and IAWI06 might lead to low effective permeability and less communication.

The simulation model of November 2016 predicted greater pressure drop for all three injectors when run with a history type strategy using the actual production rates for the producers. The simulated pressure drops were 3.2 bar for IAWI02, and 1.2 bar for IAWI04 and IAWI06. The results are shown in Table 8.1.

Table 8.1 Injector pressure drop NOV_2016_Facies_Stochastic

Well	Measured pressure drop	Simulated pressure drop
IAWI02	0.8	3.2
IAWI04	0.2	1.2
IAWI06	0.2	1.2

This discrepancy between measured and simulated pressures speaks for weaker communication between the producers and injectors than in the simulation model. The actions proposed in order to match the pressure drops were to reduce permeability and/or add additional faults. Both of these actions will reduce the communication and limit flow from the injectors towards the producers.

When hearing about the possibly weaker communication the geologist (responsible for constructing the Ivar Aasen geomodels) responded that the upcoming model was likely to have reduced properties around the wells IAWI04 and IAWI06. The new model would incorporate the well logs of the two injectors (with low NTG) and new seismic interpretations.

Some fast testing was done adding short (non-geological) faults to the model (like the one shown in Figure 8.1).

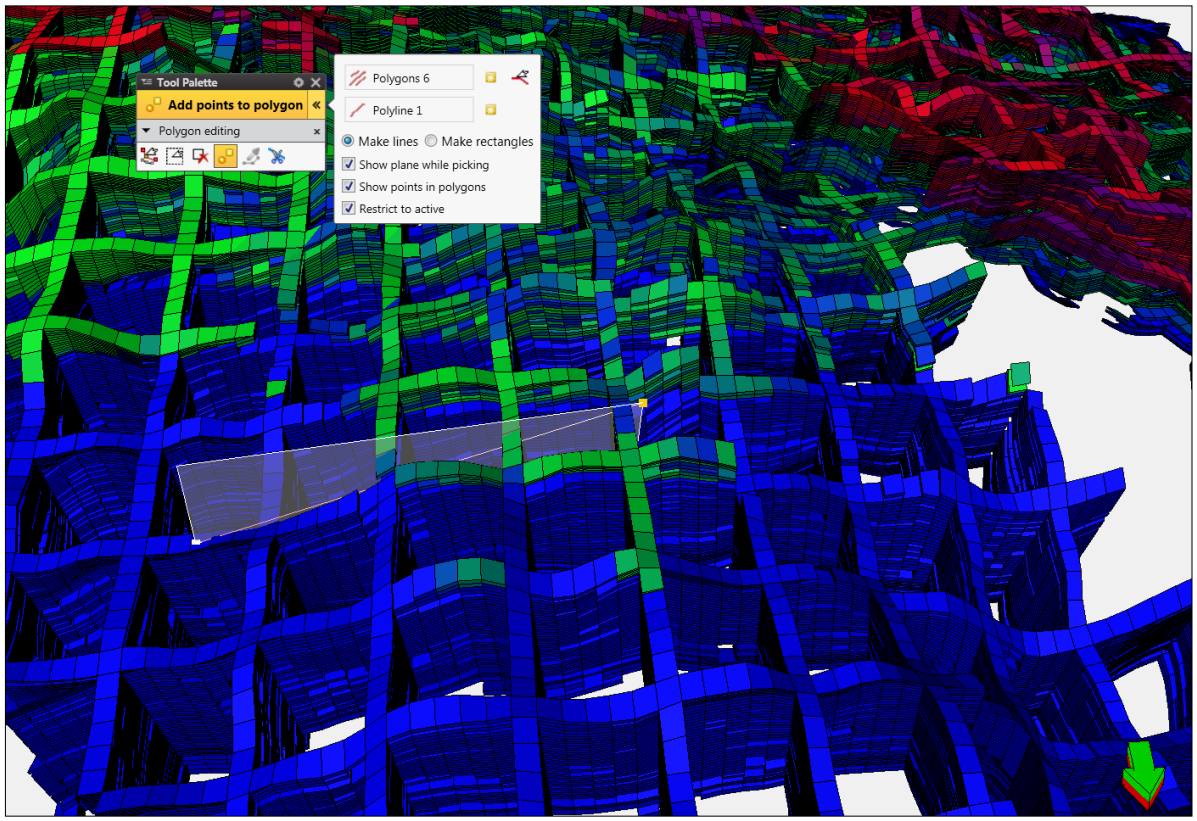

Figure 8.1 Adding faults in Petrel

The simulated pressure drops did not change significantly when introducing the faults, as the pressure pulse was able to propagate around the barriers. The faults had to be stretched out across the entire east part of the field to make an impact. The field wide faults were not in accordance with the geological understanding of the field. The adding was therefore a test of how drastic actions was needed to obtain a match. The three faults constructed are shown in Figure 8.2.

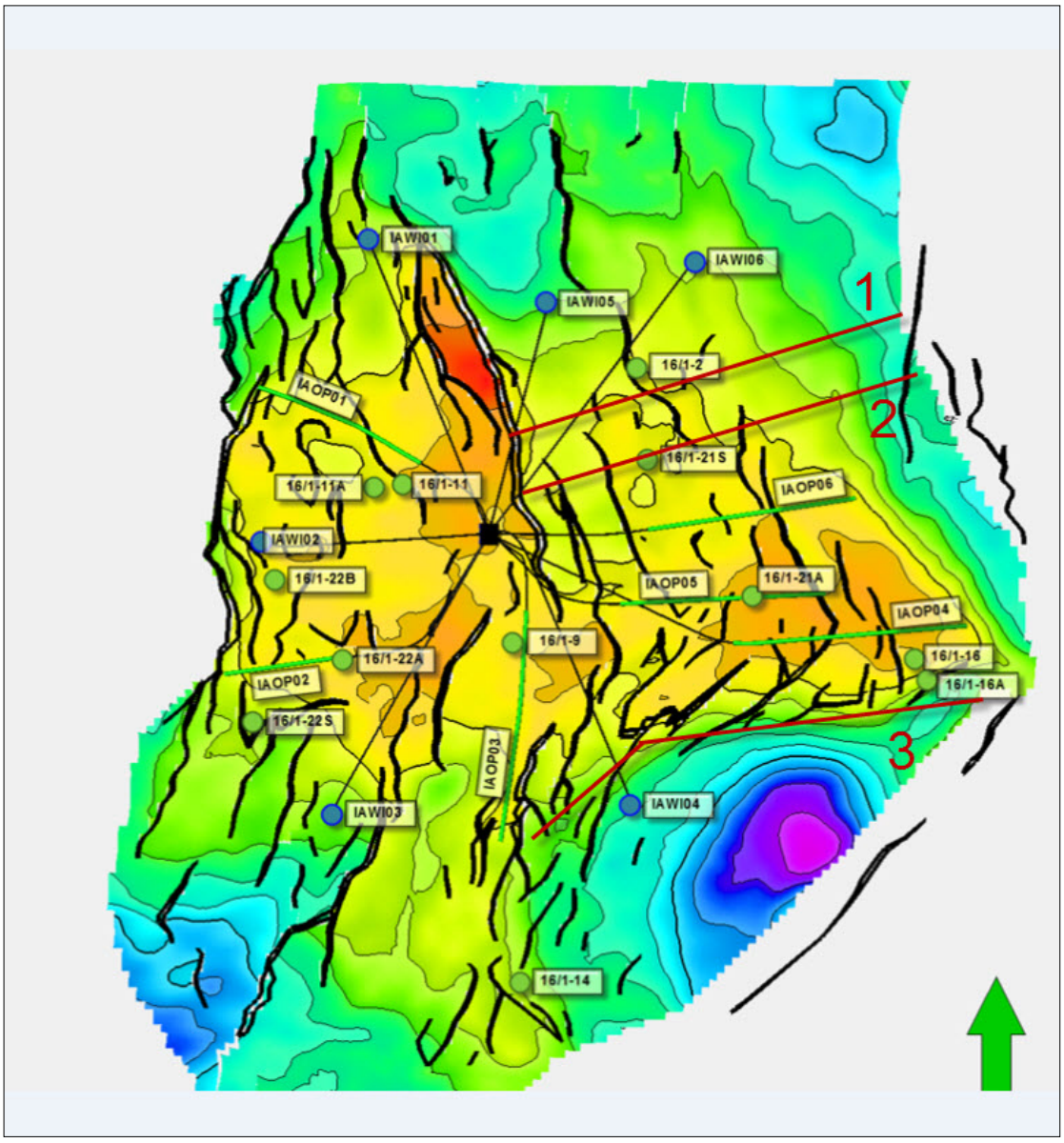

Figure 8.2 The three added faults

Changing the transmissibility multiplier of a fault changes their sealing capacity. The two variations used were Tx=0.01 and Tx=0.001, e.g. reducing the effective permeability over the cross sections by a factor 100 or 1000. As mentioned, the existing modelled faults have a transmissibility multiplier Tx=0.01.

Keeping the permeability in the model equal to the November 2016 model, and introducing the mentioned faults in the east with Tx=0.01 and Tx=0.001 (in two separate simulation runs) yielded the desired response at the two east injectors. As shown in Figure 8.3 and Figure 8.4, Tx=0.001 managed to restrict communication and reduce the pressure drops to 0.3 bar at both IAWI04 and IAWI06. However, the pressure drop did not change at the west injector IAWI02.

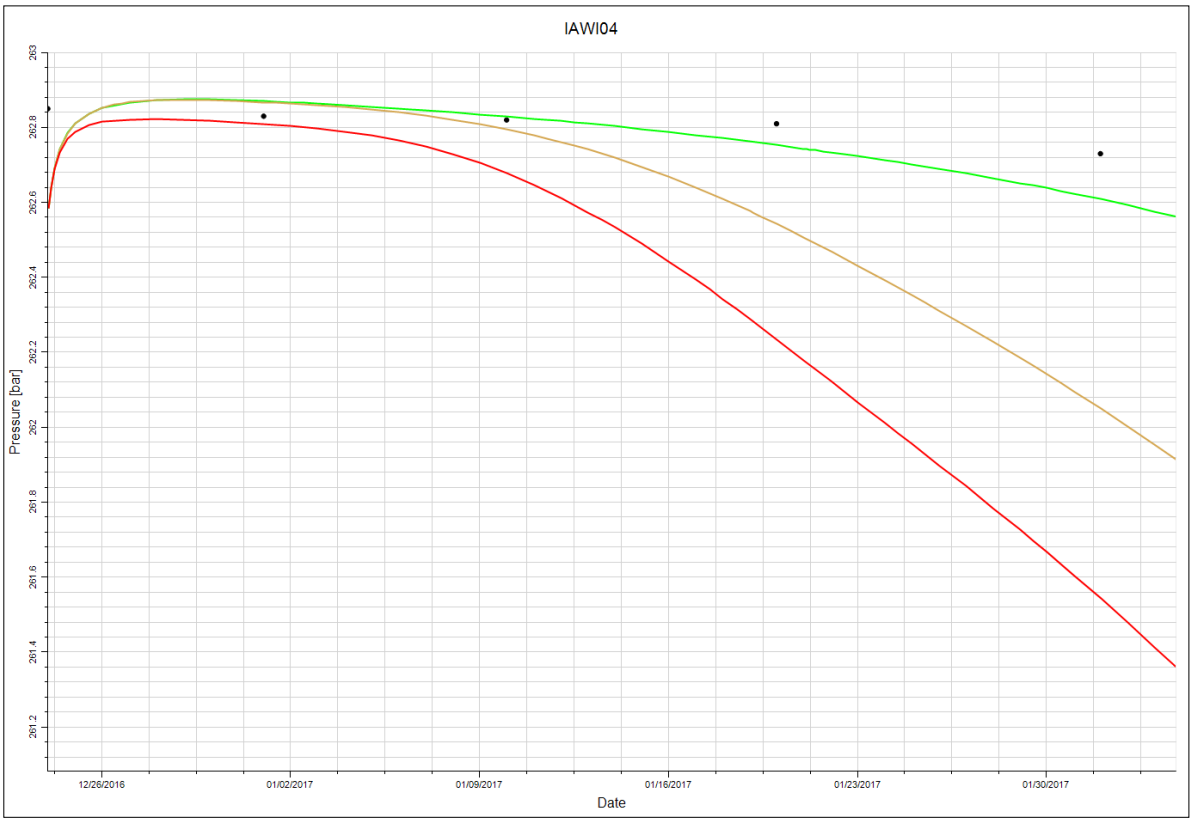

Figure 8.3 Pressure IAWI04

Black dots: Measured pressure. Red line: Base case. Brown line: Tx=0.01. Green line: Tx=0.001.

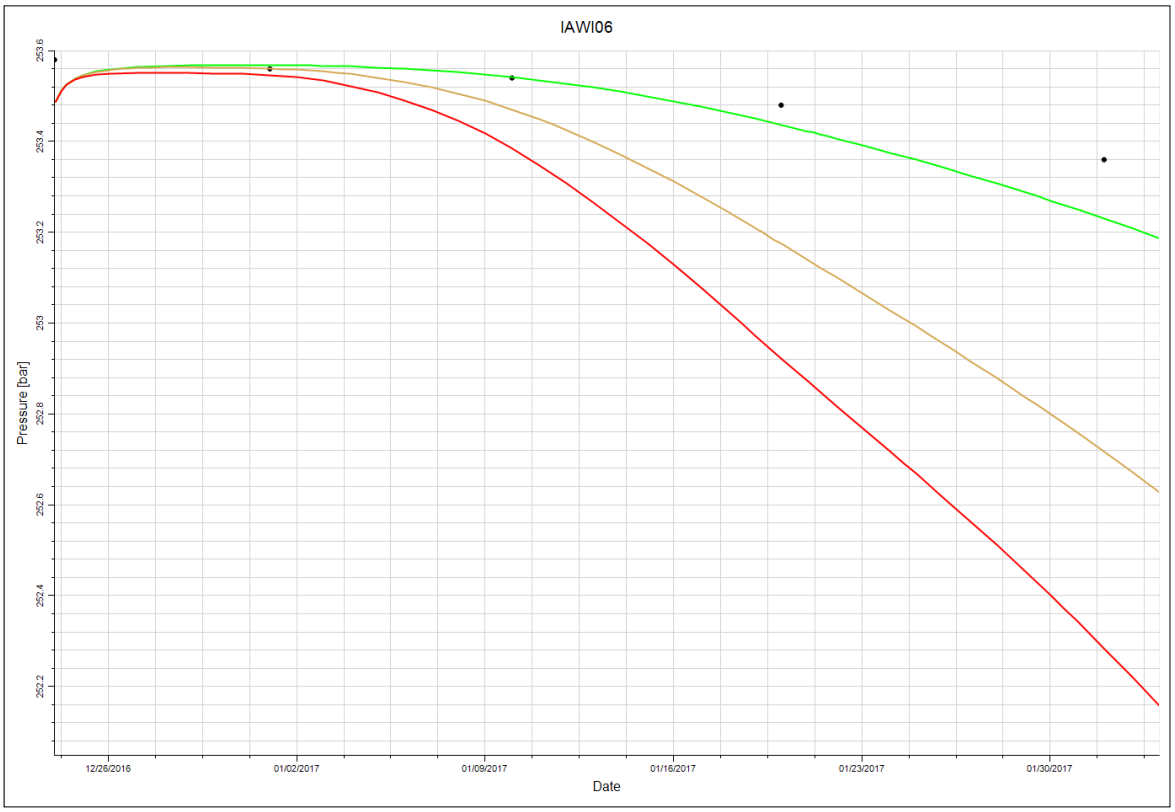

Figure 8.4 Pressure IAWI06

Black dots: Measured pressure. Red line: Base case. Brown line: Tx=0.01. Green line: Tx=0.001.

It is worth a notice that the pressure at the injectors in the models is increasing the first few days. This is because the pressure in the modelled wells was initially not in equilibrium with the reservoir. To guarantee pressure change (Δp) is compared, the measured pressure points are collectively adjusted such that the first pressure points match the equilibrium pressure in the models. This is also done in the later figures showing pressure at injectors. Similar actions are taken if the initial pressure at a modelled production well not matches the initial measured pressure.

Another way to restrict communication is to reduce the permeability. The three selected changes in permeability were:

- 90 % reduction in permeability in all water filled blocks
- 50 % reduction in permeability in all blocks situated more than 200 m away from a well (see Figure 8.5)
- 50 % reduction in permeability in all water filled blocks

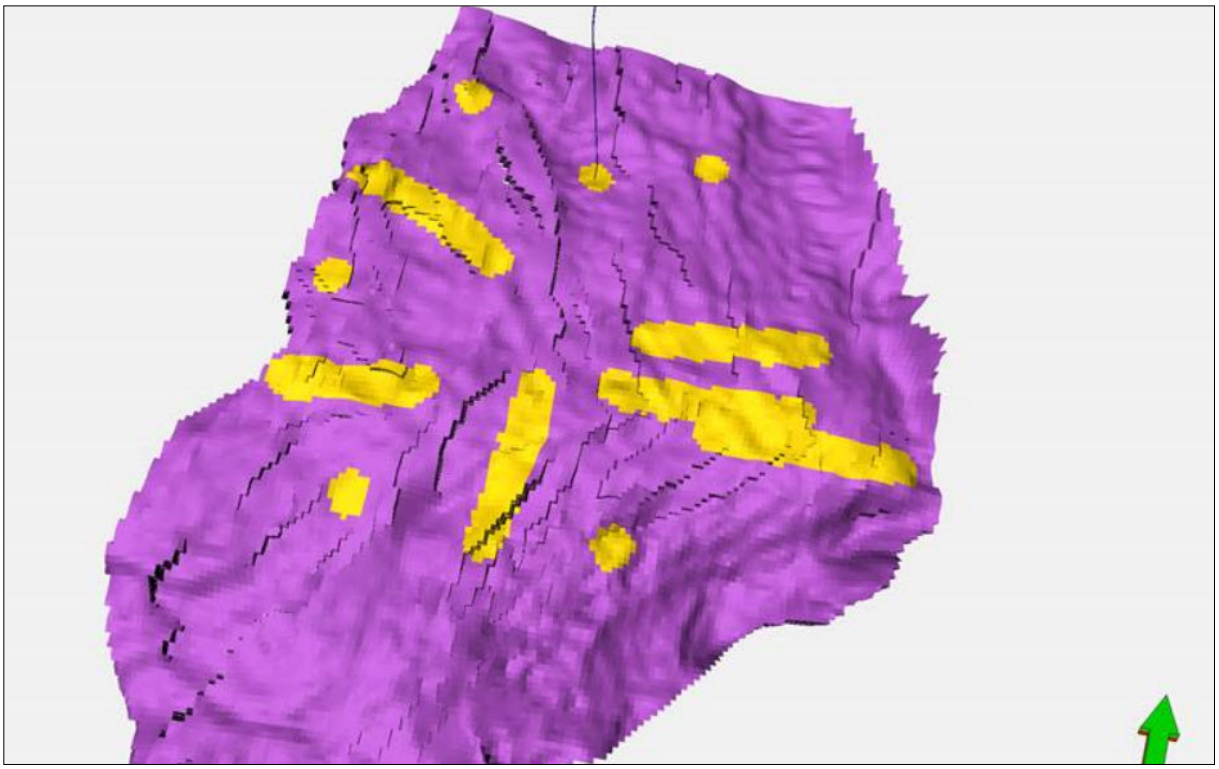

Figure 8.5 Areas around the production and injection wells not affected by the changes

The reason for not altering the permeability close to wells was to honour the permeabilities that are closest bound to the petrophysical interpretations of well logs.

All three of these permeability alterations were coupled with the different fault cases (only old faults, adding new faults with Tx=0.01 and adding new faults with Tx=0.001). When reducing the permeability in the water zone by 90 %, all the fault cases gave no pressure drop at all at IAWI04 (as seen in Figure 8.6).

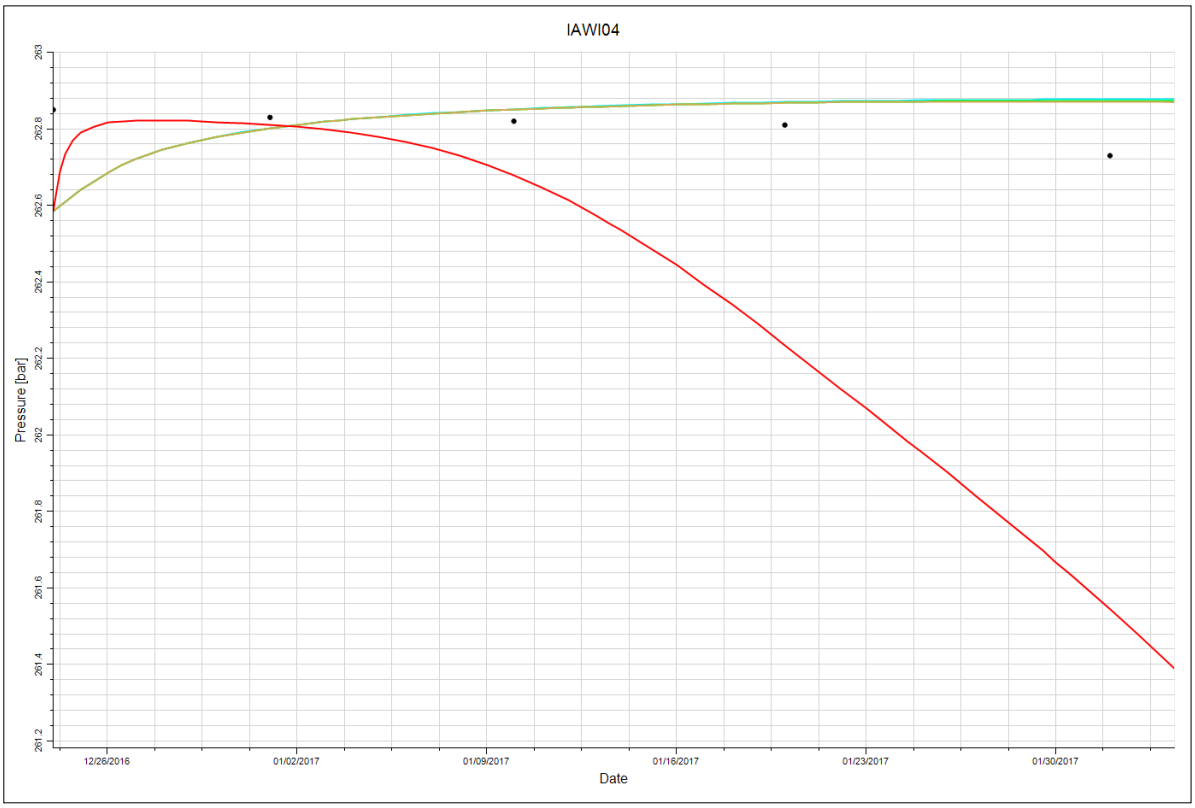

Figure 8.6 Pressure IAWI04 with 90% reduction of aquifer permeability.

Black dots: Measured pressure. Red line: Base case.

When reducing the permeability by 50 % between the wells the transmissibility multiplier needs to be reduced to 0.001 in order to get a pressure drop similar to what is measured at the IAWI04 well on Ivar Aasen (Figure 8.7).

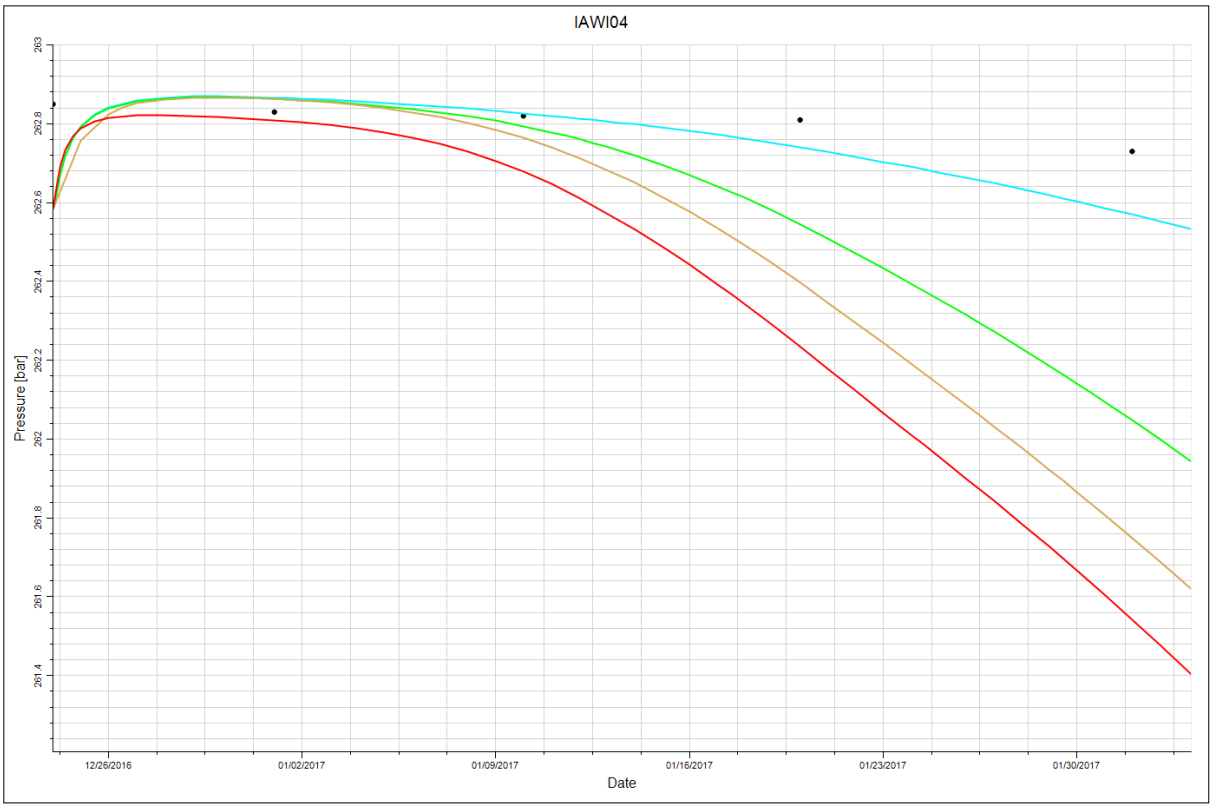

Figure 8.7 Pressure IAWI04 with 50% reduction of permeability between the wells

Black dots: Measured pressure. Red line: Base case. Brown line: Only old faults. Green line: Tx=0.01. Blue line: Tx=0.001

When reducing the permeability by 50 % in the water zone a transmissibility multiplier of 0.001 led to similar depletion as measured in the well. However, also the cases with old faults and with Tx=0.01 gave rather comparable pressure drops.

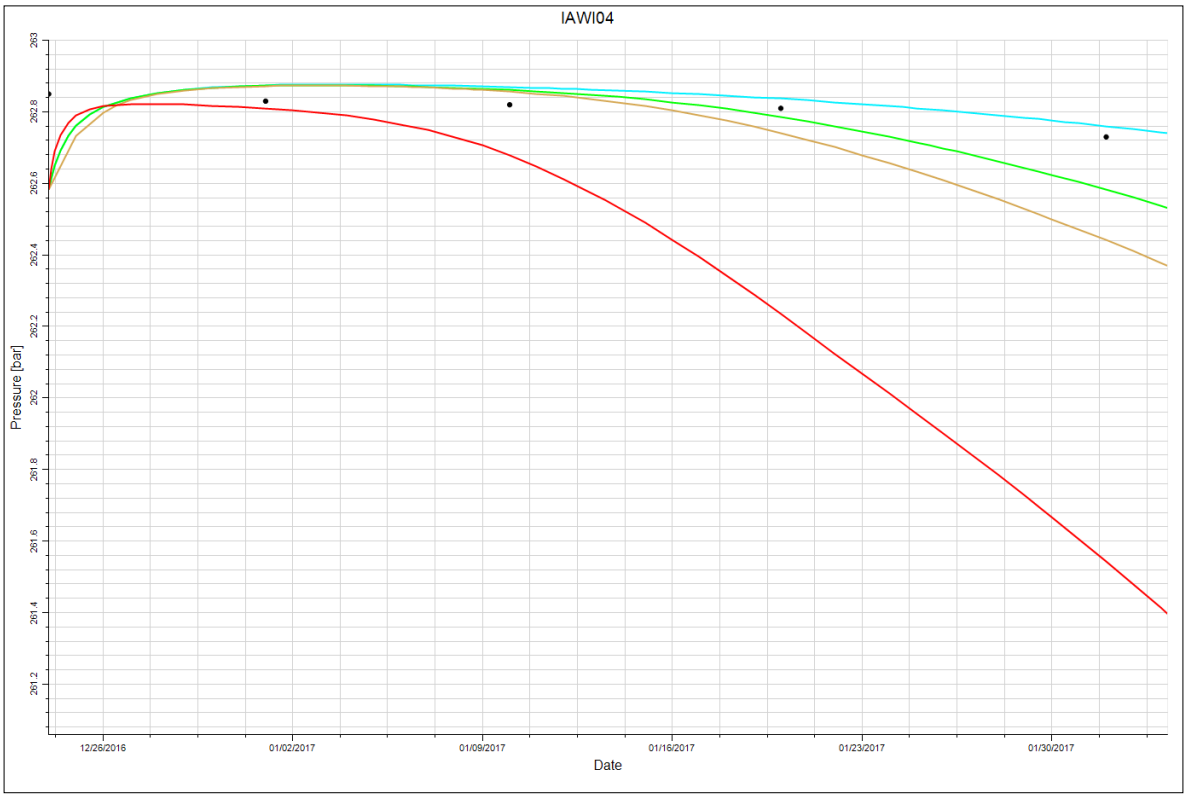

Figure 8.8 Pressure IAWI04 with 50% reduction of aquifer permeability

Black dots: Measured pressure. Red line: Base case. Brown line: Only old faults. Green line: Tx=0.01. Blue line: Tx=0.001

The main learning from this matching process was that the actions needed to make an impact were severe. Both barriers and reduced permeability were capable of reducing the depletion at the injectors in the reservoir model.

When presented with the findings, the geologist noted that the faults, especially the two towards the northeast, were not in line with geological understanding of the reservoir. In the further, these long faults are therefore not used. Thus, lowering of permeability around the injectors will have to be used to limit the communication. As discussed, the low effective permeability can be related to low NTG fluvial channels in Skagerrak 2, where the producers are perforated.

8.3.2 Matching of Pressure at Producers

In order to make a reliable history match, the depletion at the producers also needs to be matched. Based on the initial comparison of the measured and simulated pressure drops (using base case), the following general observations were made:

- IAOP01: Too severe initial pressure drop in the model
- IAOP02: Too severe initial pressure drop in the model
- IAOP03: Good match
- IAOP04: Satisfying match
- IAOP05: Satisfying match

After the initial pressure drop in the model, IAOP01 and IAOP02 show pressure developments more similar to the ones measured. This, in addition to the either good or satisfying matches at the other producers, indicates that the volumes in communication with the wells in the model have about the same size as the ones seen by the actual wells.

Based on the results from the matching of the injector pressures, the following two changes in permeability were selected:

- 50 % reduction of permeability in all blocks situated more than 200 m away from a well
- 50 % reduction of permeability in all water filled blocks (aquifer)

The two producers located in the western part of the field, IAOP01 (Figure 8.9) and IAOP02 (Figure 8.10), showed large pressure drops during the first few days of production from the specific well. The changes made in permeability did not improve the matches. Reducing the permeability between the wells had the opposite effect; it made the pressure drop even larger for both wells. The rapid pressure drop at the producers suggests that the models are missing reservoir volumes.

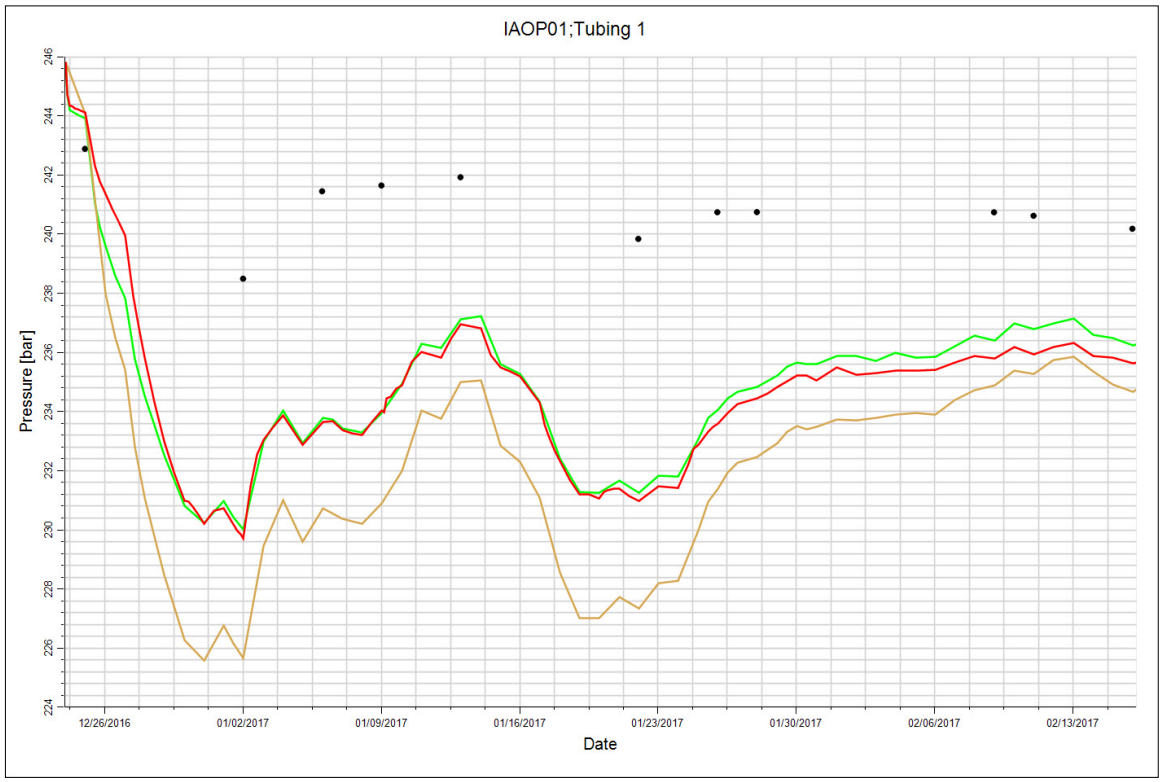

Figure 8.9 Pressure IAOP01

Black dots: Measured pressure. Red line: Base case. Brown line: 50% permeability between wells. Green line: 50% permeability in the aquifer

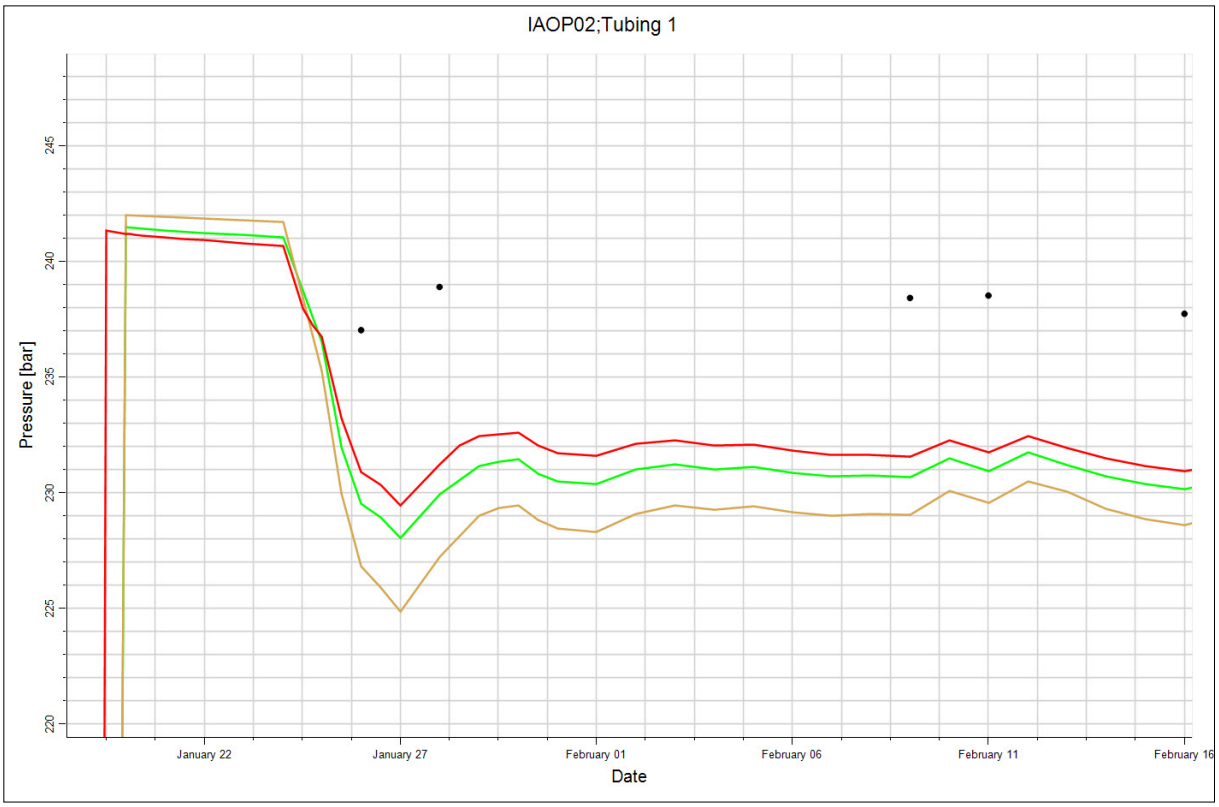

Figure 8.10 Pressure IAOP02

Black dots: Measured pressure. Red line: Base case. Brown line: 50% permeability between wells. Green line: 50% permeability in the aquifer

The base case of the model produced a good match for IAOP03 well (Figure 8.11). The area around the well seems to be accurately modelled, although the well has been heavily produced, and the pressure drop is great compared to the other wells. As for IAOP01 and IAOP02, the decreased permeability cases did not improve the match, rather the opposite.

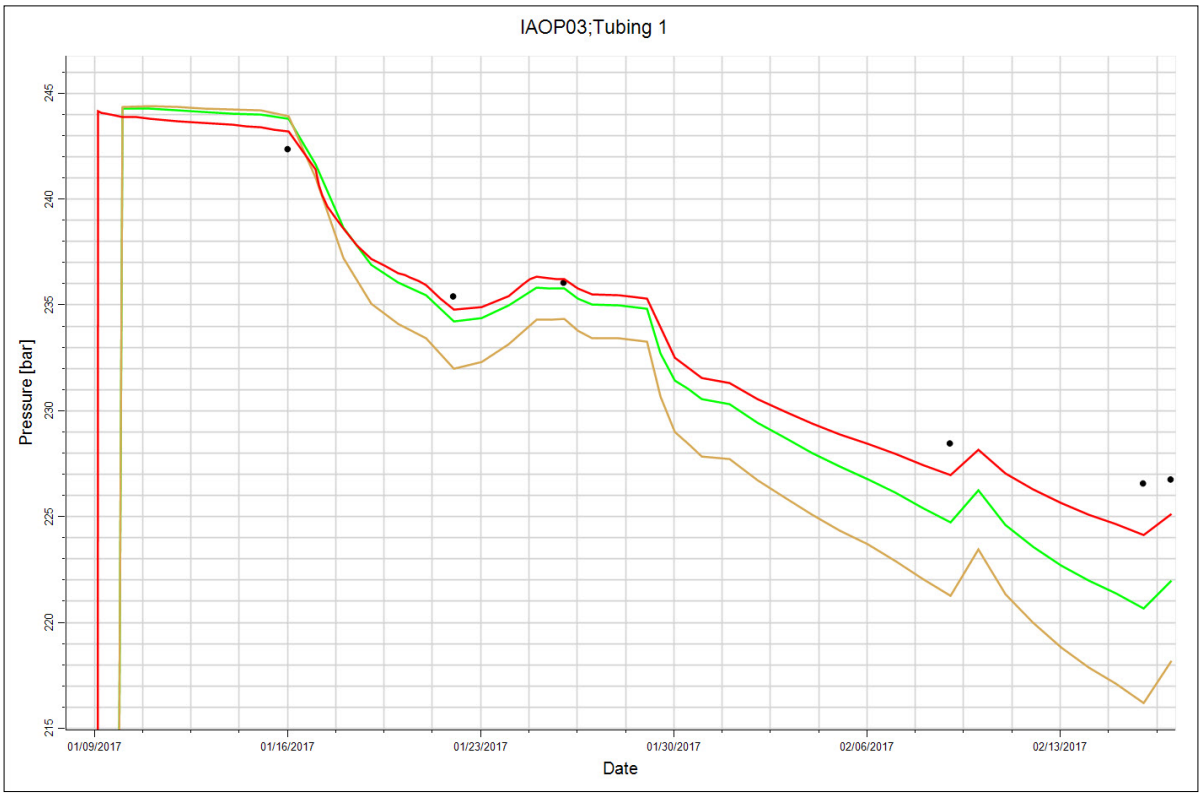

Figure 8.11 Pressure IAOP03

Black dots: Measured pressure. Red line: Base case. Brown line: 50% permeability between wells. Green line: 50% permeability in the aquifer

The two producers located in the eastern part of the field, IAOP04 (Figure 8.12) and IAOP05 (Figure 8.13), showed satisfying matches between the base cases and measured pressures. However, also the reduced permeability cases matched ok.

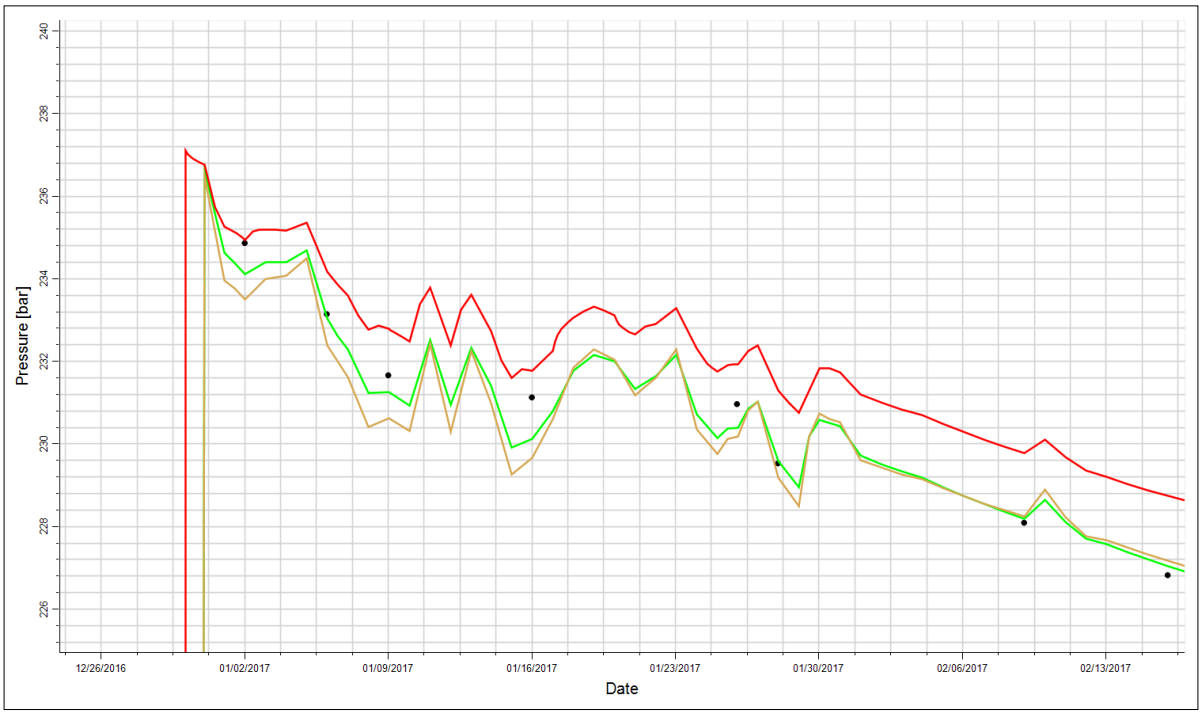

Figure 8.12 Pressure IAOP04

Black dots: Measured pressure. Red line: Base case. Brown line: 50% permeability between wells. Green line: 50% permeability in the aquifer

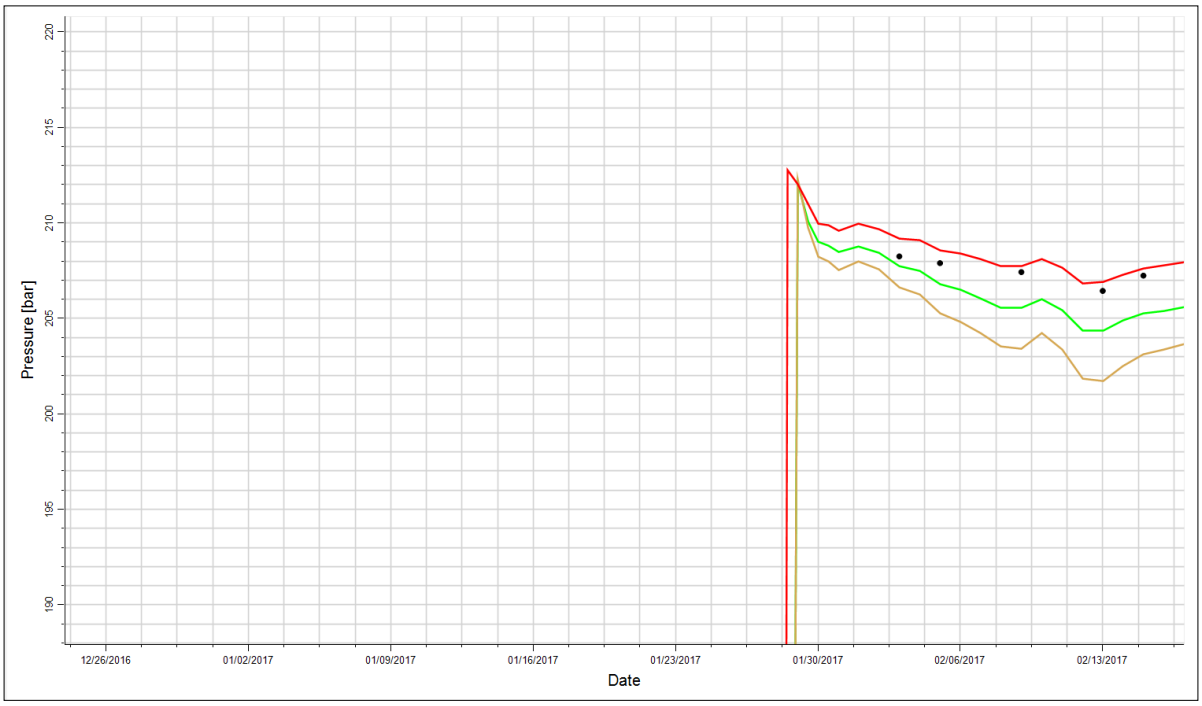

Figure 8.13 Pressure IAOP05

Black dots: Measured pressure. Red line: Base case. Brown line: 50% permeability between wells. Green line: 50% permeability in the aquifer

8.3.3 Summary

The main conclusions from the history matching work on the NOV_2016_Facies_Stochastic model were:

- The matches of the east injectors (IAWI04 and IAWI06) were improved by permeability reductions.
- The pressure development of the south and east producers (IAOP03, IAOP04 and IAOP05) were simulated rather similar to the measured ones. The permeability changes were not able to ruin the matches.
- The model was not able to reproduce the pressure development of the west producers (IAOP01 and IAOP02), and the permeability changes applied based on the injector pressure drops were not helping. Missing reservoir volumes in the western part of the field suggested as part of the explanation.

The next model, containing well logs from IAWI04 and IAWI06, was hoped to improve the match in the eastern part. However, these new logs will not affect the western part, where the model produced the weakest match. Thus, the history matching of the new model will have to be concentrated in the west.

8.4 CPI_2017_Facies_Stochastic

The new model, CPI_2017_Facies_Stochastic, did include the well logs from IAWI04 and IAWI06, but not the new seismic interpretations, and was thus a temporary model in wait for the next full model.

The initial simulations on the model showed (as predicted by the geologist) weaker communication between producers and injectors. The new simulation model predicted a smaller pressure drop for all three injectors compared to the November 2016 model. Simulated pressure drops were 2.5 bar for IAWI02, 0.8 bar for IAWI04 and 1.0 bar for IAWI06. The results are shown in Table 8.2.

Table 8.2 Injector pressure drop CPI_2017_Facies_Stochastic

Well	Measured pressure drop	Simulated pressure drop
IAWI02	0.8	2.5
IAWI04	0.2	0.8
IAWI06	0.2	1.0

The initial test of the new model showed pressure developments of the producers similar to what was seen with the old model. The south and east production wells (IAOP03, IAOP04 and IAOP05) matched ok, whereas the west producers (IAOP01 and IAOP02) still had too large pressure drops.

8.4.1 Field Wide Tests

The further testing involved broad changes in permeability. As experienced with the older model, simply multiplying the permeability with a fixed factor did not solve the problem. Again, lowering the permeability did help the match of the injectors, but had the opposite effect on the producers.

8.4.2 A Closer Look at the Western Part of the Field

The 3D visualization tool in Petrel is useful when trying to examine the distribution of different static and dynamic parameters in the reservoir. Static parameters do not change over time, whereas dynamic parameters do. In a history matching procedure pressure and fluid saturations are the main dynamic parameters to study. Among the static parameters, permeability is the most important.

Three-dimensional pressure plots of the western part of the field revealed that the initial pressure drop related to the production starts of the two producers (IAOP01 and IAOP02) was limited to small areas around the perforated zones of the wells. Figure 8.14 illustrates this. It shows absolute pressure round IAOP01 at 01.01.2017 (after one week of production), The volumes influenced by the production were relatively limited both laterally and vertically. Several nearby faults prohibited the wells pressure pulses from further lateral movement. The lack of pressure support from the lower zones was related to a non-pay zone below the main reservoir target zones (Sleipner and Skagerrak 2) of the west, where the producers are completed.

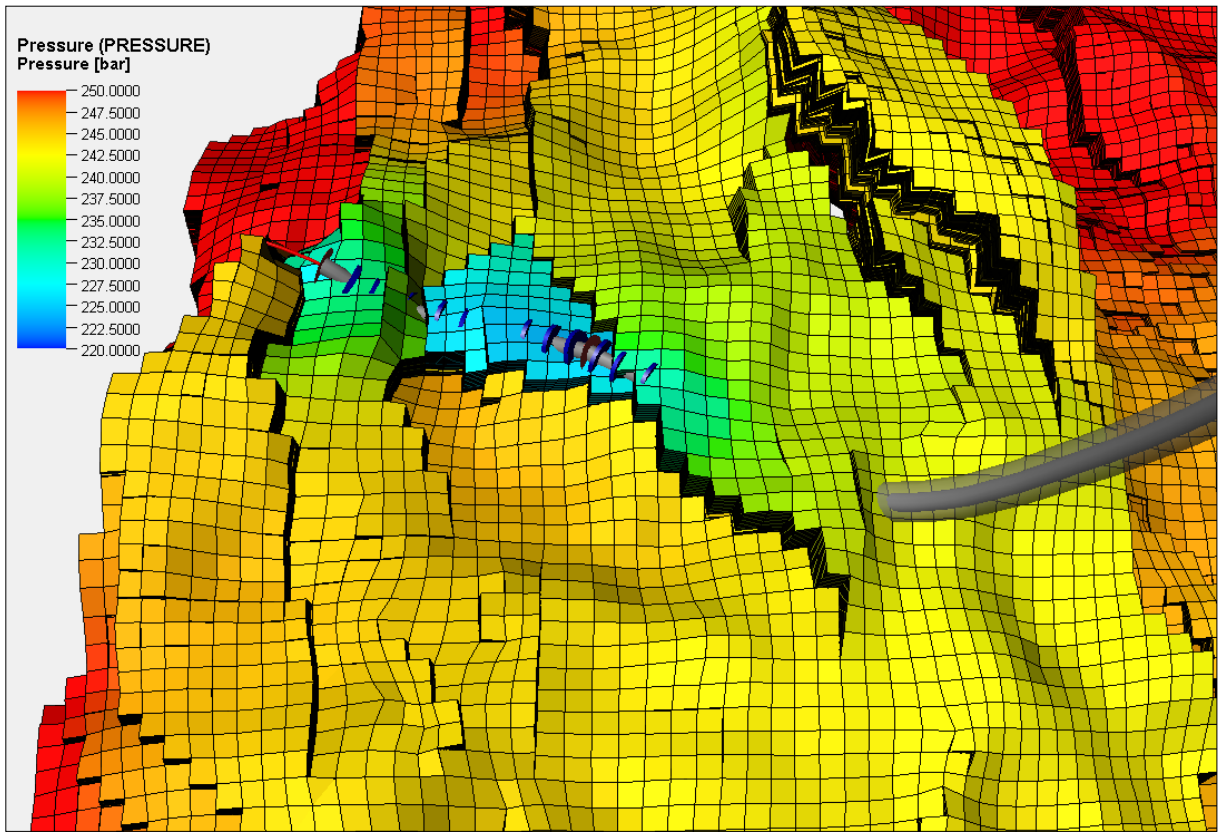

Figure 8.14 Depletion around IAOP01

Based on these insights, actions to open the western part both laterally and vertically were made. The faults of the field were made less sealing; the transmissibility was increased to 0.1 and 1.0 in two different cases. The base case transmissibility was 0.01 in order to be on the safe side (rather too tight than too open) regarding compartmentalization. The results of opening the faults were promising; the initial pressure drops of the producers were not as severe. However, the adjustments were far from enough to obtain a match, and going from 0.1 to 1.0 did not have much of an effect. The lack of effectiveness in opening the faults was

partly related to the degree of fault displacement, e.g. the good reservoir zones on each side of many faults were not communicating. Thus, long faults with large displacement were able to prevent communication, even when they in theory were non-sealing. An example of large fault displacement is marked in the middle of Figure 8.15, not far from IAOP02. A similar fault is found near IAOP01.

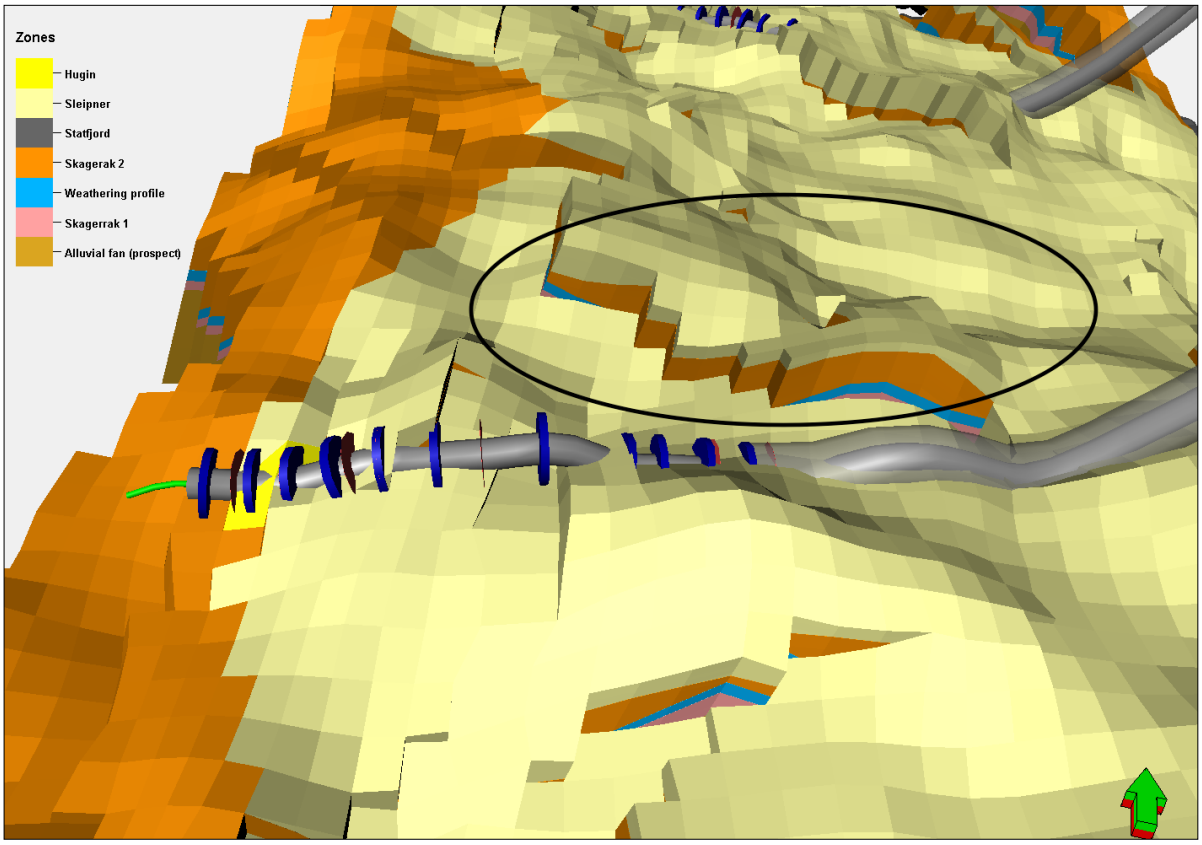

Figure 8.15 Fault near IAOP02

As expected, the hindering ability (or rather the lack of it) of the faults in the east was not much affected by the changes in transmissibility. The faults in this area are generally modelled short and not connected, making them easy to flow around. The limited influence in the east, and partly positive influence in the west, made an increase in transmissibility (to 0.1) over the faults a possible part of the solution. The adjustment did not seem to hurt the robustness of the drainage in this model, since the sealing faults were sealing no matter the transmissibility.

The search for more support and volumes further down from the main target zones soon turned out to be hard. The non-pay zone blocks were set inactive in the geomodel in order to reduce the number of blocks (the motivation for this is to reduce the computational cost of and time spent on the reservoir simulations). There is no quick fix to this. The inactive blocks

remain inactive although the permeability of all the blocks of the field (or an area) is increased. A new geomodel, where the reservoir quality of the zone is upgraded, is needed in order to establish communication with the deeper zones. More volume can appear in the form of bigger gas cap, thicker reservoir zones or communication with deeper zones. A test with doubling of pore volume (by doubling of porosity) in the communicating reservoir zones in the west, gave positive results.

8.4.3 The Match

The adjustments done to obtain the final, somehow satisfying, match with basis in the CPI_2017_Facies_Stochastic model were:

- Reduction of water zone (aquifer) permeability by a factor 10 in the entire model
- Increase of fault transmissibility from 0.01 to 0.1 in the entire model
- Increase of porosity (representing greater reservoir volumes) by a factor 2 in Sleipner and Skagerrak 2 (the main reservoir formations) in the western part of the model
- Increase of permeability by a factor 2 in Sleipner and Skagerrak 2 (the main reservoir formations) in the western part of the model

It is important not to anchor the understanding of a field to one specific case or model, and be aware of the limitations of the model. It is not THE model, but an ok model based on current information. As discussed in chapter 2, the knowledge gained is also important input to the next geomodel.

8.4.4 Discussion of the Matched Case

Discussions of the strengths and weaknesses of the history-matched model follow next. Throughout the figures (Figure 8.16 to Figure 8.28) the base case model is represented with blue lines, the matched model with red lines and the observations with black dots.

From Figure 8.16, it is apparent that the matched case gives a more similar response for IAOP01. However, the changes are too many and too severe in proximity of the well to make conclusions. In addition, the model does not seem to be able to replicate rapid pressure changes. As the production stabilizes about half way through the period, the model is able to catch up. The ability to forecast the initial response to high production rate is highly dependent on near well reservoir qualities and barriers. Later response to steady production is dependent on a greater volume, and represents the areal average. Thus, the areal match is better. To conclude; the well needs more good sand, but how large the increases in

permeability and reservoir volumes (here represented by increased porosity) should be, remain uncertain.

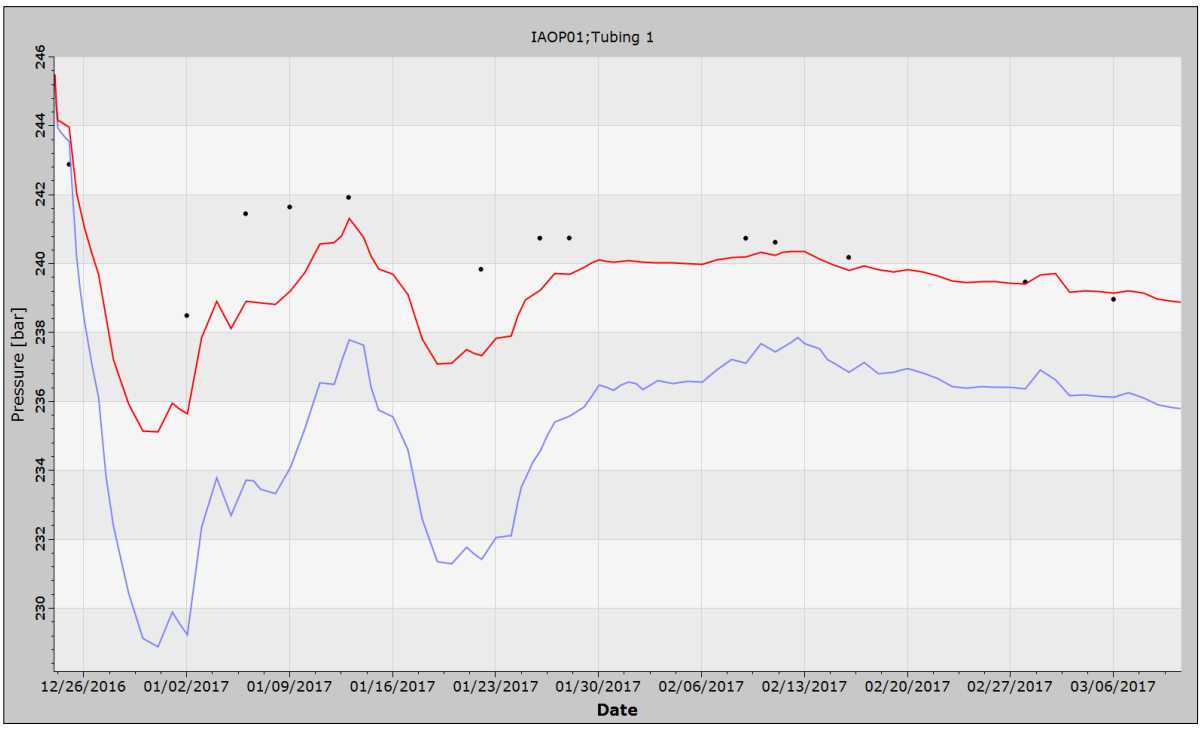

Figure 8.16 Pressure IAOP01

Black dots: Measured pressure. Blue line: Base case. Red line: History matched case

It is difficult to make any conclusions about the GOR match of IAOP01 (Figure 8.17). Part of the well is completed close to the gas cap, which makes GOR highly dependent on near well features. The GOR in the model is also dependent on the grid. These can be parts of the reason for the unsatisfying match.

In the middle of the period, the measured GOR stops to increase, stays rather stable for some weeks and then increases severely from one point to the next. It is believed that the GOR in reality was steadily increasing throughout the period. No new allocation curve was assigned to the well due to lack of accurate testing of the GOR in this period. Thus, the sudden jump in GOR is thought to be unlikely.

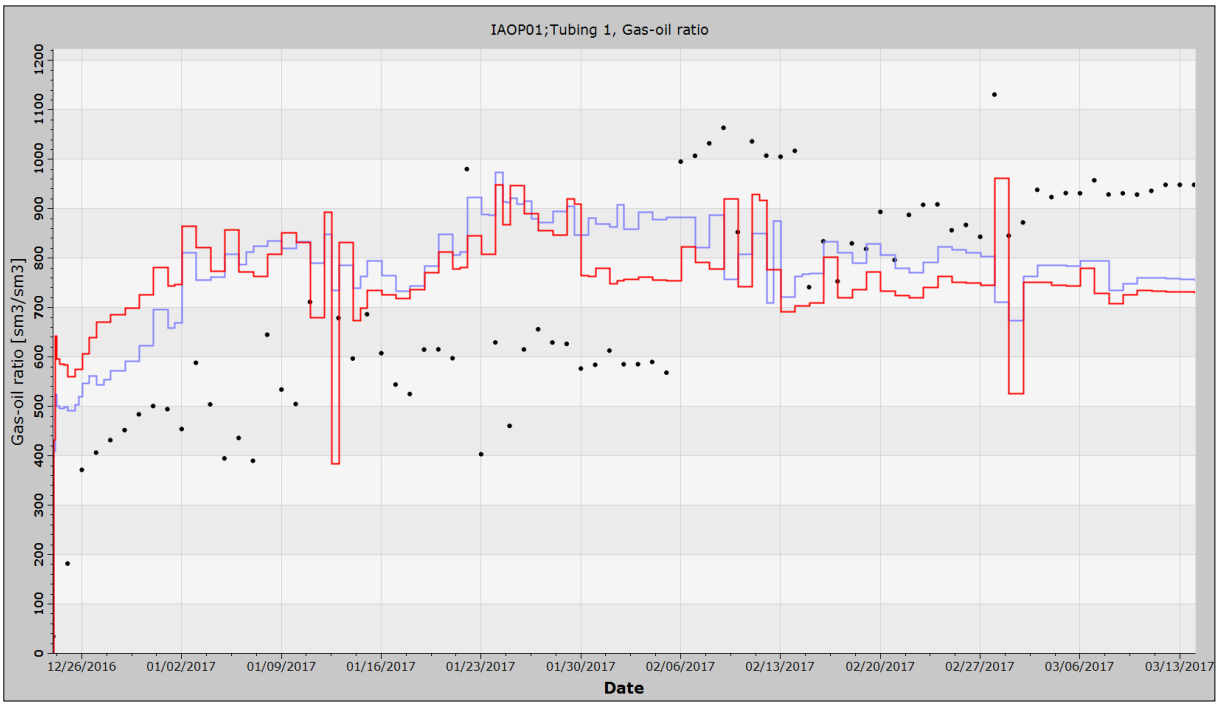

Figure 8.17 GOR IAOP01

Black dots: Measured GOR. Blue line: Base case. Red line: History matched case

The pressure response discussion of IAOP01 is also applicable for IAOP02. As with IAOP01, the history-matched model's response is greatly improved, however rapid changes are not well predicted (Figure 8.18).

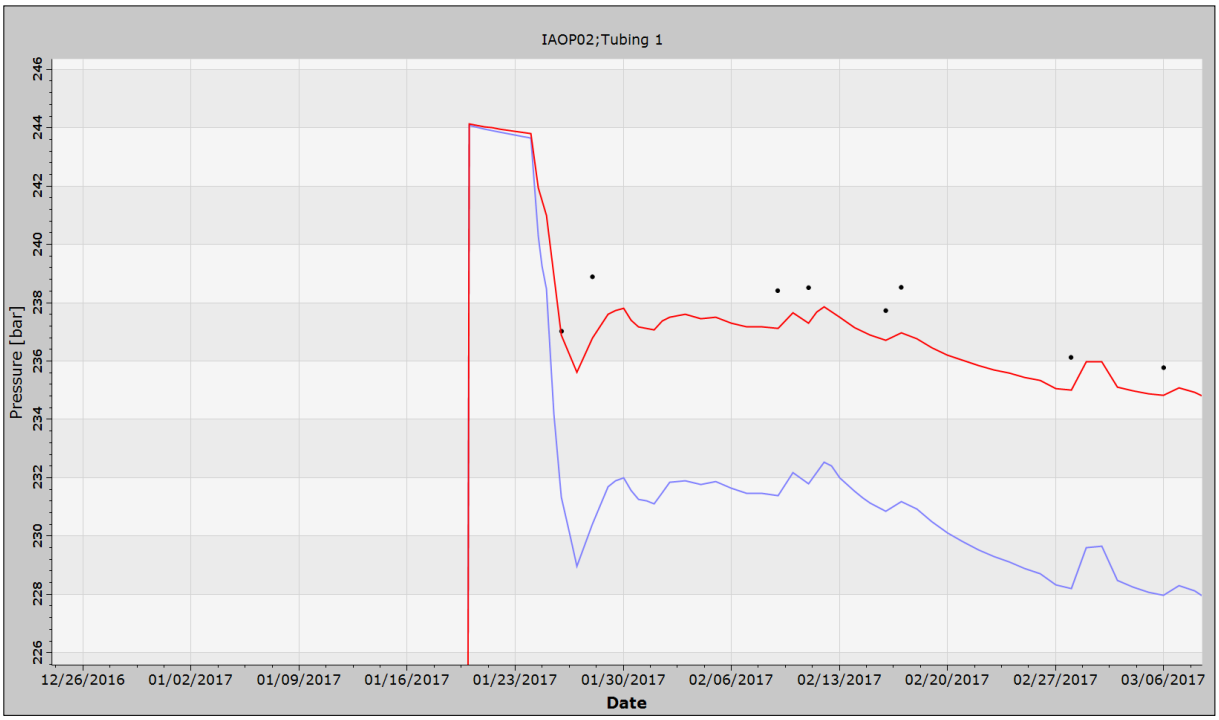

Figure 8.18 Pressure IAOP02

Black dots: Measured pressure. Blue line: Base case. Red line: History matched case

Both the base case and history matched model predicts the GOR of IAOP02 relatively closely (Figure 8.19).

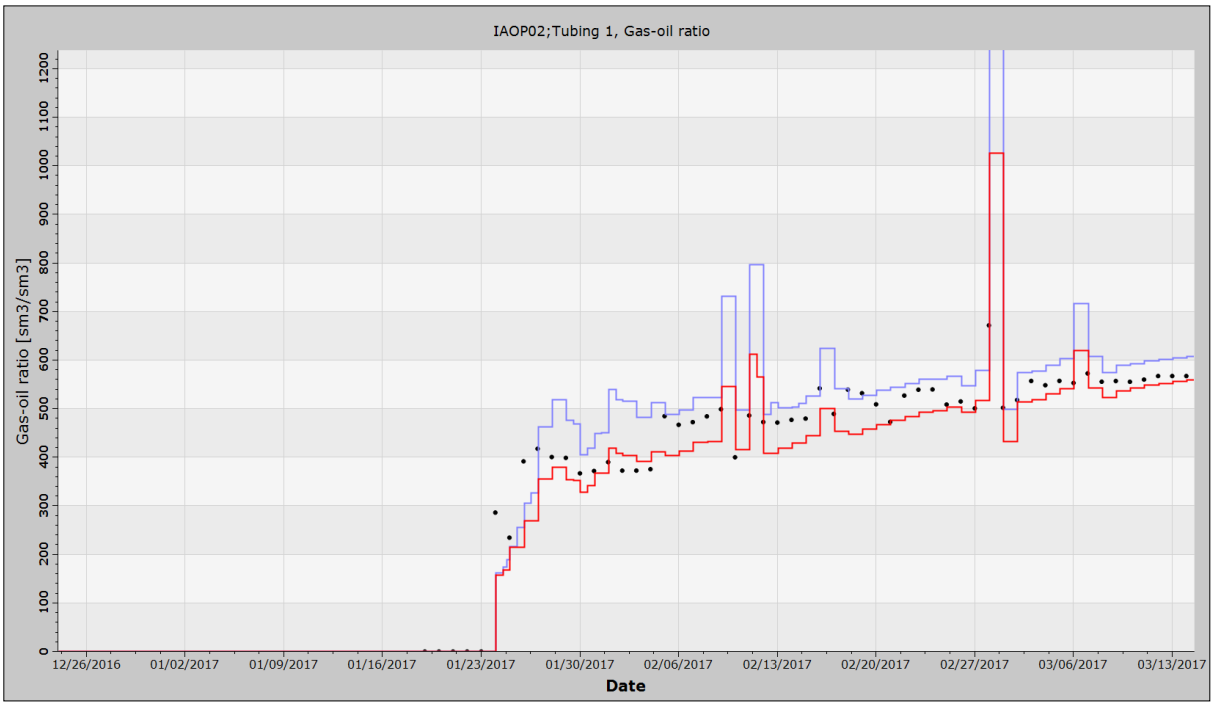

Figure 8.19 GOR IAOP02

Black dots: Measured GOR. Blue line: Base case. Red line: History matched case

The base case model was able to match the pressure at IAOP03 satisfactory. Luckily, the changes applied in the history-matched model change the depletion only mildly. This resulted in a slightly better match (Figure 8.20), although the aim was to improve matches at other wells.

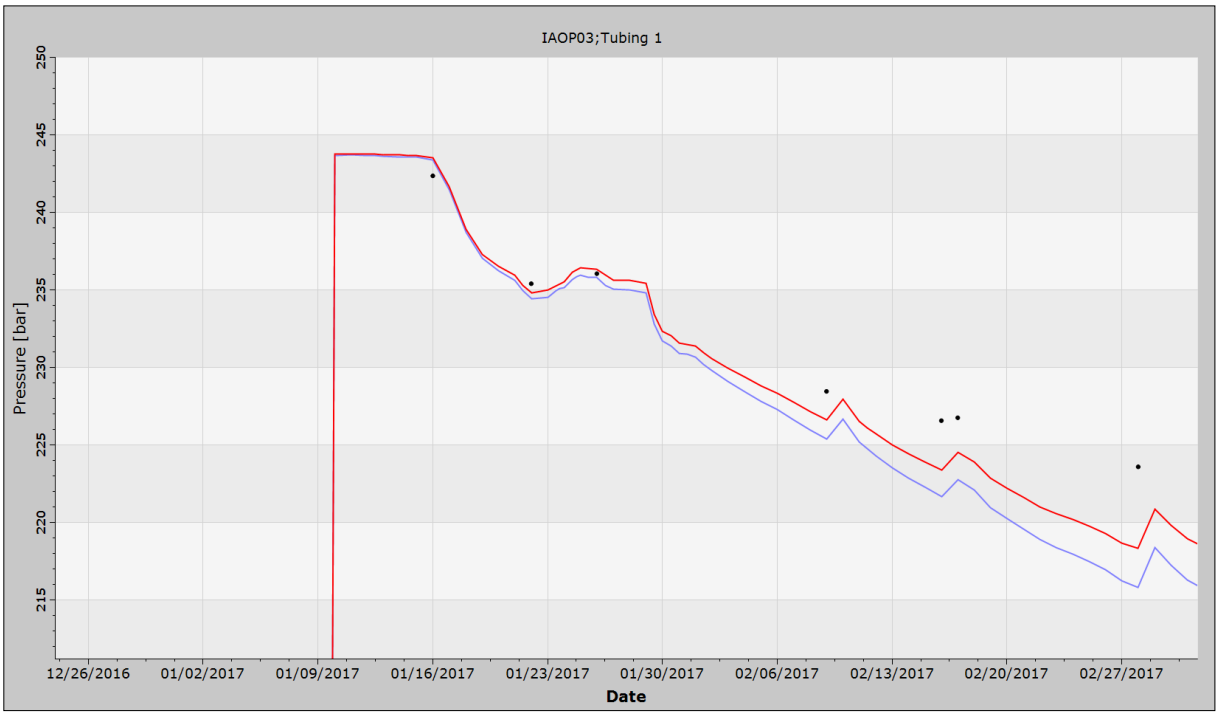

Figure 8.20 Pressure IAOP03

Black dots: Measured pressure. Blue line: Base case. Red line: History matched case

The GOR of IAOP03 is almost identical in the base case and the history-matched case. In both cases the simulated GORs are slightly higher than the measured one in the second half of the matching period (Figure 8.21). Similar to IAOP01, IAOP03 is perforated close to the gas cap. This makes the GOR highly dependent on near well features, and the grid. Thus, the deviation is acceptable.

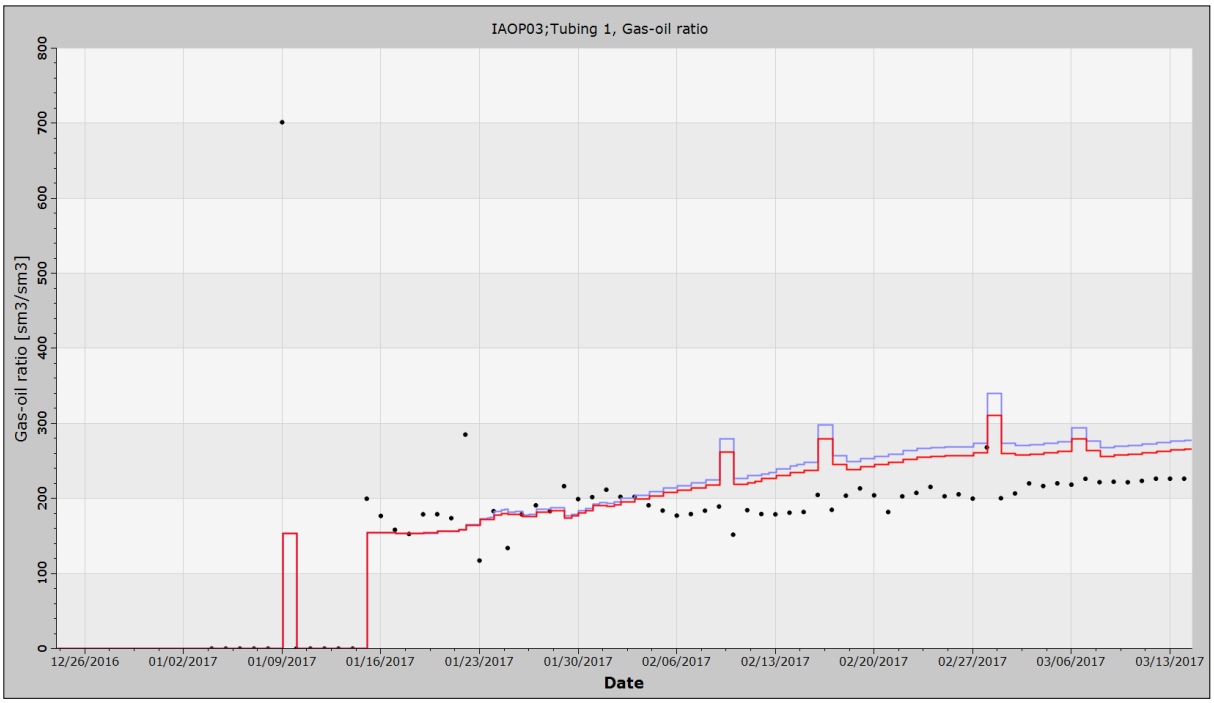

Figure 8.21 GOR IAOP03

Black dots: Measured GOR. Blue line: Base case. Red line: History matched case

The pressure development at IAOP04 is unaffected by the changes in the history matched model, i.e. the two cases are almost identical (Figure 8.22). As stated earlier, the base case produces a satisfactory match, the deviation is relatively small and the slope is similar.

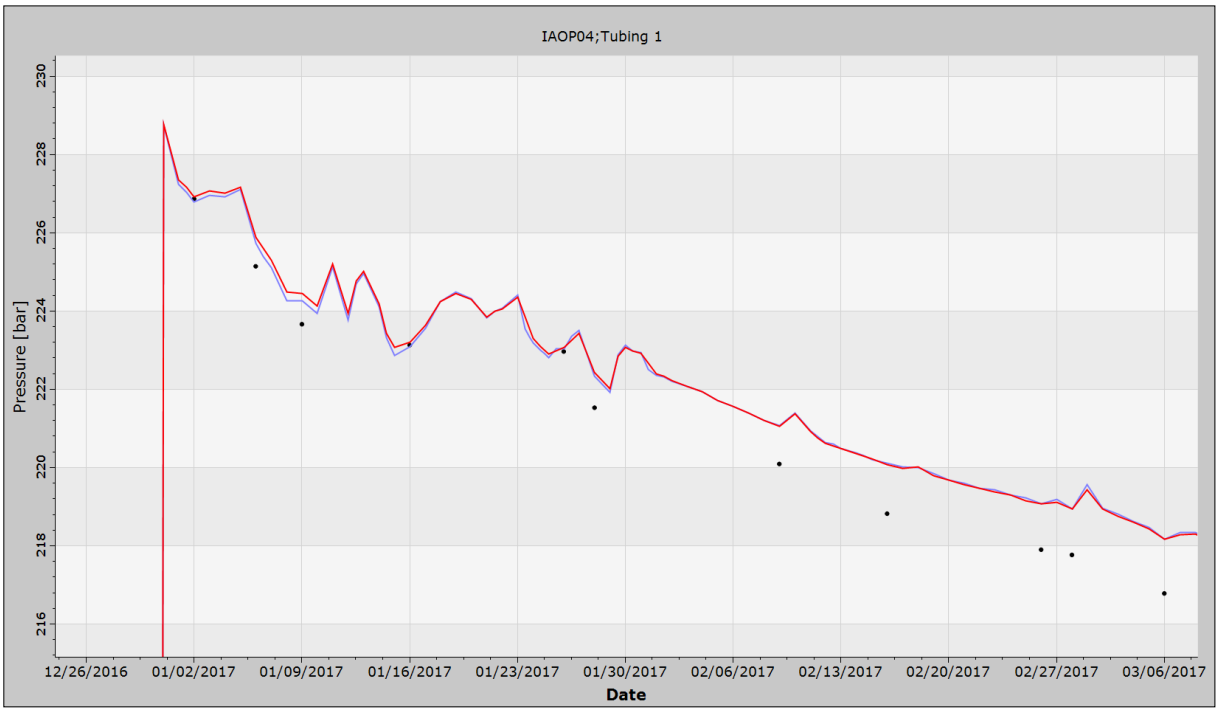

Figure 8.22 Pressure IAOP04

Black dots: Measured pressure. Blue line: Base case. Red line: History matched case

As for the pressure, the GOR of the base case and the history-matched case is almost identical at IAOP04. However, the measured GOR is considerably higher throughout most of the period (Figure 8.23). This is assumed to be, at least partly, related to the 500 m non-producing toe section of the well mentioned in chapter 7.4.1. A shorter inflow interval will naturally result in more inflow (and more depletion) of the producing areas and more coning of gas down towards the well. In addition, the missing interval is situated well below the GOC (Figure 7.10). Oil produced from this interval in the reservoir models has probably reduced the total GOR compared to the real well.

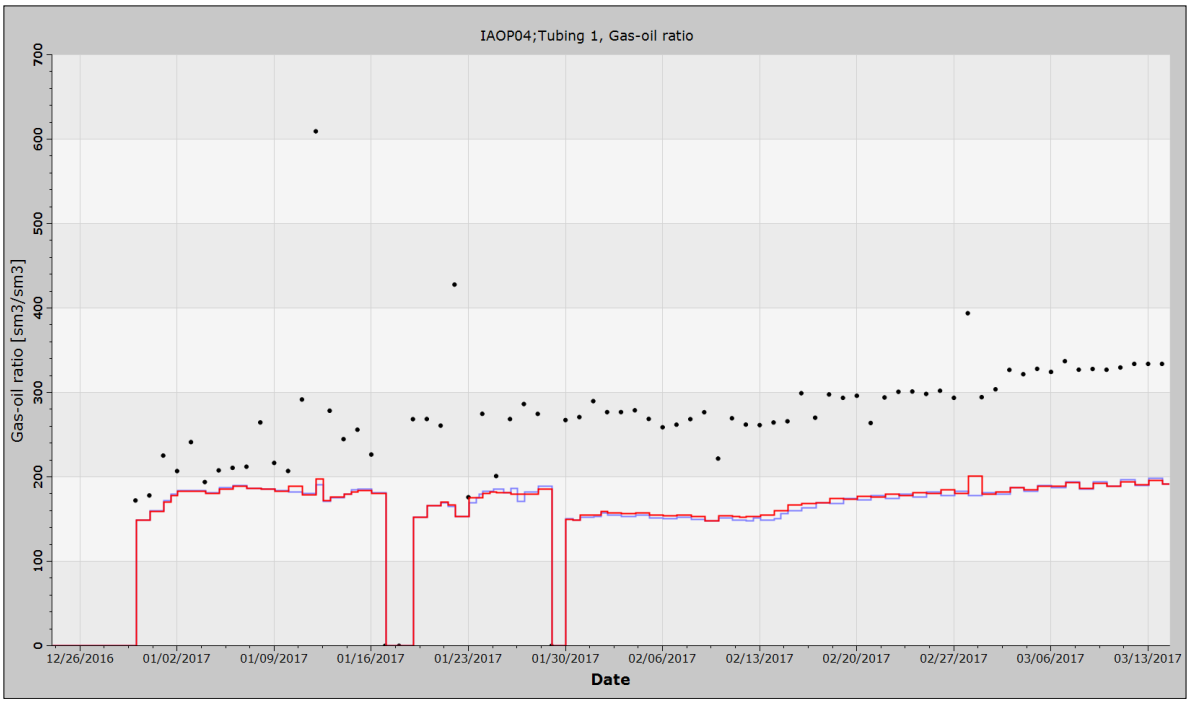

Figure 8.23 GOR IAOP04

Black dots: Measured GOR. Blue line: Base case. Red line: History matched case

Both base case and the history-matched case are able to replicate the measured pressures satisfactory at IAOP05 (Figure 8.24).

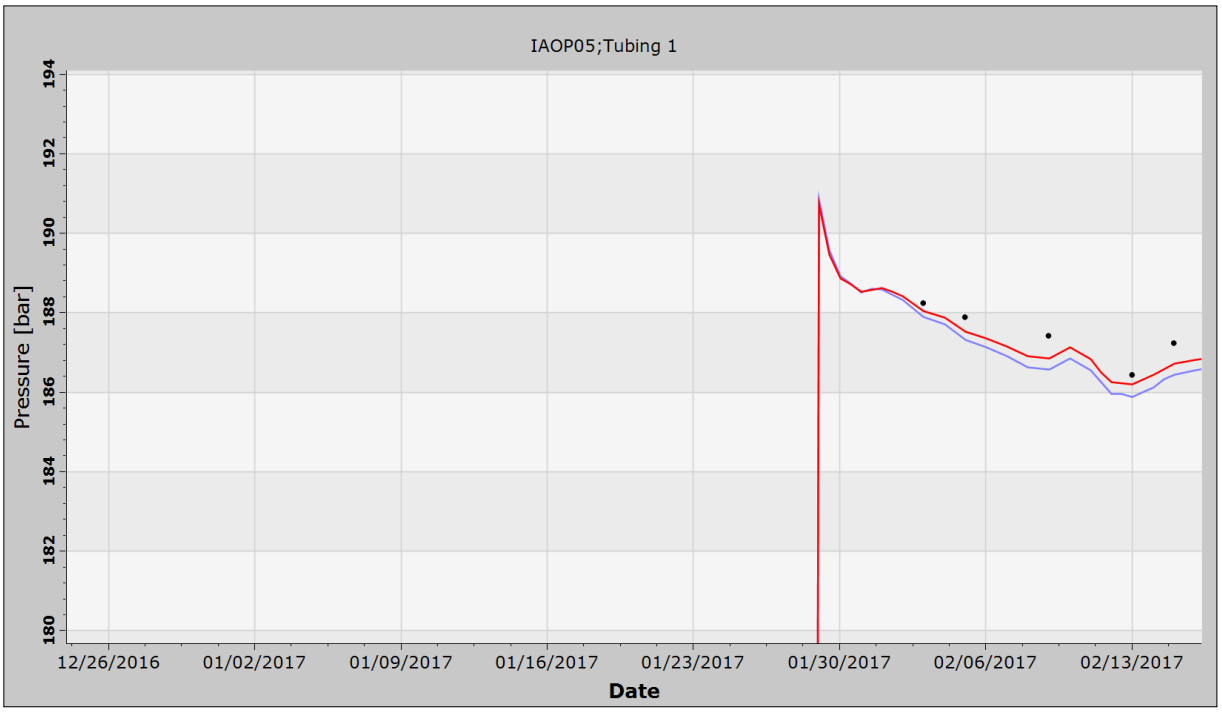

Figure 8.24 Pressure IAOP05

Black dots: Measured pressure. Blue line: Base case. Red line: History matched case

The simulated GORs from IAOP05 are at the most twice as high as the measured one (Figure 8.25). The large deviation might be related to low oil production rate, which make GOR super-sensitive to gas rate. GOR may also be influenced by how the permeability is modelled close to the well.

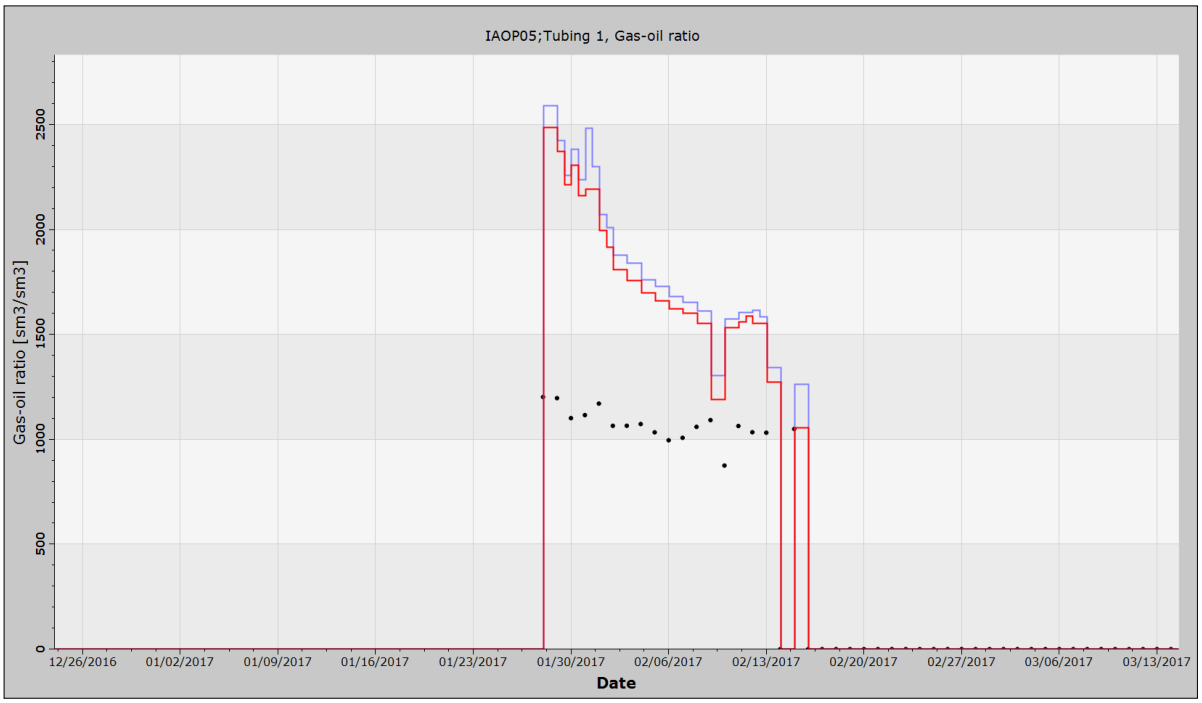

Figure 8.25 GOR IAOP05

Black dots: Measured GOR. Blue line: Base case. Red line: History matched case

As with the producers in the western part of the field (IAOP01 and IAOP02), the injector located between them, IAWI02, shows higher rate of initial depletion in the model (Figure 8.26). This behaviour supports the suggestion concerning missing volumes close to the production wells, as smaller volumes will deplete faster. The reduced aquifer permeability appears to be offset by the increased reservoir zone permeability, as the base case and history-matched model show similar depletion. A further decrease in water zone quality seems necessary in order to give as limited communication as the channel sands bring.

In the second half of the period the slope of the pressure curve (i.e. the rate of depletion) in the model becomes similar to the measured one, which indicates that similar volumes are seen.

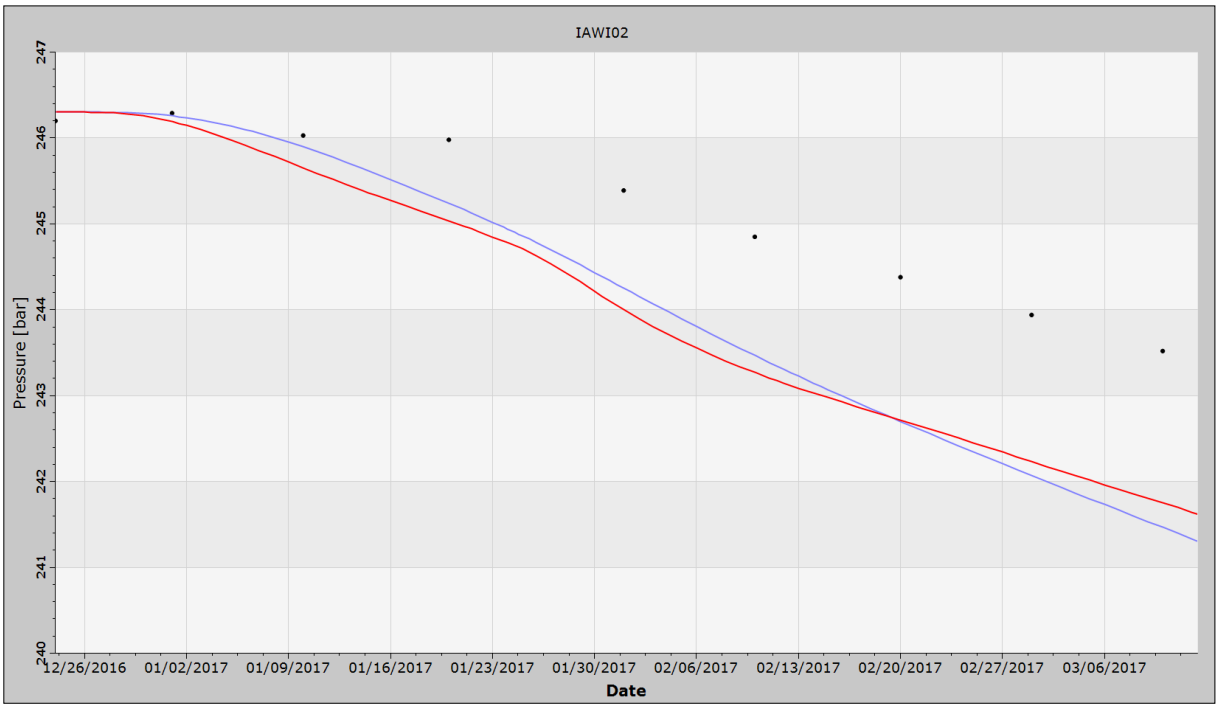

Figure 8.26 Pressure IAWI02

Black dots: Measured pressure. Blue line: Base case. Red line: History matched case.

The pressure development of IAWI04 in the history-matched model follows the measured one very close (Figure 8.27). The reduction in aquifer permeability has managed to mimic the low effective permeability set up by the low NTG fluvial channels.

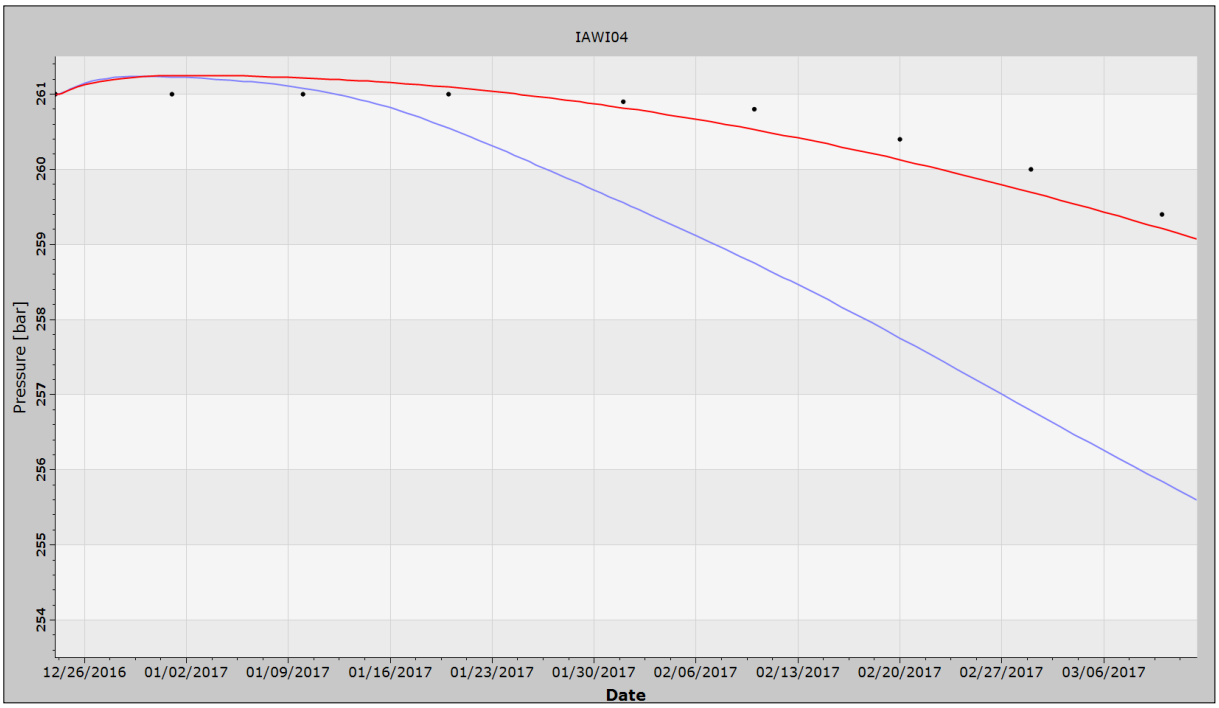

Figure 8.27 Pressure IAWI04

Black dots: Measured pressure. Blue line: Base case. Red line: History matched case

At IAWI06 the depletion rate is a bit too high in both the base case and the history-matched case compared to the measurements. The pressure drop is reduced in the matched case, but not sufficiently. The fluvial channels around the well seem to be very little connected, since the reduction in aquifer permeability is insufficient in hindering communication.

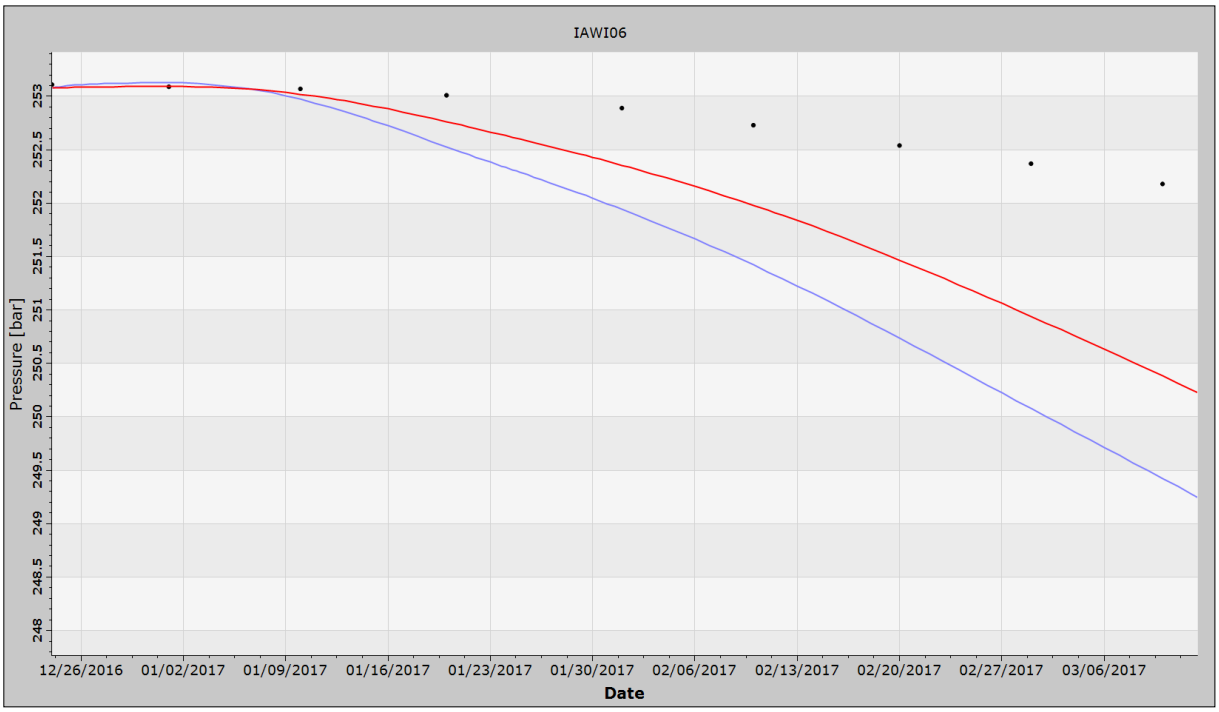

Figure 8.28 Pressure IAWI06

Black dots: Measured pressure. Blue line: Base case. Red line: History matched case

9 RFT Surveys

During drilling of the vertical injection wells IAWI03 in March 2017 and IAWI01 in April 2017, the formation pressures of the reservoir layers were measured along the well. RFT surveys typically provide valuable insight in the vertical communication, as these are the first pressure measurements with known depth performed during depletion. Reduced vertical communication will then show up as discontinuity in the pressure vs. depth plot, as equilibrium is not established. If no depletion is seen at the new injection well during production, no horizontal communication can be interpreted. No communication will of course be detrimental to the injection well, which main purpose is to serve pressure support.

9.1 IAWI03

The vertical water injector IAWI03 was drilled March 2017. Top reservoir was found at 2434 m TVD, only about 7 m shallower than what was expected. The entire reservoir interval was at first assigned to the Skagerrak 2 formation, although some meters of Sleipner were anticipated at the top. Later the upper part was however interpreted as Sleipner based on a biostratigraphic (the use of microfossils to determine age and depositional environment) study.

The RFT survey performed in IAWI03 showed pressure points falling on a water gradient down through the reservoir (blue in Figure 9.1). This confirms a water filled reservoir at this location and that there exist vertical communication between the layers. And in particular: there is communication between Sleipner and Skagerrak 2. As seen in the figure, the findings are in line with both the base case (red) and history-matched model (green).

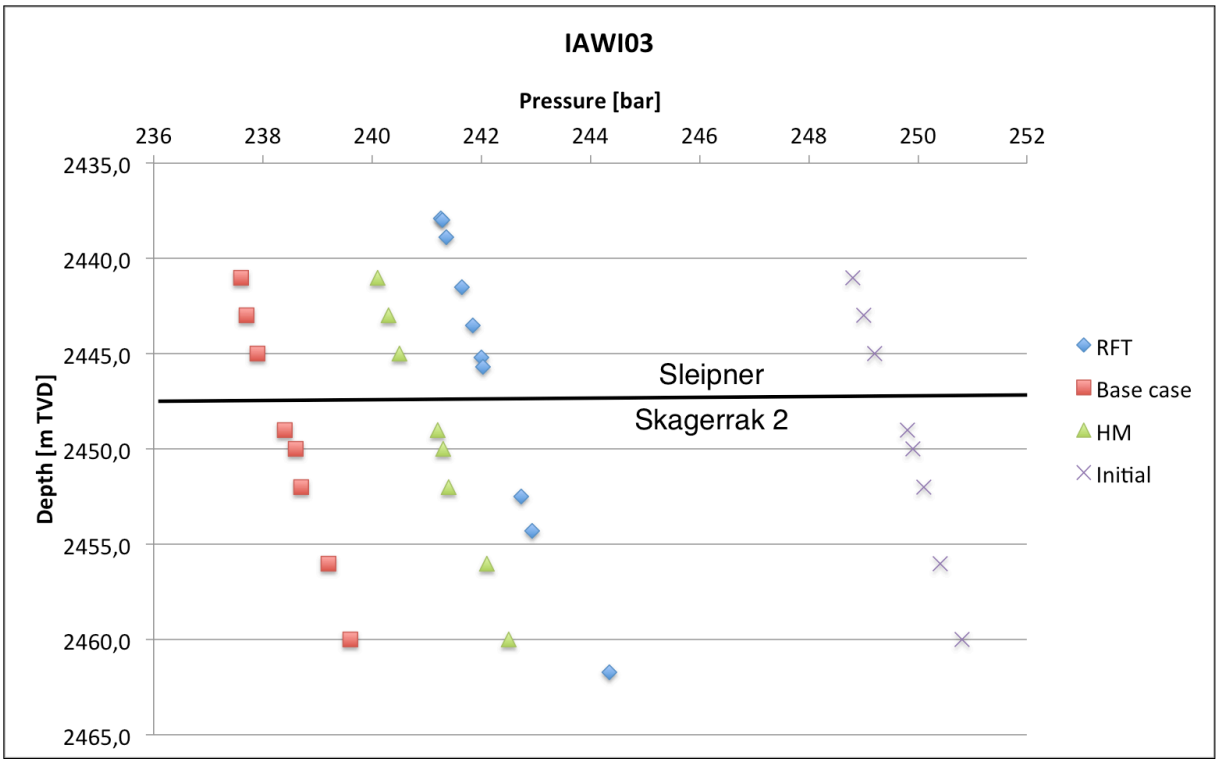

Figure 9.1 IAWI03 RFT pressures, initial pressures and simulated pressures

The initial pressure at the top reservoir at IAWI03 (2441 m TVD) is assumed to be about 249 bar (purple in Figure 9.1). The observed pressure of 242 bar gives 7 bar depletion, and promises communication between the injector and one or more of the neighbouring producers (IAOP02 and/or IAOP03). The pressure change is also similar to those seen in the simulated cases, 9 and 11 bar, for the history-matched- and base case respectively. Hopefully this means that the models are not too far from a representative one.

Although the history-matched model predicted the depletion more accurate than the base case, the difference is too small to draw conclusions regarding the predictive power of the models.

9.2 IAWI01

The vertical water injector IAWI01 was drilled April 2017. Top reservoir was found at 2450 m TVD, only about 5 m deeper than what was predicted. The upper part of the reservoir was assigned to Statfjord, contrary to the Sleipner that was expected. Further down Skagerrak 2 was found, as expected.

The RFT survey performed in IAWI01 showed pressure points forming two separate water gradients (blue in Figure 9.2). The discontinuity clearly suggests two separate pressure regimes. The four upper pressure points are proposed to belong to the Statfjord, while the

three lower points belong to the Skagerrak 2. Thus, it is inferred limited communication between Statfjord and Skagerrak 2 in this area (north-west).

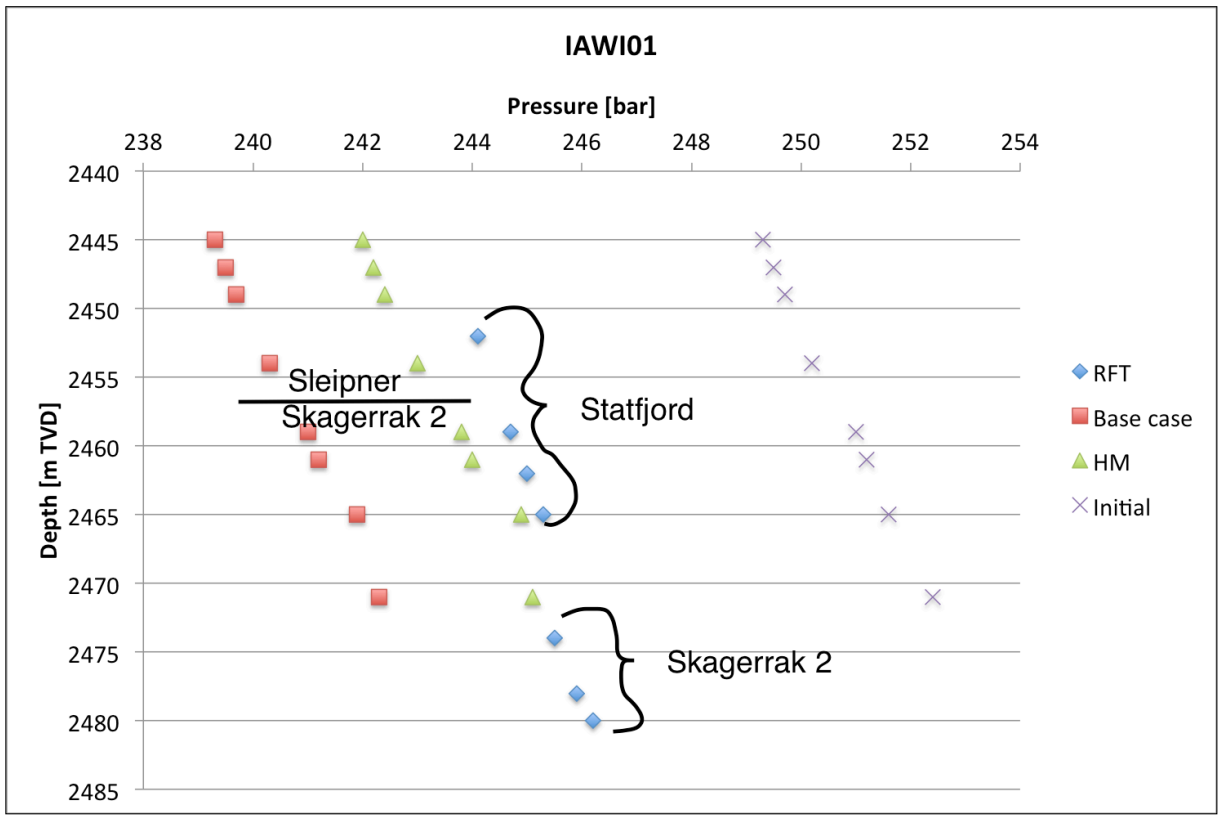

Figure 9.2 IAWI01 RFT pressures, initial pressures and simulated pressures

As seen in the figure, the finding is not in line with the base case (red) or history-matched model (green), which both form one water gradient. However, as mentioned in chapter 0, the lower part of Statfjord is believed to contain little sand, and poor vertical communication is thus not unlikely. A similar Statfjord interval is not found in the nearest well, IAOP01, which is located further south. The natural interpretation is therefor that Statfjord and the associated barrier are present only in the northern part of the western part of the field.

The next geomodel (and reservoir model) will have to include some kind of barrier to vertical flow, for instance a reduction of the transmissibility multiplier between the deepest Statfjord layer and the shallowest Skagerrak 2 layer. This reduction will be more appropriate than a change in the vertical to horizontal permeability ratio (k_v/k_h), which there is no evidence of.

The initial pressure at the actual top reservoir at IAWI01 (2450 m TVD) is assumed to be about 250 bar. The observed pressure of 244 bar gives 6 bar depletion, and promises communication between the injector and the neighbouring producer (IAOP01) through Statfjord. That is also true for the lower Skagerrak 2, where the depletion is even greater. The

difference in depletion rate may be caused by difference in drainage volume, permeability, etc.

Despite the absence of a horizontal barrier, both the history-matched- and base case models matched the depletion at this location reasonably good. With the new knowledge about the vertical communication at hand, new models will possibly give different results. Thus, no conclusions can be drawn regarding the predictive power of the models.

10 ResX Assisted History Matching Study

In April and May 2017 the Ivar Aasen subsurface team of Aker BP, with support from Resoptima, performed a computer assisted history matching and forecasting study using the ensemble based ResX software. The aim of the study was to integrate all available production data into the current reservoir model. A forecast to quantify the uncertainties associated with production profiles resulting from the ensemble of history-matched models.

The general impression left among the members of the subsurface team of Ivar Aasen was that not enough time had been set aside for the ResX study. In addition, technical problems slowed the process. With a tight deadline for delivering of a large ensemble of history-matched models, a sufficient amount of time was not at hand to properly learn to use the software and quality check all inputs and steps of the process.

As a result of the sparse time, the fact that the production wells were modelled without ICDs was first encountered after the study was completed. By then there was not enough time to do the study over again. Modelling the wells as open hole during the history matching is of course adding another layer of uncertainty to the results. Production wells are completed with ICDs to control the inflow to the well, and ensure production from the entire perforated interval. Therefore, the production in the models might be more concentrated in the wells heel sections.

The rush to complete the study resulted in that only a set of standard plots was made. No in-depth analysis of the results was performed. A selection of the plots is nevertheless examined in the following, to illustrate what results are produced, and possibly spot some trends.

Normally the history-matched ensemble is analysed closely and significant changes are confirmed. With more time at hand, Resoptima recommend to make use of the knowledge gained from the creation of the first ensemble, and the results of the history matching of them, to produce a new ensemble.

10.1 History Matching Parameters

As explained in chapter 0 concerning ResX, the foundation of the AHM study is laid in the construction of an ensemble of reservoir models spanning all possible outcomes given the available information, and the related uncertainty. Since the ensemble is made with this aim, the initial models will produce widely different results for bottom hole pressures, GOR etc. The models may also deviate significantly from the measured values. The history matching

algorithm will then tune all models until they resemble the actual production data more accurately.

10.1.1 Bottom Hole Pressure

The BHP of all the wells before and after history matching is shown in Figure 10.1 and Figure 10.2, respectively. In some of the wells the BHP matched reasonably well already in the initial ensemble (with pressure on the y-axis going from 0 to 300 bar). In the less consistent wells, the history matching procedure manages to improve the match to an acceptable level.

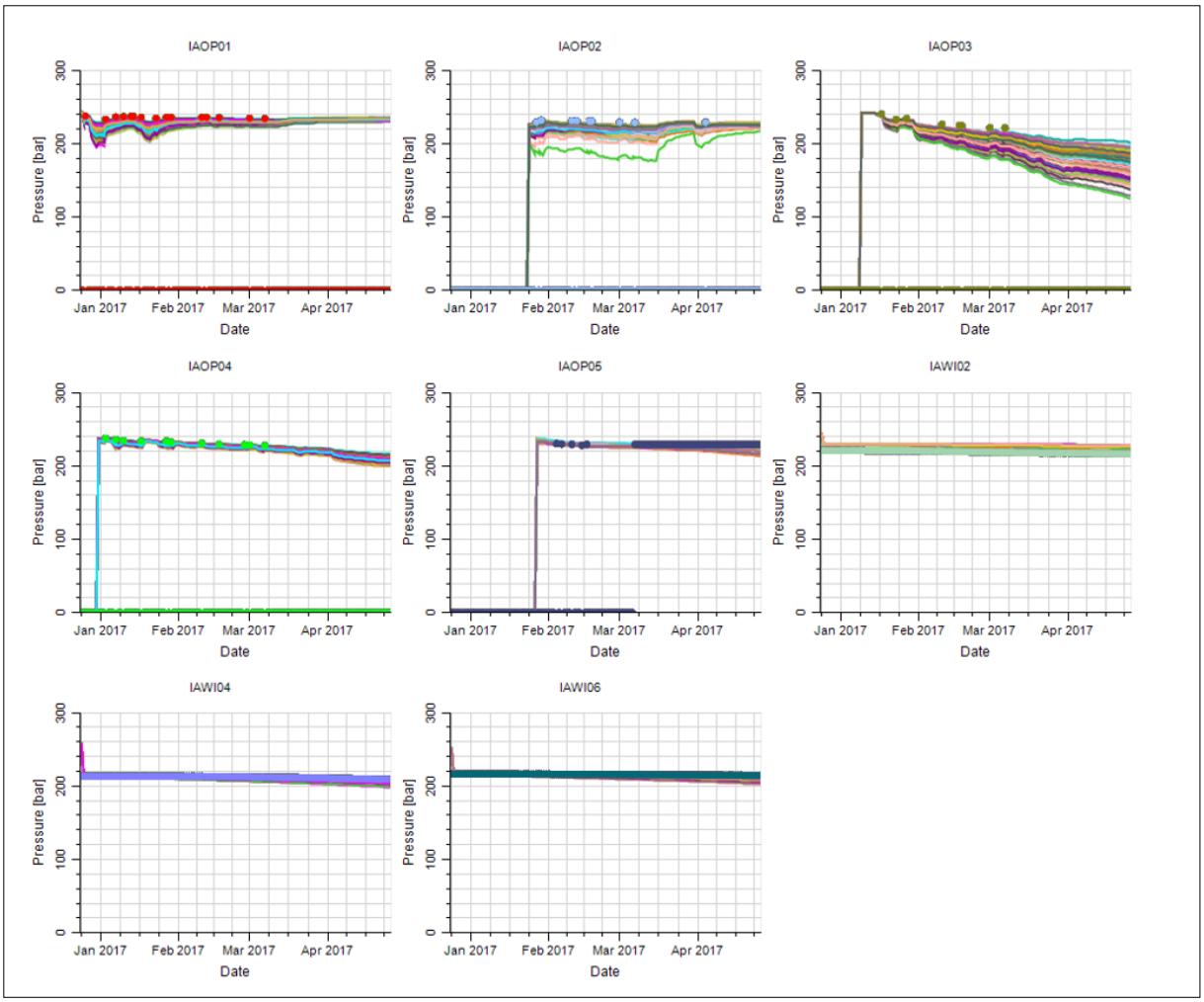

Figure 10.1 Bottom hole pressure in the wells before history matching

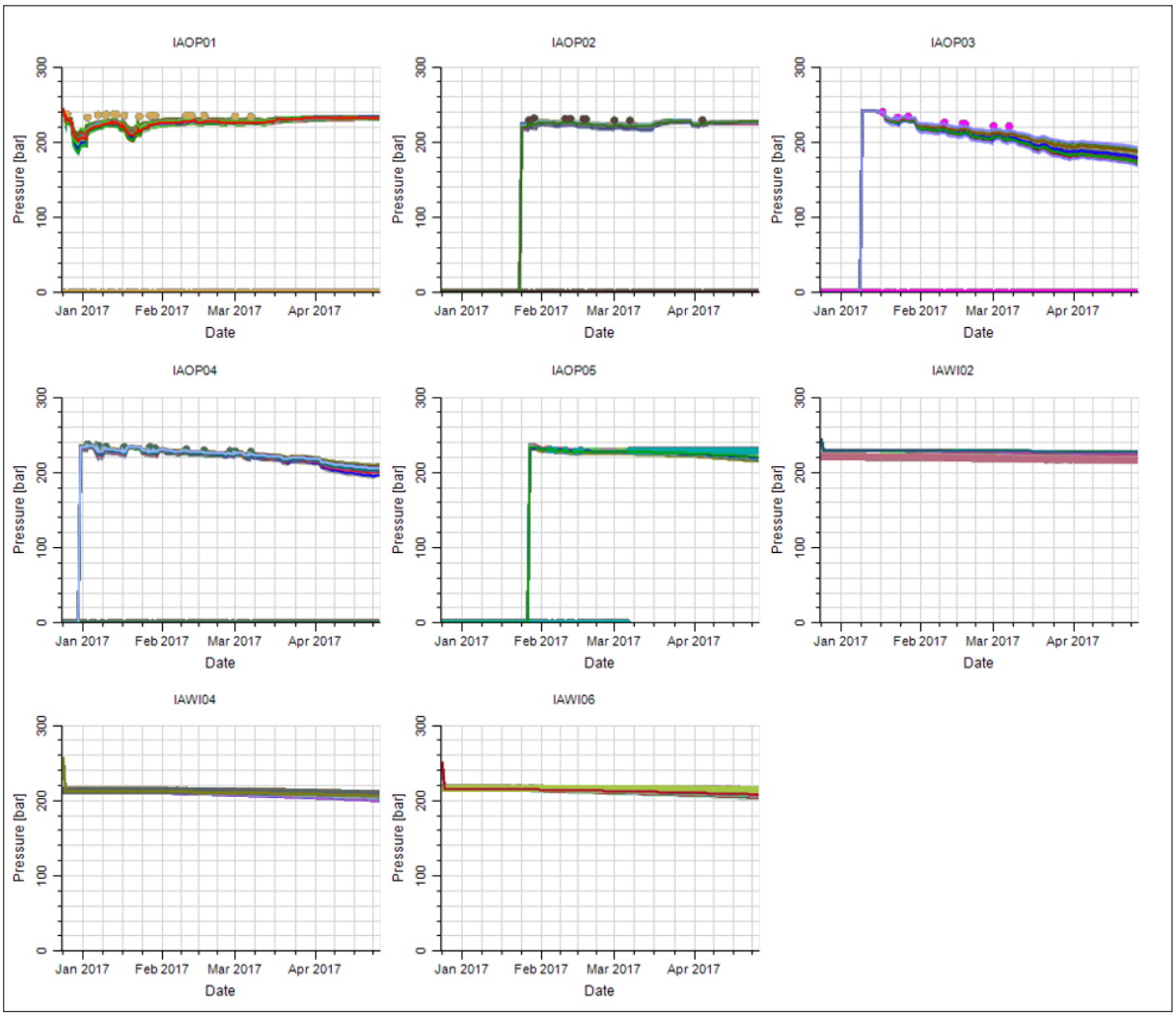

Figure 10.2 Bottom hole pressure in the wells after history matching

As in the manual history matching, the west and south production wells IAOP01, IAOP02 and IAOP03 have experienced the largest changes in bottom hole pressure. This suggests the most effective changes are done in these areas.

10.1.2 Gas/Oil Ratio

The GOR of all the production wells before and after history matching is shown in Figure 10.3 and Figure 10.4, respectively. Most of the producers experienced a wide range of GORs in the initial ensemble. Through the adjustments of the ensemble, ResX succeeded in forcing the GORs much closer to what was measured in the real wells.

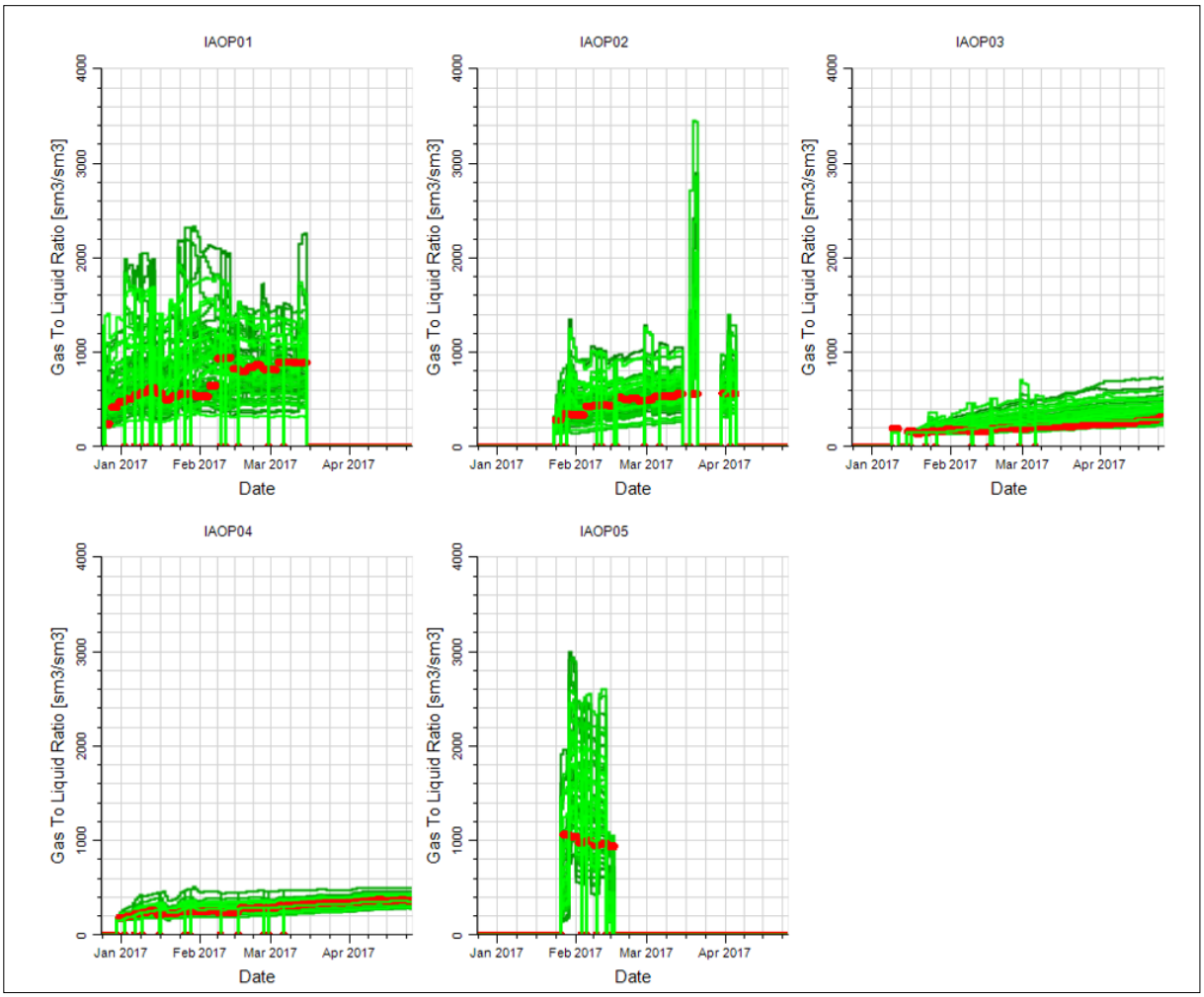

Figure 10.3 GOR in the wells before history matching

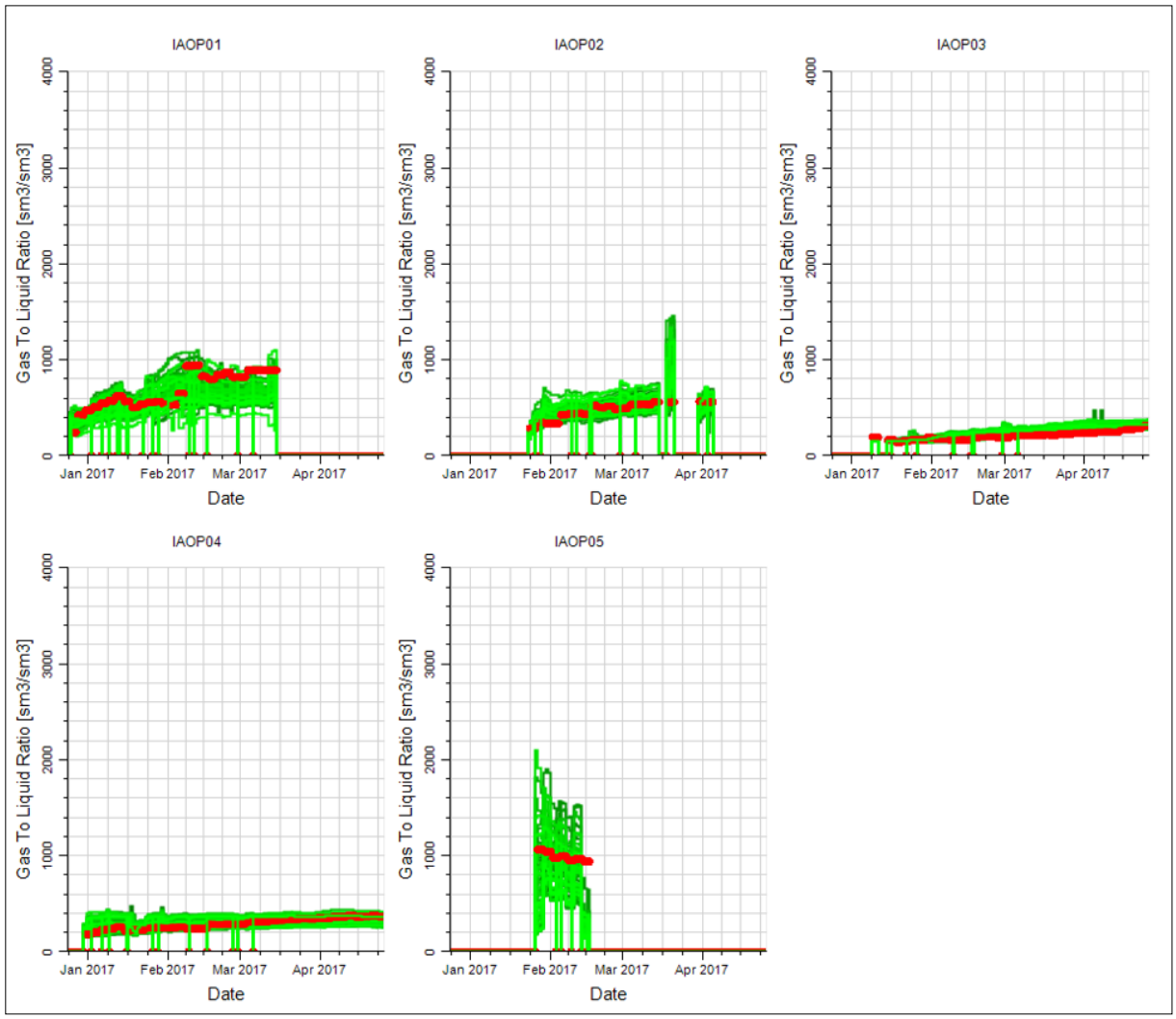

Figure 10.4 GOR in the wells after history matching

Given the rough axis in plots of BHP and GOR for the Ivar Aasen wells, it seems like ResX is better at improving GOR than BHP.

10.2 History Matching Variables

In order to obtain the history-matched ensemble, variables like fault transmissibility multiplier, permeability and porosity are adjusted. Next follows a review of some of the adjustments performed. Where applicable, the results are compared to those found in the manual history matching.

10.2.1 Fault Transmissibility Multiplier

The transmissibility multiplier of each fault in the reservoir model is adjusted individually in the assisted history matching procedure. This is in contrast to the approach selected for the manual history match, where a common multiplier for all the faults was selected for each

simulation run. Individual transmissibility multipliers are of course more realistic. However, to keep track of vast amounts of adjustments simultaneously is an overwhelming task. This is a classic limitation for manual history matching.

After the assisted history matching, a few faults were categorized as sealing since they ended up with a transmissibility multiplier smaller than 0.001. The sealing faults are shown in Figure 10.5. Among the faults found sealing, three are situated very close to wells. The production wells IAOP01 (north-west) and IAOP02 (south-west) are virtually cut by sealing faults. This can be an effective change, since it efficiently reduces production. The sealing fault neighbouring the IAWI04 (sout-east) will help reduce depletion related to heavy production at IAOP03.

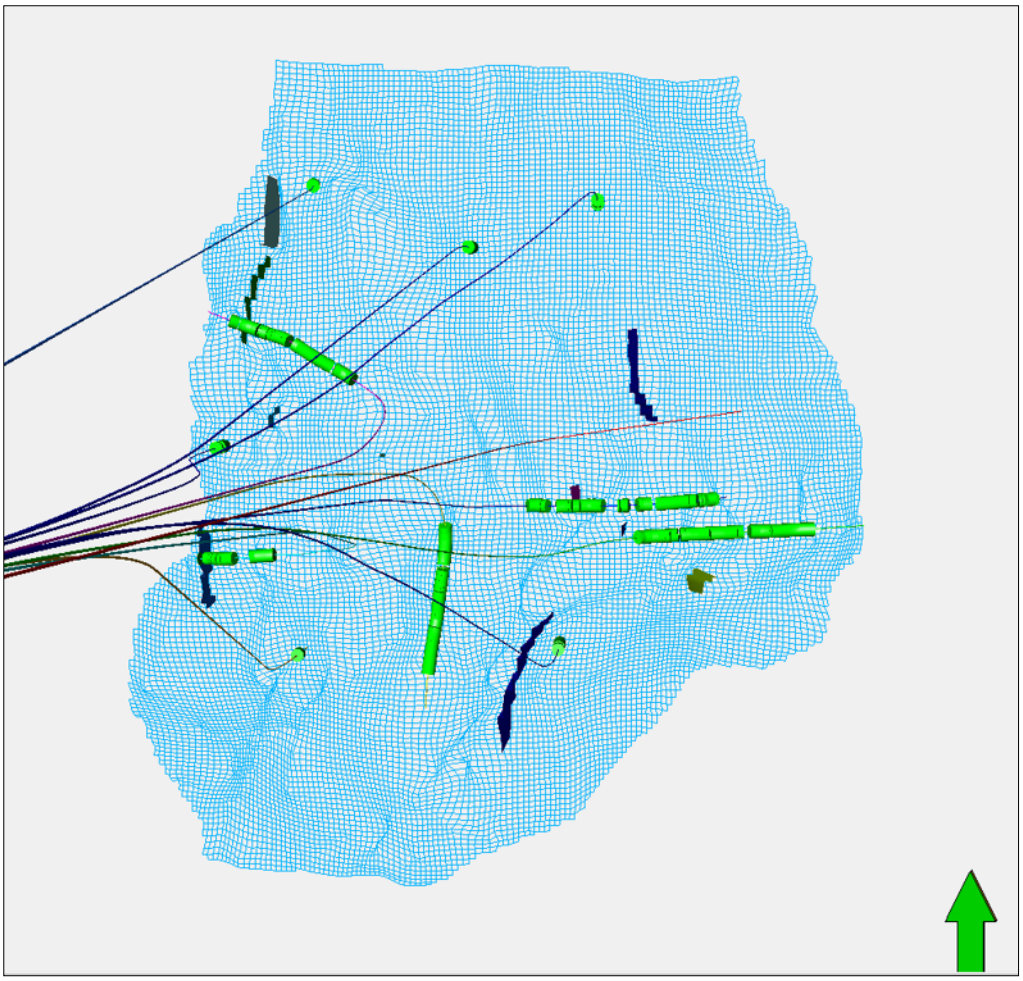

Figure 10.5 Sealing faults after history matching

The sealing fault seen in the central eastern part of the field in Figure 10.5 is worth to notice. The north-south direction of the fault makes it parallel to fluid flow towards IAOP04 and

IAOP05. The impact it has on the flow between the injector to the north and the producers to the south is thus questionable.

A substantial amount of the field's faults were assigned with a transmissibility multiplier larger than 0.1, and are thus considered open (Figure 10.6). However, as discussed earlier, a fault might end up sealing if the fault displacement prevents contact between good reservoir zones on each side of the fault. This is true for many of the faults seen in the figure. Especially the two faults with north-south direction in the centre of the field have large displacements, and will stay sealing no matter how high the transmissibility multipliers are set.

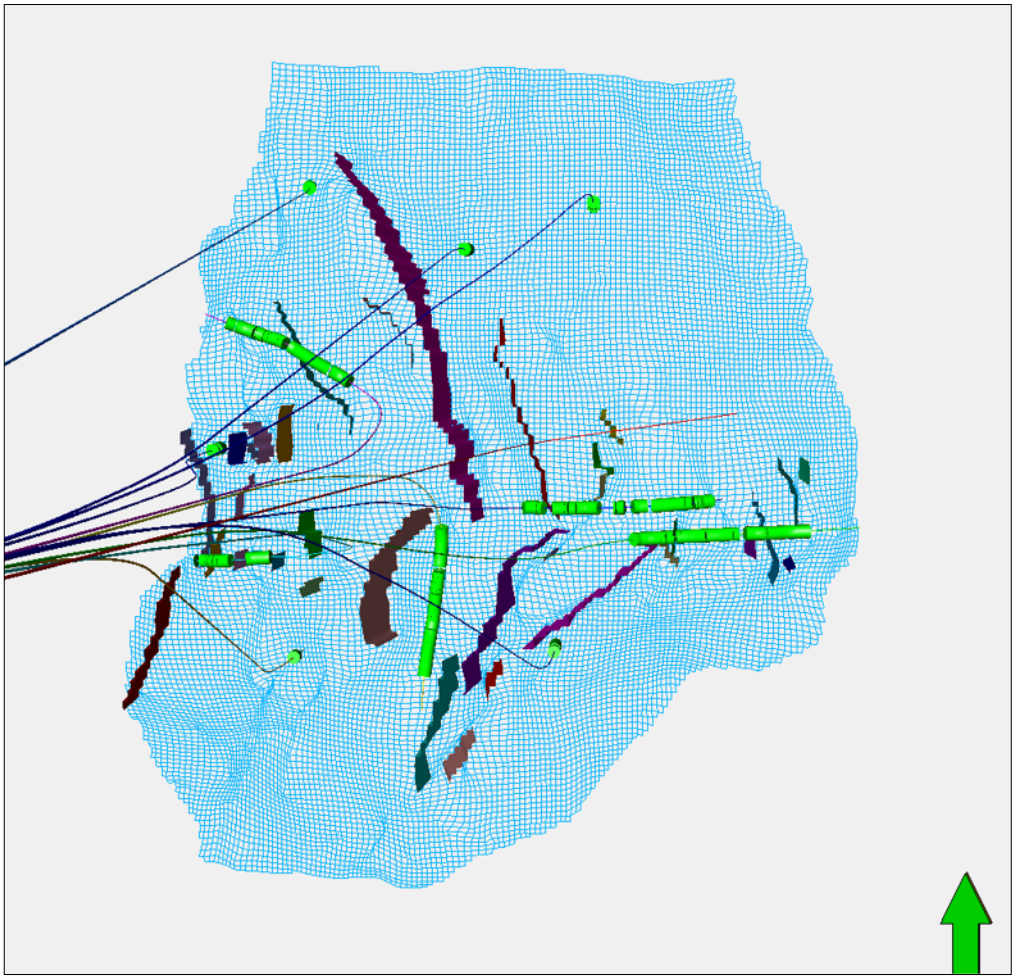

Figure 10.6 Open faults after history matching

There exist about 150 faults in the grid used in this study. The majority of the faults did thus end up with a transmissibility multiplier somewhere in between, i.e. partly sealing. This general result is in line with the results of the manual history match, where all faults ended up

with transmissibility multiplier equal to 0.1. The trend towards more open fault seen in the manual study, is however not evident.

10.2.2 Porosity

During the assisted history matching, the porosity of each individual cell in the model was subject to change. The porosity distribution in the P50 model, representing the ensemble average, was modified through the conditioning of the ensemble to production data. The average of the initial ensemble will be similar to the base case model in the manual history matching. As seen in Figure 10.7, the number of cells with porosity less than 2 %, in practice inactive, increased substantially. At the same time, the share of cells with porosity between 6 and 16 % decreased. However, the number of high porosity cells, between 17 and 24 %, increased significantly.

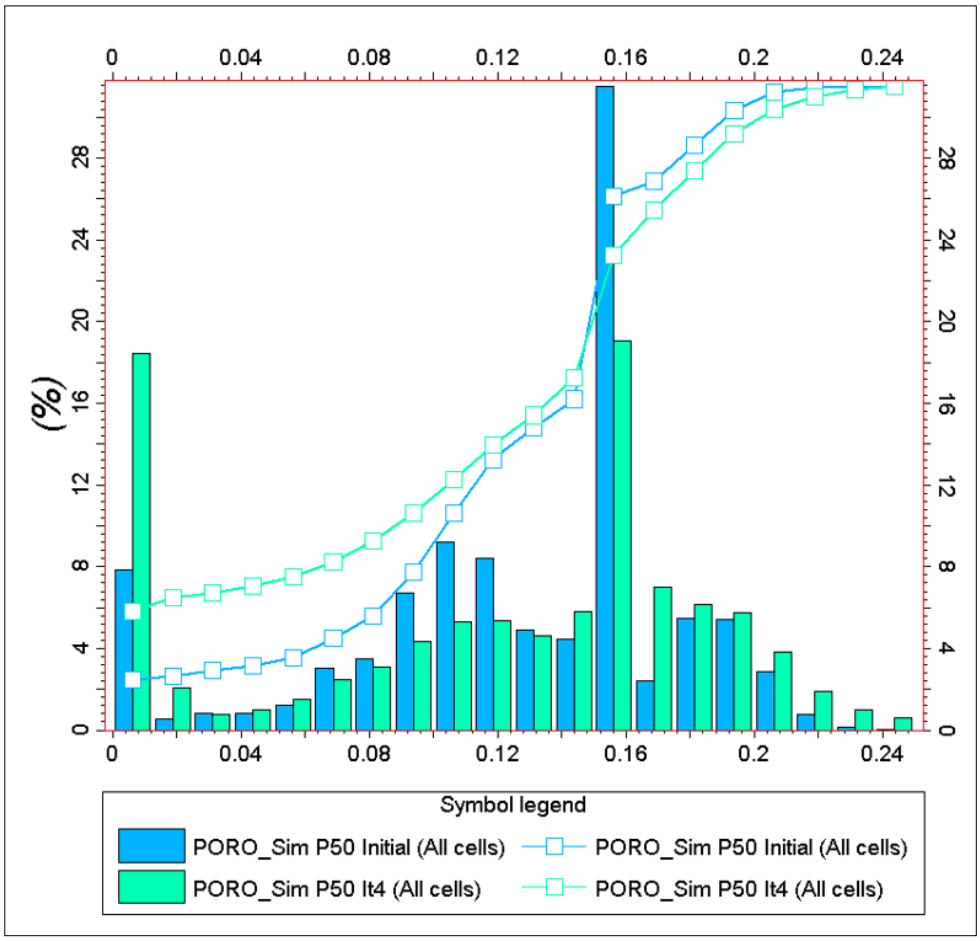

Figure 10.7 P50 porosity distribution

Before (blue) and after (green) history matching

In the manual history matching, adjustments of the porosities were tried avoided in order to reduce the number of variables. When done, the porosity of all cells inside an area, or box, was adjusted with a common factor to represent greater reservoir volumes. In the final match, the porosity in Sleipner and Skagerrak 2 in the western part of the field was increased with a factor 2, to add reservoir volumes around the producers IAOP01 and IAOP02. Similarly, the significant increase in the high end of porosity suggests volumes have been added to the reservoir in order to reduce the depletion at the producers seen in the initial ensemble.

10.2.3 Permeability

The permeability of each individual cell was also adjusted during the process. The P50 permeability distribution, representing the ensemble average, was modified through the conditioning of the ensemble to production data. As seen in Figure 10.8, the number of cells with permeability of about 0.0001 mD, in practice inactive, increased considerably. At the same time the share of cells with permeability between 0.1 and 10 mD decreased drastically.

These changes will probably not affect depletion around a production well, as the flow capacity of cells with permeabilities below 10 mD is rather limited anyway. However, if the cell is situated close to an injection well the change might be substantial.

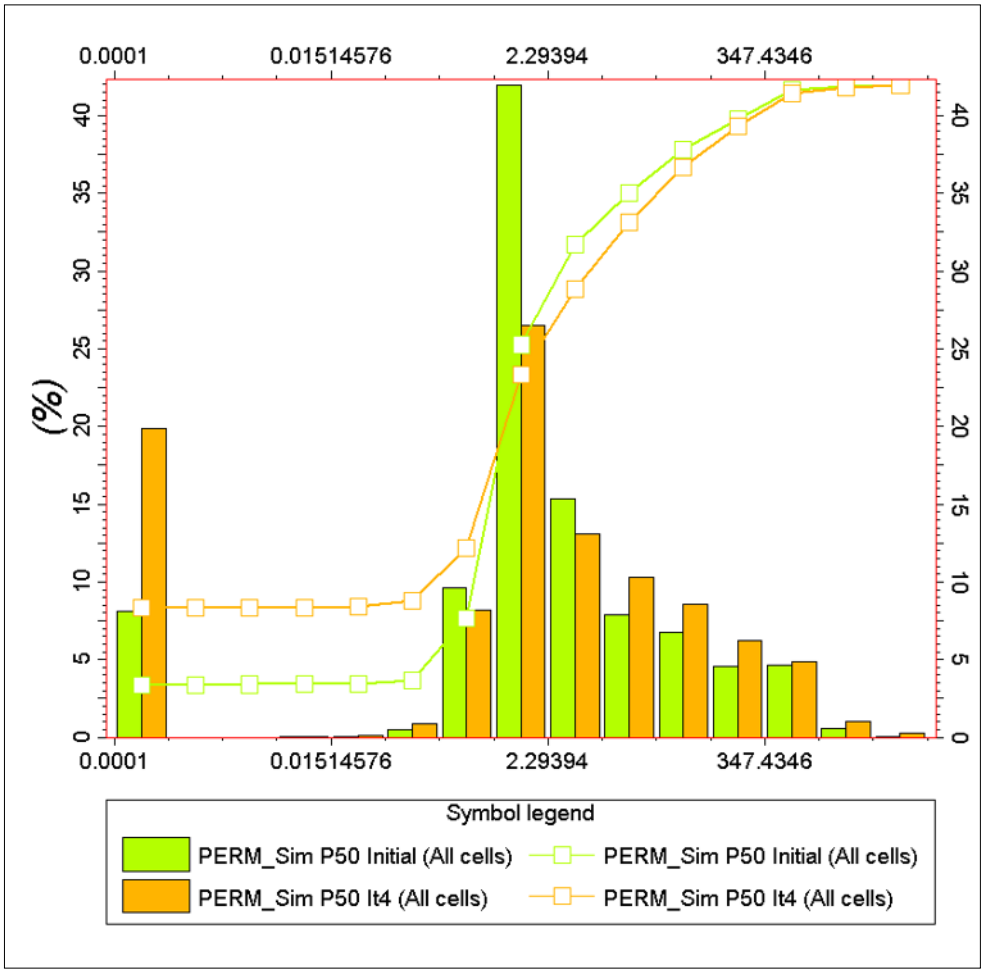

Figure 10.8 P50 permeability distribution

Before (green) and after (orange) history matching

The significant increase in number of cells with permeability above 10 mD will most likely contribute to the reservoir communication of the field. Increased permeability does not automatically increase communication, as the cell need a permeable neighbouring cell to allow flow. However, the AHM algorithm is (in theory) set up such that changes are avoided when they have little impact.

As for the porosity, changes of permeability were conducted by adjusting the permeability of all cells inside an area, or box, with a common factor in the manual history matching. In the final match the permeability was reduced by a factor 10 in the aquifer, and increased by a factor 2 in Sleipner and Skagerrak 2 in the western part of the field.

The aggregate nature of P50 makes it hard to confidently compare the changes made in the assisted and manual matching. However, for the algorithm to improve the BHP matches at the west and south producers, the permeability was probably increased in these areas. This will be further deliberated in the following subchapter.

10.2.4 Sand Quality

The reservoir simulator shows little interest in what geologic facies is assigned to each grid cell in the reservoir model. However, the simulator uses the permeability (and porosity etc.) in the flow calculations. Facies with similar permeability are therefore lumped together into the three categories; poor sand, medium sand and good sand, when setting up the ResX study.

In the P50 model of the initial ensemble, the probability of encountering good sand in Sleipner was about 80 % almost anywhere the zone is found, as shown in the left part of Figure 10.9. In the right part of the figure, the history-matched counterpart indicates only minor changes. A slightly lower probability of good sand in an area in the central eastern part of the field encourages further investigation of the permeability there. The permeability in rest of Sleipner in this model does not seem to work against the imitation of production data (as they are not changed). One would then assume that the permeability in Sleipner is reasonably well understood.

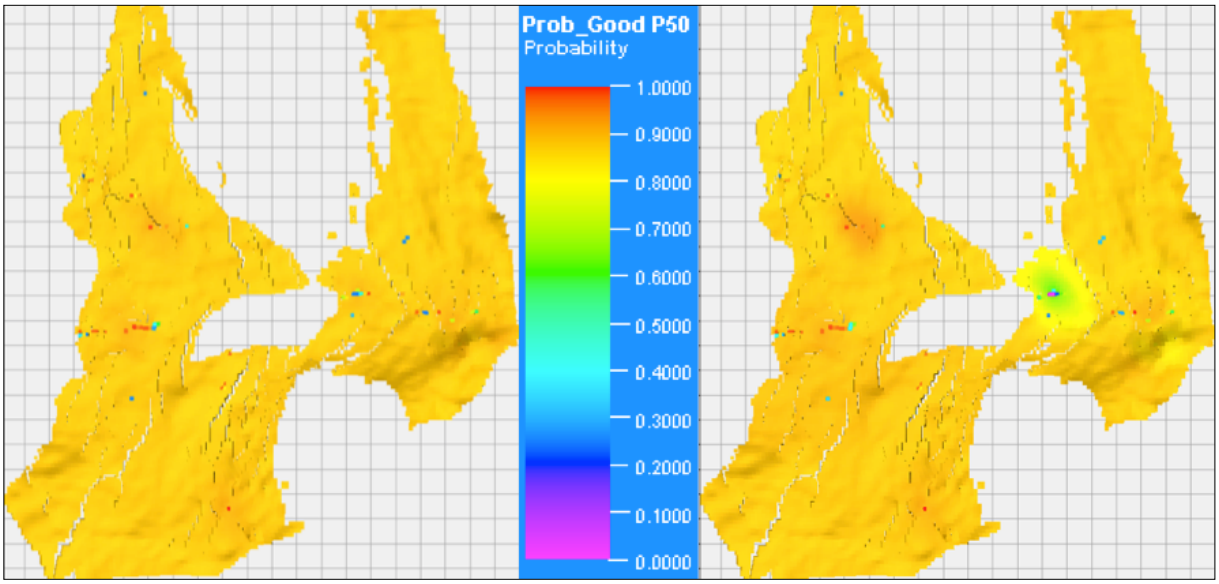

Figure 10.9 Probability of good sand in Sleipner

Before (left) and after (right) history matching

The plots are hardly comparable to the changes done in manual history matching. The increased permeability in the west in the manual study would not show up in similar (before and after) maps. A grid cell that is already categorized as good sand will not change category if the permeability is doubled.

In the P50 model of the initial ensemble, the probability of encountering medium sand in underlying Skagerrak 2 was about 25 % almost anywhere the zone is found, as shown in the left part of Figure 10.10. In the right part of the figure, the history-matched counterpart indicates several changes. A lower probability of medium sand in areas in the central eastern and western parts of the field is interpreted as higher probability of good sand. Large parts of the area between the west producers IAOP01 and IAOP02 have experienced a reduction in probability of medium sand to below 20 %. This corresponds to the area modified in the manual history matching in order to reduce the depletion at the production wells. It seems like also ResX increased permeability with the goal of improving the match.

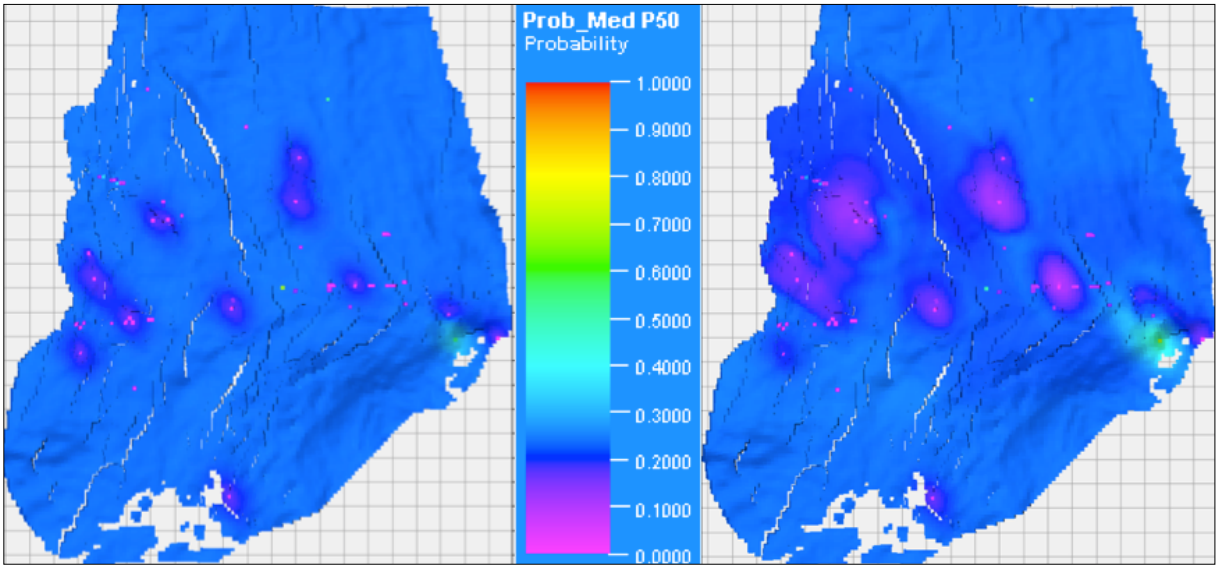

Figure 10.10 Probability of medium sand in Skagerrak 2

Before (left) and after (right) history matching

The study also concluded that the areas around the injectors need less communication or poorer permeability in order to counteract the rapid depletion seen in the model.

10.2.5 Volumes

As a consequence of the adjustments of the porosity of the grid cells throughout the field, the static in place volumes are subject to change. The initial ensemble of the study contained models with a wide range of volumes, but although fairly concentrated around the P50 value (Figure 10.11). The high upper and low lower values of the ensemble stem from the porosity ranges that are set in order to capture uncertainty. If the extremes are deemed unlikely when confronted with production data, they are adjusted.

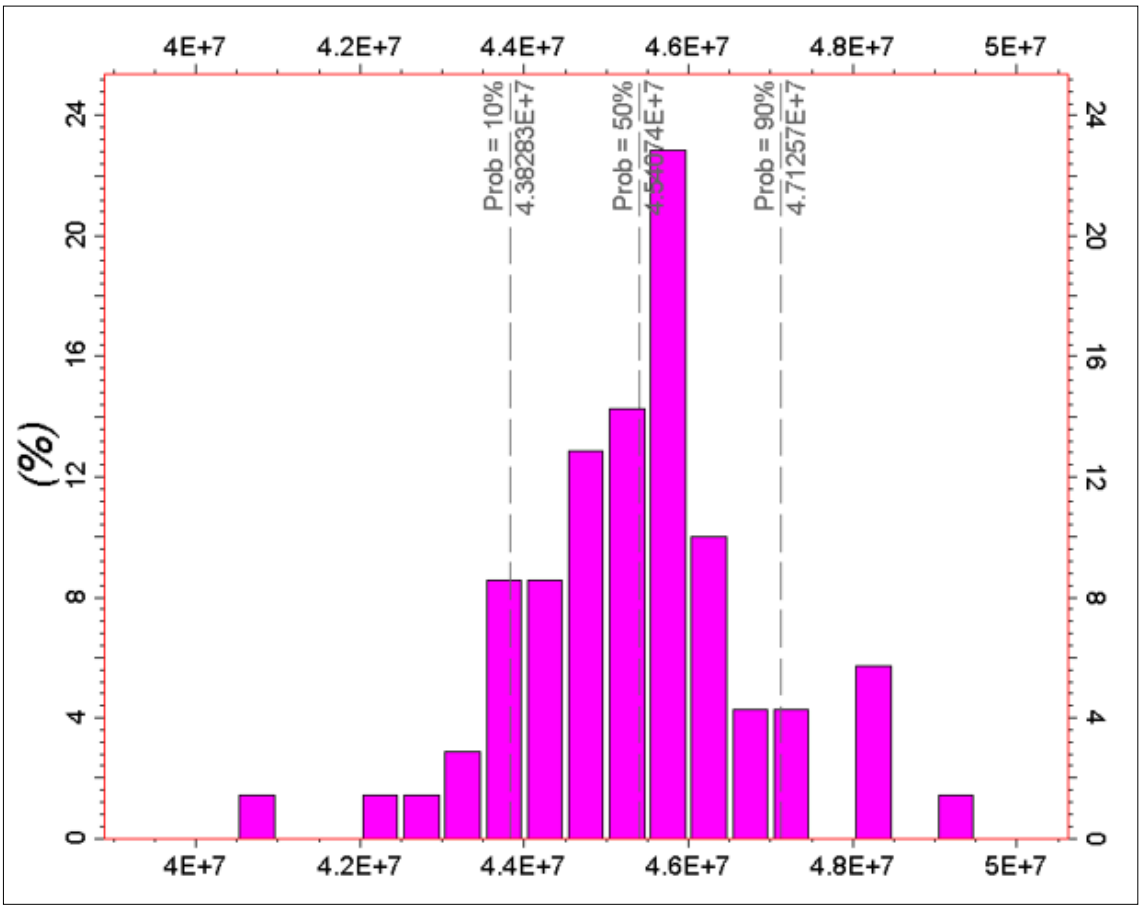

Figure 10.11 Probability distribution of static in place volumes before history matching

In the probability distribution of static volumes after history matching the P50 value is slightly increased. However, the probability is more uniformly distributed between P10 and P90 (Figure 10.12) (Be aware of inconsistent axis). The probability for the highest and lowest value seen before the history matching is now zero, and the models are generally more concentrated. This infers that the uncertainty in static volumes is reduced after conditioning to production data.

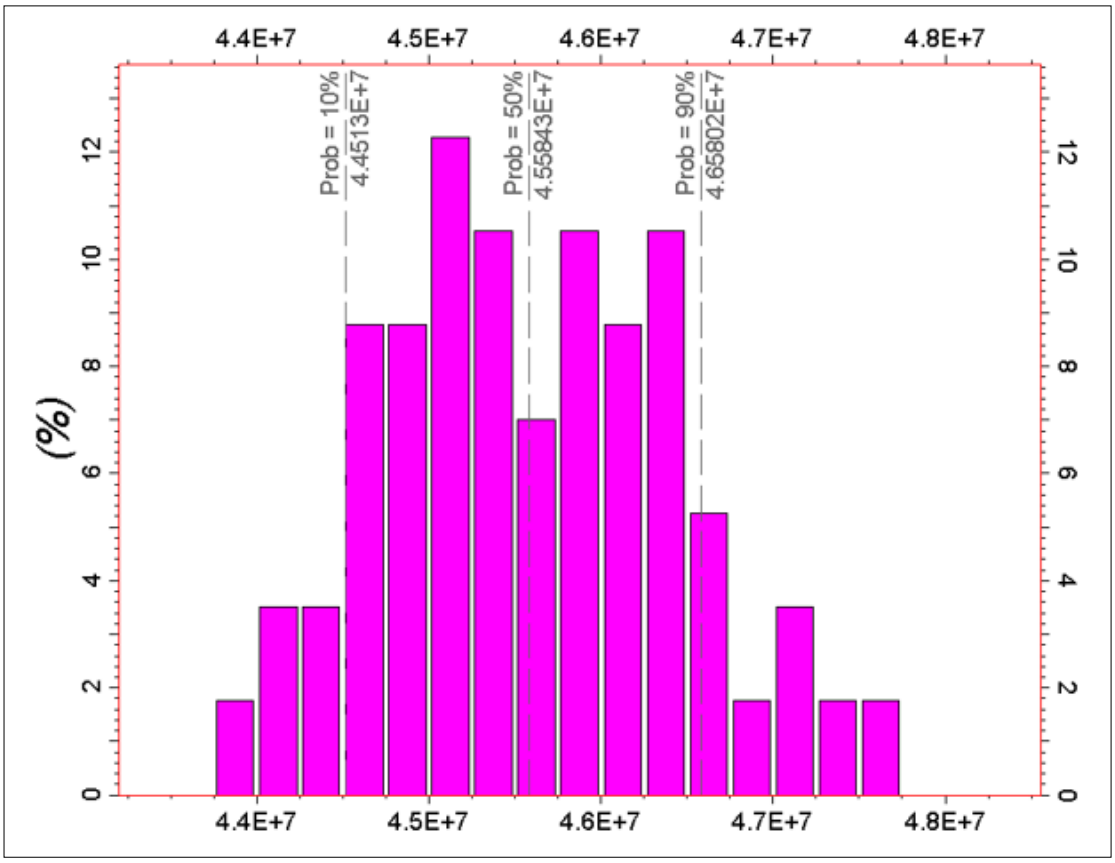

Figure 10.12 Probability distribution of static in place volumes after history matching

The dynamic (movable) in place volumes did also increase during the history matching. This is in line with the results of the manual history matching, where the reservoir volume was increased by a factor 2 (represented by a doubling of porosity) in Sleipner and Skagerrak 2 in the western part of the field.

10.3 Prediction Runs

After a successful history matching had produced an ensemble of matched models, the ensemble was used to make predictions about future reservoir performance of the Ivar Aasen field. Although all models matched the same production history, the forecasts for pressure development, oil production and WCT over the first five years of production vary widely across the ensemble.

10.3.1 Field Pressure

From the initial pressure of the field of 246 bar, the pressure of all models fall to about 230 during the matching period, since all models are conditioned to the same pressure data. Figure 10.13 shows that as soon as the prediction period starts, the differences between the models

became apparent. By the end of the five years of production shown in the figure, the field pressure in the models ranges from 155 to 235 bar, with the majority of the models between 170 and 220 bar.

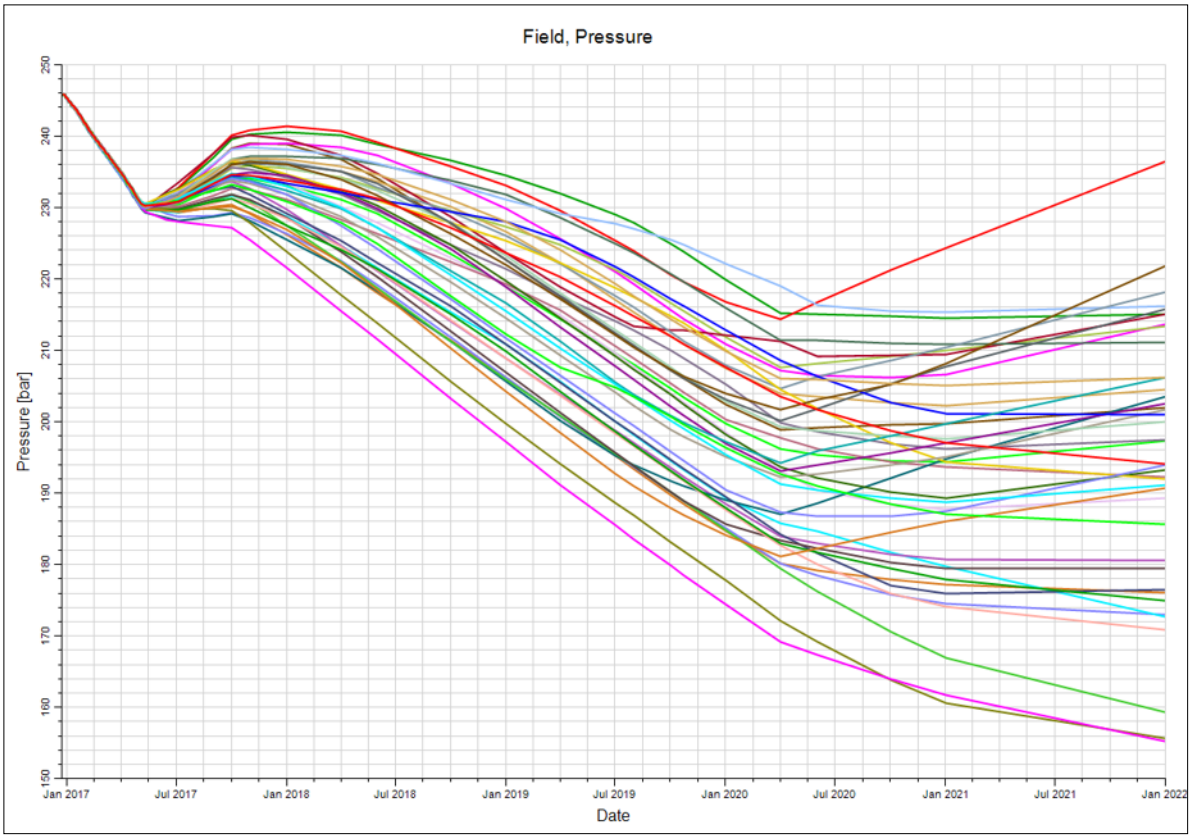

Figure 10.13 Prediction of field pressure development

The drainage strategy for the Ivar Aasen field is three months of depletion, followed by pressure maintenance by water injection. The rapid falling pressure in the prediction period is related to problems with water injection in the models. The models were unable to inject the desired amounts of water, and therefore unable to maintain the pressure.

The wide range in depletion between the models highlights one of the main arguments against manual history matching. One will not know where in the spectrum of possible models the single matched case actually is. Thus, the uncertainty is not well captured. However, more effective injectors might have lead to a more consistent answer in this prediction.

10.3.2 Oil Production

Figure 10.14 shows the cumulative oil production of the field predicted by the same ensemble. Again the diversity in the models leads to rather different production rates, adding up to huge volumes over the years. This is especially true for the second half of the period, when the oil production is limited by water production as the wells are suffering from high levels of water cut. The mentioned issues regarding low injection rates and resulting depletion also caused disappointing oil production.

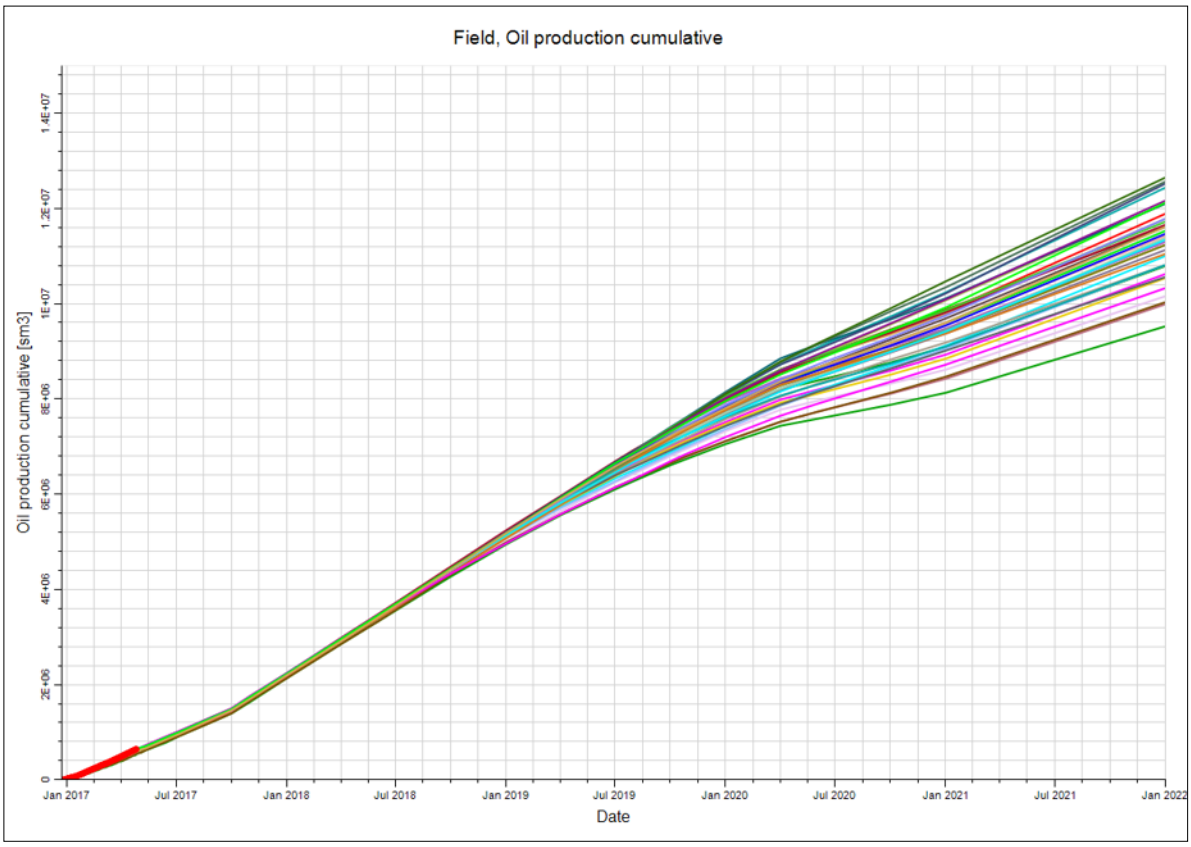

Figure 10.14 Prediction of cumulative field oil production

The base case model constructed through a manual history match is also typically used to predict future production. The prognoses are in turn useful input to development and investment decisions, and reservoir management in general. The decisions are thus highly dependent on where in the spectrum the single matched model ends up. However, if the entire ensemble models from an AHM study show significantly lower oil production than expected (due to low injection rates in this particular study), it does not bring a lot of insight either.

10.3.3 Water Cut

The future water cut was also predicted by simulating the history-matched models forward in time. The differences in time of water break through, seen as the point where the water cut becomes higher than zero, is fairly small. However, the spread in level of water cut seems to accelerate as the water cut increases. When they level off, the water cut in the different models range from 40 to 60 %. This deviation is significant, and suggests that the success of drainage is highly dependent on the changes done.

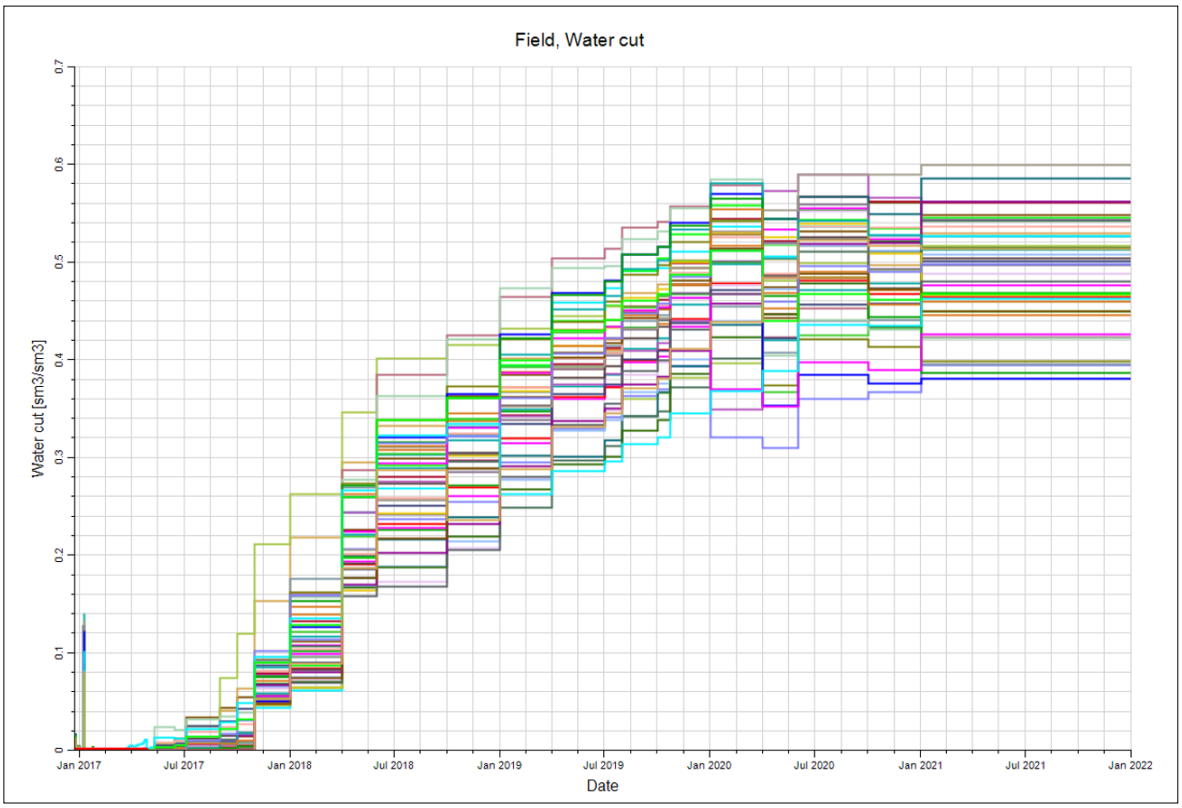

Figure 10.15 Prediction field water cut

No water production during the matching period makes any predictions about future two-phase flow inherently difficult. No information, not even indirectly, about two-phase flow is available until water breakthrough. Any adjustments of the relative permeability functions, how easily the phases are flowing at different saturations, will be speculative at this stage. Both manual and assisted history matching will become more reliable with known water breakthroughs.

11 Results

11.1 Manual History Matching

- Improved match compared to base case.
- Lower aquifer permeability.
- More good sand in the central west.
- More open faults.

11.2 RFT Surveys

- All reservoir zones found in the drilled injectors IAWI01 and IAWI03 were communication with their neighbouring producers.
- No Sleipner, but Statfjord on top of Skagerrak 2 in IAWI01 (north-west). Barrier to vertical flow between Statfjord and Skagerrak 2.
- Sleipner and Skagerrak 2 present in IAWI03 (south-west). Vertical communication between Sleipner and Skagerrak 2.

11.3 ResX Assisted History Matching Study

- Improved match compared to the initial ensemble.
- Porosity and permeability throughout the model are distributed more heavily towards extreme values. More low- and high-quality cells and fewer in between. The improved quality is assigned to the central west, while the poorer is assigned to the areas around the injectors.
- Increased static and dynamic in-place volumes.
- Trouble with reaching desired water injection levels during the prediction period led to unreliable forecasts for field pressure and oil production.

12 Discussion

12.1 Ivar Aasen Reservoir

The manual history matching of the Ivar Aasen reservoir model led to a better representation of the production data and measurements. More rapid depletion in the model than the field at two of the producers (IAOP01 and IAOP02) was fixed by increasing the reservoir volume and permeability in the area. Reducing the permeability in the aquifer mitigated large depletion at injectors seen in the model. In addition, all the faults were made less sealing by increasing the fault transmissibility multiplier from 0.01 to 0.1.

The adjustments were partly confirmed by the ResX study. Increased total reservoir volumes and improved reservoir quality between the mentioned production wells support the results of the manual study. Some support to the reduced aquifer permeability was found in the ResX results, as less communication or poorer permeability is suggested in the areas around the injectors (which is in the aquifer). The fault transmissibility multipliers did not show a clear tendency to increase in assisted study, as in the manual one.

Although the match was improved (in both studies), there is still a lot of uncertainty associated with the reservoir. As long as the production wells have not yet experienced water breakthrough, all two-phase flow properties are heavily based on assumptions. Short production history also adds uncertainty.

RFT surveys in IAWI01 and IAWI03 confirmed communication between the injectors and their neighbouring producers. This is vital for the efficiency of the injectors.

12.2 History Matching

The choice between manual and assisted history matching is a trade-off between detailed control and better uncertainty management. In manual history matching one is in control of every change, the risk of anchoring to one model is however imminent. In ensemble based computer assisted history matching one has limited control over the single changes. However, the numerous small changes to the model variables will (given a well-prepared study) help explore every possibility.

Although the user is not adjusting the reservoir variables in an assisted history matching, the process is far from automatic when considering all the preparations and quality checks that is needed in order to obtain meaningful results. The improved matches in the ResX study

suggest that the main challenge in AHM is not related to the matching procedure itself, but rather setting up the study efficiently.

Knowledge about the reservoir and experience with the history matching software is both needed in order to perform a successful AHM study. For better use of all reservoir knowledge present in the subsurface team, a great effort has to be made to get as many as possible familiar with the software and its methodology. Sufficient amounts of time are also of great importance.

12.3 General

Drilling of injectors after production start is an excellent source of information. The RFT-surveys brought insight into the vertical communication. However, depletion of the reservoir is needed in order distinguish between layers in communication and not. Determining vertical communication will not be possible with injection and pressure maintenance from the start of, since the entire reservoir will remain at initial pressure. The pre-drilled injectors also provided valuable pressure monitoring.

12.4 Further Work

A new manual history matching, integrating more production history, will probably be more robust. When time of water breakthrough becomes available, one can be even more confident.

A new, more thorough, ResX study will be beneficial. The discussed pitfalls revealed in the first study will then hopefully be avoided. More time at hand is however crucial in order to improve the results significantly.

13 Conclusion

13.1 Ivar Aasen Reservoir

The history matching studies suggest increased total reservoir volume, improved reservoir quality between IAOP01 and IAOP02, and reduced reservoir quality around the injectors. However, the lack of water breakthrough, and short production history make the results uncertain.

13.2 History Matching

Neither manual nor assisted history matching can be done quickly and easily if expected to yield high quality results. The superiority in optimization and uncertainty quantification of the AHM methods is limited by the quality of the preparations. A sound use of both classes of history matching may be the best solution at the moment, since both have their flaws.

13.3 General

RFT proved very useful in determining communication between producers and injectors, and in determining vertical communication.

Nomenclature

Abbreviations

AHM	Assisted history matching
BHFP	Bottom hole flowing pressure
BHP	Bottom hole pressure
EnKF	Ensemble Kalman filter
EnKS	Ensemble Kalman smoother
ES	Ensemble smoother
GOC	Gas oil contact
GOR	Gas/oil ratio
HM	History matching
ICD	Inflow control device
MCMC	Markov chain Monte Carlo
NTG	Net to gross ratio
Pdf	Probability density function
PDO	Plan for Development and Operation
PI	Productivity index
RFT	Repeat formation tester
RML	Randomized maximum likelihood
TVD	True vertical depth
WCT	Water cut
WOR	Water/oil ratio

Symbols

c	Compressibility
$\boldsymbol{C}_{qq}$	Model error covariance
$\boldsymbol{C}_{\varepsilon\varepsilon}$	Covariance of measurement errors
$\boldsymbol{C}^{\mathbf{a}}_{\psi\psi}$	Error covariance matrix for the analysed estimate
$\boldsymbol{C}^{\mathbf{f}}_{\psi\psi}$	Error covariance matrix for the predicted estimate
$\boldsymbol{d}_{obs}$	Observed reservoir behaviour vector
$\boldsymbol{d}$	Vector of measurements
$f(\psi)$	Probability density
F	Distribution function
$g( )$	Reservoir behaviour model
$\boldsymbol{G}$	Model operator for a vector state
$h( )$	Arbitrary function
k	Permeability
k_h	Horizontal permeability
k_v	Vertical permeability
$\boldsymbol{K}$	Kalman gain matrix
$\boldsymbol{m}$	Reservoir model variables vector
$\boldsymbol{M}$	Measurement matrix
N	Ensemble size
p	Pressure
p_e	Reservoir boundary pressure
p_w	Well pressure
PI	Productivity index
q	Production rate
$\boldsymbol{q}$	Stochastic error of vector model
r	Radius

r_e	External radius
r_w	Well radius
S	Skin factor
t	Time variable
Tx	Transmissibility multiplier
$\boldsymbol{\varepsilon}$	Measurement errors
μ	Viscosity or sample mean
φ	Porosity
Φ	Random scalar variable
$\boldsymbol{\psi}$	State variable vector
Ψ	Random scalar variable
σ	Standard deviation
σ^2	Variance
$\Re$	Space of real numbers

Reference List

Cancelliere, M., Verga, F., Viberti, D. 2011. Benefits and limitations of assisted history matching. Society of Petroleum Engineers.

Chen, Y., Oliver, D.S. 2013. History Matching of the Norne Full Field Model Using an Iterative Ensemble Smoother-(SPE-164902).

Dadashpour, M. 2009. Reservoir characterization using production data and time-lapse seismic data. In.

Det norske oljeselskap. 2014. *Ivar Aasen Reservoir Management Plan 2014*.

Evensen, G. 1994. Sequential data assimilation with a nonlinear quasi‐geostrophic model using Monte Carlo methods to forecast error statistics. In *Journal of Geophysical Research: Oceans* **99** (C5): 10143-10162.

Evensen, G. 2009. *Data assimilation: the ensemble Kalman filter*, Springer Science & Business Media.

Evensen, G., Van Leeuwen, P.J. 2000. An ensemble Kalman smoother for nonlinear dynamics. In *Monthly Weather Review* **128** (6): 1852-1867.

Fossum, K., Mannseth, T., Oliver, D. et al. 2012. Numerical comparison of ensemble Kalman filter and randomized maximum likelihood.

Gjesdal, A. 2017. History Matching – what is sufficient HM for prediction/well planning. Force, http://www.force.org/Global/Seminars/2015/Presentation 10 Dec - History Matching what is succesful History matcing.pdf (accessed 24.04 2017).

Hølland, Ø. 2016. Comparing expected and observed reservoir communication during first years of production for selected North Sea oil fields, Specialization Project, NTNU.

Jafarpour, B., Tarrahi, M. 2011. Critical evaluation of the ensemble Kalman filter for reservoir parameter estimation under incorrect and uncertain prior models. Society of Petroleum Engineers.

Jelmert, T.A. 2013. *Introductory Well Testing*.

Khaninezhad, M., Jafarpour, B. 2013. Bayesian history matching and uncertainty quantification under sparse priors: a randomized maximum likelihood approach. Society of Petroleum Engineers.

Ma, X., Hetz, G., Wang, X. et al. 2017. A Robust Iterative Ensemble Smoother Method for Efficient History Matching and Uncertainty Quantification.

Mattax, C., Dalton, R. 1990. *Reservoir Simulation, Monograph Series, SPE, Richardson*, TX.

Nichols, G. 2009. *Sedimentology and stratigraphy*, John Wiley & Sons.

NPD. 2017. Factpage Ivar Aasen, http://factpages.npd.no/factpages/Default.aspx?culture=nb-no&nav1=field&nav2=PageView%7CAll&nav3=23384520 (accessed 24.03 2017).

Oliver, D.S., Chen, Y. 2011. Recent progress on reservoir history matching: a review. In *Computational Geosciences* **15** (1): 185-221.

Perrone, A., Pennadoro, F., Tiani, A. et al. 2017. Enhancing the Geological Models Consistency in Ensemble Based History Matching an Integrated Approach. Society of Petroleum Engineers.

Resoptima. 2016. *ResX Reference Manual 3.4.0 2016*.

Resoptima. 2017. ResX, http://resoptima.com/solutions/ (accessed 22.05 2017).

Schlumberger. 2015. Transmissibility calculations. In *Eclipse Technical Description 2015.1*, Chap. 72, 960-966.

Skjervheim, J.-A., Evensen, G. 2011. An ensemble smoother for assisted history matching. Society of Petroleum Engineers.

Sætrom, J., Selseng, H., MacDonald, A. et al. 2016. Consistent Integration of Drill-Stem Test Data into Reservoir Models on a Giant Field Offshore Norway. Society of Petroleum Engineers.

Tan, T.B. 1995. A computationally efficient Gauss-Newton method for automatic history matching. Society of Petroleum Engineers.

Aanonsen, S.I., Nævdal, G., Oliver, D.S. et al. 2009. The ensemble Kalman filter in reservoir engineering--a review. In *Spe Journal* **14** (03): 393-412.

14 Appendix A Statistical Definitions

The following statistical fundament is based on the work of Evensen (2009).

Probability density function

A variable Ψ, with continuous random outcome can be described by the distribution function $F(\psi)$. The function defines how likely Ψ is to take a value less than or equal to ψ. It is linked to $f(\psi)$, the continuous probability density function, by

$$F(\psi) = \int_{-\infty}^{\psi} f(\psi')d\psi', \tag{14.1}$$

$f(\psi)$ is then the derivative of the distribution function

$$f(\psi) = \frac{dF(\psi)}{d\psi}. \tag{14.2}$$

How likely the random variable Ψ is to take the exact value of ψ is given by the probability density function (pdf).

The following conditions must be satisfied by the pdf;

$$f(\psi) \geq 0 \quad \text{for all } \psi, \tag{14.3}$$

the probability must be non-negative, and

$$\int_{-\infty}^{\infty} f(\psi)d\psi = 1, \tag{14.4}$$

the probability of finding Ψ is equal to one.

The likelihood that the value of Ψ is found in the interval $[\psi_a, \psi_b]$ is

$$Pr(\Psi \in [\psi_a, \psi_b]) = \int_{\psi_a}^{\psi_b} f(\psi)d\psi \tag{14.5}$$

The normal (or Gaussian) distribution is a bell shaped distribution, fully defined by its mean μ and variance σ^2. The pdf of the normal distribution is

$$f(\psi) = \frac{1}{\sigma\sqrt{2\pi}} exp\left(-\frac{(\psi-\mu)^2}{2\sigma^2}\right) \tag{14.6}$$

To describe the probability of two events happening together, a joint pdf can be used. The joint pdf $f(\psi, \phi)$ is defined given the two random variables Ψ and Φ.

Given the event Φ, the probability that some other event Ψ happens is described by the conditional pdf, $f(\psi|\phi)$. The pdf for Ψ given Φ is also called the posterior pdf.

When ignoring information of one event Φ, the pdf of the other event Ψ is the marginal pdf, or the prior pdf. Integrating the joint pdf over the ignored event gives the marginal pdf for Ψ:

$$f(\psi) = \int_{-\infty}^{\infty} f(\psi, \phi) d\phi \tag{14.7}$$

We also have that

$$f(\psi|\phi) = \frac{f(\psi, \phi)}{f(\phi)} \tag{14.8}$$

or

$$f(\psi, \phi) = f(\psi|\phi) f(\phi) = f(\phi|\psi) f(\psi) \tag{14.9}$$

If $f(\psi,\phi) = f(\psi)\, f(\phi)$, the variables Ψ and Φ are independent

We can rewrite (5.10) to Bayes' theorem:

$$f(\psi|\phi) = \frac{f(\psi) f(\phi|\psi)}{f(\phi)} \tag{14.10}$$

The theorem is giving the conditional probability distribution of Ψ given Φ, in terms of the posterior probability distribution of Ψ given the "data" Φ and the prior probability distribution of Ψ.

The probability density function $f(\boldsymbol{\psi})$ for the event $\boldsymbol{\psi} \in \Re^n$ is related to the distribution function $F(\boldsymbol{\psi})$ of the random variable $\boldsymbol{\Psi} \in \Re^n$ through the equation

$$F(\psi_1, \dots, \psi_n) = \int_{-\infty}^{\psi_1} \dots \int_{-\infty}^{\psi_n} f(\psi_1', \dots, \psi_n') d\psi_1' \dots d\psi_n' \tag{14.11}$$

Again the pdf is defined as the derivative of the distribution function.

$$\int_{-\infty}^{\infty} \dots \int_{-\infty}^{\infty} f(\psi_1', \dots, \psi_n') d\psi_1' \dots d\psi_n' = 1 \tag{14.12}$$

Also here the probability of finding ψ is equal to one. It is also called the joint pdf for $(\psi_1, \ldots, \psi_n)$.

It can be factorized into

$$f(\psi_1, \ldots, \psi_n) = f(\psi_1) f(\psi_2|\psi_1) f(\psi_3|\psi_1, \psi_2) \cdots f(\psi_n|\psi_1, \ldots, \psi_{n-1}) \tag{14.13}$$

In case $(\psi_1, \ldots, \psi_n)$ are independent, (14.13) can be written

$$f(\psi_1, \ldots, \psi_n) = f(\psi_1) f(\psi_2) \cdots f(\psi_n) \tag{14.14}$$

The likelihood function for a vector of measurements **d** given a model state $\boldsymbol{\psi}$ is $f(\mathbf{d}|\boldsymbol{\psi})$. The probability density function for the state and measurements happening together is then

$$f(\psi, d) = f(\psi) f(d|\psi) = f(d) f(\psi|d) \tag{14.15}$$

which leads to

$$f(\psi|d) = \frac{f(\psi) f(d|\psi)}{f(d)} \tag{14.16}$$

This is again Bayes' theorem, which here shows proportionality between the pdf of the model state given a set of measurements and the pdf of the model state times the likelihood function for the measurements.

Statistical moments

In order to make the probability density function easier to work with, some statistical moment of the density can be defined based on the general expression of the expected value of a function $h(\Psi)$

$$E[h(\Psi)] = \int_{-\infty}^{\infty} h(\psi) f(\psi) d\psi \tag{14.17}$$

Expected value

For a random variable Ψ with distribution $f(\psi)$, the expected value is defined as

$$\mu = E[\psi] = \int_{-\infty}^{\infty} \psi f(\psi) d\psi \tag{14.18}$$

The expected value is to be read as an average outcome (given a large number of samples) rather than the most likely outcome.

Variance

Given randomness of the variable Ψ, the variance can be expressed as

$$\sigma^2 = E[(\Psi - E[\Psi])^2] = \int_{-\infty}^{\infty} (\psi - E[\Psi])^2 f(\psi) d\psi = E[\Psi^2] - E[\Psi]^2 \qquad (14.19)$$

The variance is the expected value of its square deviation from its mean, the mean squared deviation. The last term, the second moment minus the square of the first moment, is used for calculation.

Covariance

The covariance of two random variables Ψ and Φ with pdfs $f(\psi)$ and $f(\phi)$is defined as

$$\begin{aligned} &E[(\Psi - E[\Psi])(\Phi - E[\Phi])] \\ &\qquad = \iint_{-\infty}^{\infty} (\psi - E[\Psi])(\phi - E[\Phi]) f(\psi, \phi) d\psi d\phi \\ &\qquad = \iint_{-\infty}^{\infty} \psi \phi f(\psi, \phi) d\psi d\phi - E[\Psi] E[\Phi] \end{aligned} \qquad (14.20)$$

Working with samples from a distribution

To evaluate the integrals using numerical integration becomes impractical when the dimension of the probability function becomes more than 3-4. This is clearly the case for reservoir simulation, where the number of unknowns is often much larger. Luckily the Markov chain Monte Carlo (MCMC) methods can substitute the direct numerical integration for high dimensional systems. It assumes the availability of a large number N of realizations from the distribution $f(\psi)$.

Sample mean

This sample of N independent realizations from $f(\psi)$, i.e. ψ_i for i = 1,…, N, give a sample mean of

$$\mu = E[\psi] \simeq \bar{\psi} = \frac{1}{N} \sum_{i=1}^{N} \psi_i \qquad (14.21)$$

Sample variance

The formula used to compute the variance is

$$\sigma^2 = E[(\Psi - E[\Psi])^2] \simeq \overline{(\psi - \bar{\psi})^2} = \frac{1}{N-1}\sum_{i=1}^{N}(\psi - \bar{\psi})^2 \tag{14.22}$$

Sample covariance

The following equation can be used to calculate the covariance

$$\begin{aligned} Cov(\psi, \phi) &= E[(\Psi - E[\Psi])(\Phi - E[\Phi])] \simeq \overline{(\psi - \bar{\psi})(\phi - \bar{\phi})} \\ &= \frac{1}{N-1}\sum_{i=1}^{N}(\psi_i - \bar{\psi})\,(\phi_i - \bar{\phi}) \end{aligned} \tag{14.23}$$

Statistics of random fields

In so-called random fields $\Psi(\mathbf{x})$, Ψ is a function of **x** = (x, y, z,…).

Sample mean

The sample mean for an ensemble of independent samples from the distribution $f(\psi(\mathbf{x}))$, i.e. $\psi_i(\mathbf{x})$ for $i = 1, \ldots, N$, is given by

$$\mu(x) \simeq \overline{\psi(x)} = \frac{1}{N}\sum_{i=1}^{N}\psi_i(x) \tag{14.24}$$

Sample variance

The sample variance of the same ensemble is given by

$$\sigma^2(x) \simeq \overline{\left(\psi(x) - \overline{\psi(x)}\right)^2} = \frac{1}{N-1}\sum_{i=1}^{N}\left(\psi_i(x) - \overline{\psi(x)}\right)^2 \tag{14.25}$$

Sample covariance

For the random fields the covariance between two different locations $\boldsymbol{x_1}$ and $\boldsymbol{x_2}$ are given by

$$C_{\psi\psi}(x_1, x_2) \simeq \overline{\big(\psi(x_1) - \overline{\psi(x_1)}\big)\big(\psi(x_2) - \overline{\psi(x_2)}\big)} = \frac{1}{N-1}\sum_{j=1}^{N}\big(\psi_j(x_1) - \overline{\psi(x_1)}\big)\big(\psi_j(x_2) - \overline{\psi(x_2)}\big) \tag{14.26}$$

The covariance defines how values of Ψ at different locations are varying together. The covariance are regarded a measure of smoothness.

Correlation

For the random variables $\Psi(\boldsymbol{x_1})$ and $\Psi(\boldsymbol{x_2})$ the correlation between them is defined by

$$Cor\big(\psi(x_1), \psi(x_2)\big) = \frac{C(x_1, x_2)}{\sigma(x_1)\sigma(x_2)}, \tag{14.27}$$

the normalized covariance.

Central limit theorem

Some conclusions about the convergence of different moments of a sample with increasing sample size can be drawn using the central limit theorem. By drawing a number of samples of Ψ with sample size N, we can expect:

- No matter the distribution of Ψ, the sample mean $\mu(\psi)$ from a set of samples, will follow a normal distribution
- The sample mean from a set a of samples converges towards $\sigma(\Psi)/N^{1/2}$

Then the error of a computed sample mean can be expected to be normally distributed and given by $\sigma(\Psi)/N^{1/2}$. Notably, the error will decrease proportional to $1/N^{1/2}$.